ISSN 2074-272X

науково-практичний журнал 2018/3

Електротехніка і Електромеханіка

Electrical Engineering & Electromechanics

З 2016р. журнал індексується у міжнародній наукометричній базі Web of Science Core Collection: Emerging Sources Citation Index

«ELECTRICAL ENGINEERING & ELECTROMECHANICS»

SCIENTIFIC & PRACTICAL JOURNAL

Journal was founded in 2002

Founders:

National Technical University «Kharkiv Polytechnic Institute» (Kharkiv, Ukraine)

State Institution «Institute of Technical Problems of Magnetism of the NAS of Ukraine» (Kharkiv, Ukraine)

ISSUE 3/2018

TABLE OF CONTENTS

Editorial office address: Dept. of Electrical Apparatus, NTU «KhPI», Kyrpychova Str., 2, Kharkiv, 61002, Ukraine

phones: +380 57 7076281, +380 67 3594696, **e-mail:** a.m.grechko@gmail.com (**Grechko O.M.)**

ISSN (print) 2074-272X
ISSN (online) 2309-3404

Printed 08 June 2018. Format 60 x 90 ⅛. Paper – offset. Laser printing. Edition 200 copies.
Printed by Printing house «Madrid Ltd» (11, Maksymilianivska Str., Kharkiv, 61024, Ukraine)

UDC 621.3: 537.8: 910.4 **doi: 10.20998/2074-272X.2018.3.01**

M.I. Baranov

AN ANTHOLOGY OF THE DISTINGUISHED ACHIEVEMENTS IN SCIENCE AND TECHNIQUE. PART 44: TRADITIONAL POWER ENGINEERING. NUCLEAR POWER STATIONS: RETROSPECTIVE VIEW, STATE AND PROSPECTS OF THEIR DEVELOPMENT

Purpose. ***Preparation of brief scientific and technical review about a retrospective view, modern state, achievements, problems, tendencies and prospects of development of world nuclear energy. Methodology. Known scientific methods of collection, analysis and analytical treatment of the opened scientific and technical information, present in scientific monographs, journals and internet-reports, world level in area of nuclear energy. Results. A brief analytical scientific and technical review is resulted about a retrospective view, modern state, basic achievements, existent problems, tendencies and prospects of development of nuclear energy in the industrially developed countries of the world. Considerable progress is marked in development and creation of technical base of modern nuclear energy, including the nuclear power stations (NPP) such their basic devices as nuclear reactors, steam generators, steam turbines and turbogenerators. The basic charts of construction of NPP producing in the world now about 11 % are described annual production electric power. It is indicated that in Ukraine a production of electricity volume at NPP makes more than 50 %, and in France − more than 70 % in annual power balance of country. Nuclear-physical bases of work of nuclear reactor are resulted on thermal-neutron, widely in-use at NPP. The design of most safe water-waters of nuclear power-reactor of type of WWER-1000 is described by thermal power 1000 MW, applied presently at NPP of Ukraine. Basic classification of nuclear reactors is presented. Technical information is resulted about largest NPP of the world. Master data are indicated about a nuclear fuel and radio-active offcuts of nuclear reactors of NPP. Basic measures and facilities are described for the increase of safety of nuclear reactors and NPP. Advantages and lacks of NPP are marked by comparison to the thermal power plants. Nuclear energy of Ukraine is considered and basic technical descriptions of operating domestic NPP are indicated. Basic problems, tendencies and possible prospects of development, are marked in the world and to Ukraine of nuclear energy. Originality. Systematization of the scientific and technical materials touching functioning of such important sector of world economy as nuclear energy known from the sources opened in outer informative space is executed. It is shown on the basis of approach of the systems that in spite of row of existent problems in area of world nuclear energy has the real prospects in the further development and to service society at satisfaction of his increasing requirements in electric and thermal energies. Practical value. Popularization and deepening for students, engineer-technical and scientific workers of scientific and technical knowledge in area of modern nuclear physics and energy, extending their scientific range of interests and further development of scientific and technical progress in society.*** References 20, figures 13, tables 1.

Key words: **nuclear physics and energy, nuclear reactor, nuclear power station, safety of nuclear reactor and nuclear power station, problems and prospects of development of nuclear energy.**

Приведен краткий научно-технический обзор о ретроспективе, современном состоянии и тенденциях в развитии мировой ядерной энергетики. Приведены ядерно-физические основы функционирования и описаны основные устройства ядерного реактора на уране и тепловых нейтронах, широко используемого на атомных электрических станциях (АЭС). Представлена классификация ядерных реакторов. Приведены данные о применяемом на АЭС ядерном топливе и радиоактивных отходах ядерных реакторов АЭС. Указаны меры для повышения безопасности ядерных реакторов и АЭС. Отмечена важная роль АЭС в годовом объеме выработки электроэнергии в мире и ряде стран. Указаны преимущества и недостатки АЭС. Рассмотрена ядерная энергетика Украины. Обозначены основные проблемы и перспективы развития в мире и Украине ядерной энергетики. Библ. 20, рис. 13. табл. 1.

Ключевые слова: **ядерная физика и энергетика, ядерный реактор, атомная электрическая станция, безопасность ядерного реактора и атомной электрической станции, проблемы и перспективы развития ядерной энергетики.**

Introduction. As is known, for the first time in the world, a controlled chain nuclear reaction in natural uranium $_{92}^{238}$U containing not more than 0.71 % per unit weight a rare isotope of uranium $_{92}^{235}$U fissioning by slow (thermal) neutrons [1], was carried out on December 2, 1942 by a group of physicists and engineers of the University of Chicago (USA) headed by the Nobel Prize winner in physics for 1938, Professor Enrico Fermi [2, 3]. The world's first uranium-graphite nuclear reactor in the form of an ellipsoid of rotation (with polar by vertical radius of about 3.09 m and equatorial by horizontal radius of about 3.88 m) known as «Chicago Pile-1» or CP-1 and containing 57 layers of uranium-graphite blocks (with 46 tons of natural uranium, of which 6 tons was metal uranium and 40 tons uranium dioxide and 385 tons of block uranium graphite of extraordinarily high purity [3]), ensured the receipt of a self-sustaining controlled (due to the radial neutrons of the cadmium rods, radiated through five three-level horizontal channels into the active zone of the reactor), the chain nuclear reaction [2]. With a minimum energy release power level (about 0.5 W) and radioactivity for personnel in this uncooled nuclear reactor, the multiplication factor k_p of neutrons was almost equal to unity [3]. By k_p which determines the reactivity $\rho_p = (k_p–1)$ of the nuclear reactor we mean the ratio of the number of neutrons in one of the succeeding generations from the fission of the nuclei of the uranium isotope $_{92}^{235}$U to their number in the previous generation from the fission of these nuclei [1]. It was the creation of a uranium-graphite nuclear reactor that opened the main path to the military and peaceful use of the nuclear energy of a number of radioactive chemical elements (for example, the uranium isotope $_{92}^{235}$U and the isotope of plutonium $_{94}^{239}$Pu [1, 3]). It should be noted that in the framework of the Uranium project of Nazi Germany (the scientific advisor of the project was Nobel Prize winner in physics for 1932, Professor Werner Heisenberg), a fully-

fledged controlled nuclear chain reaction in uranium $_{92}^{235}U$ was obtained only in February 1945 in an experiment conducted in the mining near Haigerloch [2]. After almost two months, Germany's nuclear program, due to the defeat of the latter in the Second World War, ceased to exist. Let us also point out that in the former USSR the first Soviet experimental uranium-graphite nuclear reactor created under the scientific supervision of Academician of the Academy of Sciences of the USSR Igor Vasilievich Kurchatov at Laboratory No. 2 (now Russian Research Center «Kurchatov Institute», Russian Federation (RF), Moscow) and called F-1 (in my opinion, the letter «F» in the name of the reactor comes from the name of the outstanding Italian-American nuclear physicist Fermi, the first to invent this type of heterogeneous nuclear reactor; this is a kind of homage of Soviet nuclear physicists to this all worldwide known scientist), on December 25, 1946 was put into its critical state ($k_p \approx 1$) [2]. Reactor F-1 was almost a ball with a diameter of up to 7.5 m, in the central part of which a diameter of about 6 m along the holes in the graphite blocks were placed working uranium and controlled cadmium rods. It did not have a cooling system and therefore operated at minimum power levels. Based on the experimental data obtained at the F-1 reactor, in July 1948 in the Southern Urals (Ozersk city), the first Soviet industrial uranium-graphite reactor, called A-1, was designed to produce weapons grade plutonium $_{94}^{239}Pu$ for the first Soviet atomic bombs [2, 4]. It is important to emphasize that as early as 1948 (before the completion of the work on the creation of the first Soviet plutonium atomic bomb successfully blown up at the Southern Nuclear Test Site of the USSR on August 29, 1949 [4, 5]) Academician of the Academy of Sciences of the USSR I.V. Kurchatov achieved, by the appropriate decision of the Government of the USSR, the initiation of experimental and development work on the practical peaceful use of atomic energy to generate electricity. In May 1950, in Obninsk (Kaluga region, RF), where one of the Soviet leaders in the field of reactor building, the «Physico-Energy Institute» (now the world-famous State Research Centre of the RF «Physics and Power Institute named after A.I. Leypunsky» [6]) placed, construction of the Obninsk nuclear power plant (NPP) with installed capacity of 5 MW began [2]. June 27, 1954 Obninsk NPP (Fig. 1) was put into trial operation. It was the first in the world NPP connected to a common electrical network [2].

Fig. 1. General view of the main building of the world's first pilot industrial Obninsk NPP with installed power of 5 MW (Obninsk, Kaluga region, RF, 1954) [7]

In 1958, the first stage of the Siberian NPP (Tomsk city) was commissioned in the former USSR with power of 100 MW (soon this NPP was brought to design power of 600 MW) [2]. On April 26, 1964, the first stage of the Beloyarsk NPP (Middle Urals, RF) gave electric current to its consumers. In September 1964, the 1st power unit of the Novovoronezh NPP was commissioned with installed power of 210 MW [2, 7]. The 2nd power unit of this NPP with installed power of 365 MW was launched in December 1969. In 1973, the first power unit of the Leningrad NPP with installed power of 1000 MW was commissioned. We point out that outside the former USSR the first industrial NPP with installed power of 46 MW was put into operation in 1956 in Calder Hall (Great Britain) [2]. In 1957, the US launched its first NPP in Shippingport with installed power of 60 MW. In 1959, France built its first NPP, Germany in 1961, Canada in 1962, Sweden in 1964 and Japan in 1966 [2, 7]. In 1976, around the world, work was begun on the construction of a record number of NPP in the history of world nuclear power, numbering 44 new nuclear power plants. In 1979, a serious accident occurred in the United States at the Three Mile Island nuclear power plant, which led to the long-term «freezing» of the US nuclear power program [2]. It should be noted that in the United States the idea of putting into operation new peaceful nuclear facilities was not returned until the beginning of the 21st century. Only during 1984-1985, in the world 33 new nuclear power plants were built [2]. The massive catastrophe on April 26, 1986 at the Chernobyl nuclear power plant (the explosion of the nuclear reactor of the 4th power unit with power of 1000 MW) had a negative impact not only on the nuclear power of the former USSR and then on independent Ukraine, but on the entire nuclear power industry of the industrialized countries. Undoubtedly, the recent catastrophe at the Fukushima-1 nuclear power plant, which occurred in March 2011 in Japan due to a strong earthquake in the nearby fault zone of the Earth's crust and the huge ocean waves (tsunami) that followed it, had a negative impact on the world nuclear power industry [8]. Undoubted scientific, technical and educational interest is an overview of the current state and possible prospects for the development of world nuclear energy, which has great socio-economic significance for mankind.

The goal of the paper is compilation on the basis of published materials of a scientific and technical review on the retrospective, current state, main achievements, problems and prospects for the development of nuclear power in the world with its powerful nuclear power plants.

1. General characteristics of nuclear power plant, its main construction schemes and power units. As is known, NPP is an important strategic object of any country in the world, containing a nuclear installation with the necessary technical facilities and technological systems, intended for industrial production of electricity (heat) [7, 8]. The cost of building a NPP according to modern expert estimates is about USD 2300 per 1 kW of electric power of this nuclear installation, commonly called a «*nuclear reactor*» [8]. Proceeding from this, the approximate cost of building at a NPP of its one 1000

MW power unit will be at least USD 2.3 billion. As we can see, nuclear power is the branch of the country's economy that requires huge investments. In Fig. 2, 3 in enlarged form the schemes of construction of modern nuclear power plants with powerful nuclear reactors and power units of increased safety are given [2, 7, 8].

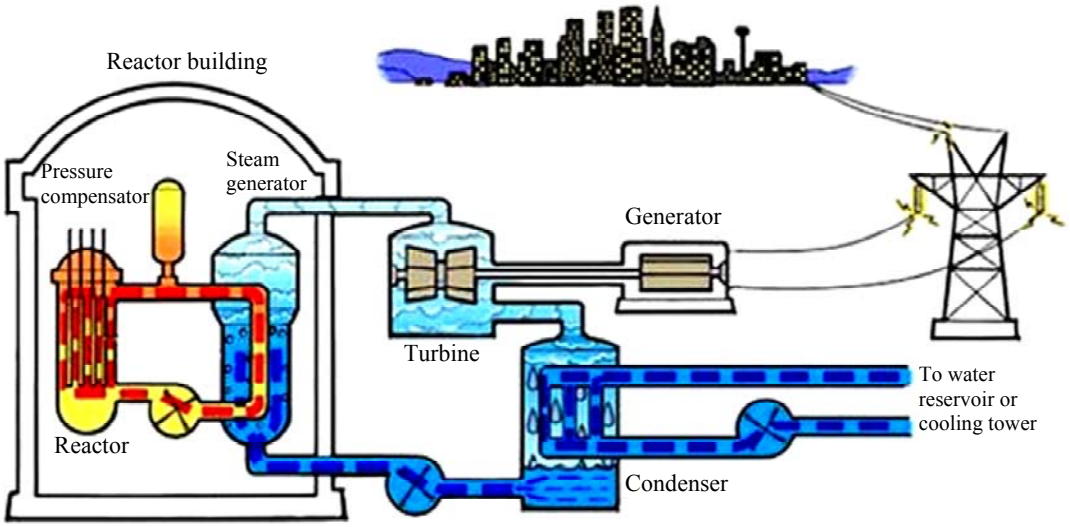

Fig. 2. Scheme of modern NPP on a two-circuit water-water power nuclear reactor of the WWER-1000 type [8]

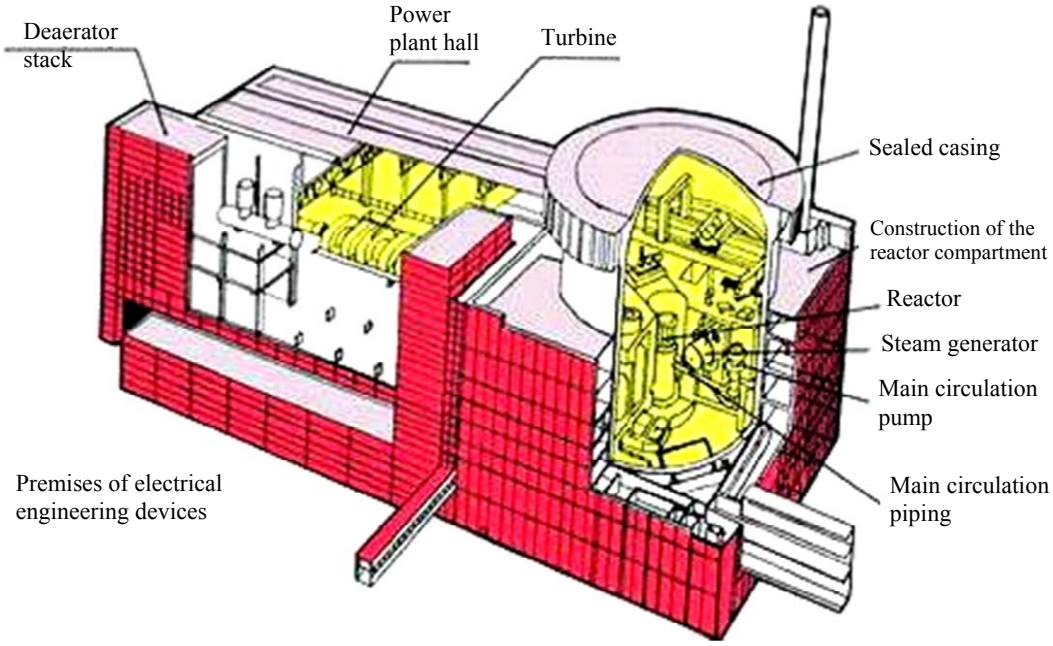

Fig. 3. Scheme of the structure of a powerful power unit of a modern NPP with a nuclear reactor of the WWER-1000 type [8]

According to Fig. 2, 3, the core of the NPP and its each power unit is a nuclear reactor (our accepted abbreviation WWER-1000 stands for «1000 MW water-water power reactor») which converts purified water with the addition of a solution of boric acid to a non-boiling boron mixture with a temperature of up to 320 °C, directed by the main circulation pump along the first radioactive circuit to the steam generator.

The operating pressure of the boron-water mixture in the first circuit of a nuclear reactor of the WWER-1000 type is up to 160 atm (16.2 MPa) [8]. The pressure compensator in this circuit serves to equalize the pressure fluctuations caused by the thermal expansion of its coolant. In the heat exchanger of the steam generator, this mixture heats the water of the second non-radioactive closed circuit to boiling, the superheated steam is directed to a steam turbine at pressure of about 63 atm (see Fig. 2, 4) rotating the rotor of a synchronous generator producing electricity. From the outlet pipe of the steam turbine, the spent steam is sent to a condenser, where it is cooled by water flows from the cooling pond (cooling tower) and by means of a circulating pump of this closed circuit is fed back to the heat exchanger of the steam generator. Note that the use of liquid metal coolant (for example, sodium) in the primary circuit instead of water makes it possible to simplify considerably the design of its metal casing in the core (the pressure of its liquid metal coolant does not exceed atmospheric pressure) and to get rid of it from the pressure compensator [7, 8]. Let us dwell further on the nuclear-physical features of the operation of powerful nuclear reactors of nuclear power plants.

Fig. 4. Installation of a powerful domestic steam turbine ПТ-1000 (in the right side of the turbine axis, the body of the corresponding turbogenerator is visible) in the power plant hall of the NPP [9]

1.1. Nuclear physics and nuclear reactor. From atomic physics it is known that the energy barrier hinders the spontaneous transition of a microparticle of matter to a different state. It can overcome this barrier only in two ways [1]: either due to the kinetic energy of the colliding particles, or due to the binding energy of the joining particle. The excitation of matter by the attached particles does not require large values of their kinetic energy. The main thing here is to have these particles, leading to «*exoenergetic reactions*» occurring in the excited substance, in which, in the subsequent transformation of the substance, energy is released more than required for its excitation itself. When energy is obtained in this way on a macroscopic scale, such reactions in matter must be chain-like, following one after another. *Chain reactions* in a substance can arise only when the particles that excite it in the exoenergetic reaction appear again as a product of the course of these exoenergetic reactions. Nuclear physicists have long been looking for a similar substance (chemical element) and similar microparticles, leading to the emergence of «*chain nuclear reactions*» in it and, accordingly, to the allocation of large values of intranuclear energy. In January 1939, the Austrian-German «tandem» of physicists Otto Frisch and Lisa Meitner, interpreting the results of a nuclear experiment conducted in December 1938 by German scientists Otto Hahn and Fritz Strassmann, concluded that in the natural uranium $_{92}{}^{238}$U the *nuclear reaction of dividing* the «mother» nuclei of its$_{92}{}^{238}$U isotope into two fragments with their «daughter» nuclei and the emission of several fast neutrons [3, 10]. The scientific discovery of the chain nuclear fission reaction in the uranium isotope $_{92}{}^{238}$U pointed to the practical reality of mastering nuclear energy for both military and peaceful purposes. Now we know that for each act of fission of one nucleus of the uranium isotope $_{92}{}^{238}$U, energy of about 197 MeV ($3.15 \cdot 10^{-11}$ J) is released and an average of 2.47 fast neutrons are «born» (produced) [1, 3]. Most of the fast neutrons (with energies up to 0.7 MeV [1]) are emitted almost instantaneously (in a time on the order of the relaxation time of free electrons in a copper conductor − 10^{-14} s [1]), and about 0.75 % of all secondary neutrons is emitted by nuclear fission fragments with delay in time equal to (0.05 - 60) s [1, 3]. Such neutrons in nuclear physics are called «delayed», which play an important role in the management of nuclear chain reactions in nuclear power plant reactors operating on thermal neutrons. For a stable course of the nuclear chain reaction in the uranium isotope $_{92}{}^{235}$U, impurities that absorb neutrons should be absent in it, and a minimum amount of a nuclear substance called the *critical mass* should be present [1, 3]. In addition, the neutron energy in the core with nuclear fuel should be sufficient to cause fission of the nuclei of the uranium isotope $_{92}{}^{235}$U. When using slow neutrons in the reactor for these purposes, their energy is ~0.025 eV [1, 3]. A controlled chain nuclear reaction in the uranium isotope $_{92}{}^{235}$U underlies the construction of nuclear reactors operating on slow neutrons and used at nuclear power plants. Fig. 5 shows a unique photo image of the core of a working water-cooled nuclear reactor [2].

Fig. 5. The rarest view of active zone of the active research water-water nuclear reactor (in the active zone of this type of reactor there is clearly observed a blue glow caused by Vavilov-Cherenkov radiation) [2]

The nuclear reactor (Fig. 6) consists of the following main parts [2]: an active zone with nuclear fuel and a neutron moderator; a neutron reflector surrounding the active zone of the reactor; liquid (usually purified water) coolant that takes heat from nuclear assemblies of fuel assemblies and transmits it to the steam generator of the power unit of the nuclear power plant; nuclear chain reaction control systems in the reactor core; emergency protection of the reactor; radiation protection of the reactor; remote control systems for reactor operation.

The data of Fig. 5 clearly demonstrate to the reader the complex nuclear-physical processes taking place in the active zone of a water-water nuclear reactor operating on thermal neutrons. In these processes, the formation of powerful neutron fluxes and fast charged microparticles, which cause intensive Vavilov-Cerenkov radiation in the water coolant of the reactor, takes place in the reactor core. We recall that the Vavilov-Cerenkov effect is due to

the emission of electromagnetic energy (light) by a charged microparticle moving rapidly with velocity v_e in an optically transparent medium, when $v_e > c/n$ [1, 3], where $c = 3 \cdot 10^8$ m/s is the speed of light in vacuum; n is the refractive index of the coolant (for water $n \approx 1.33$ [1]).

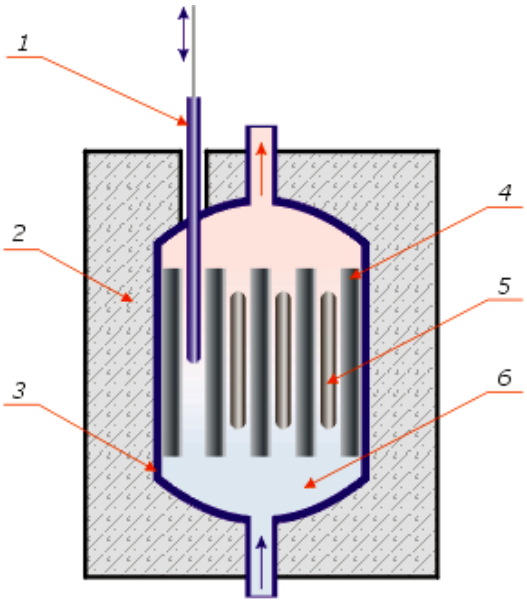

Fig. 6. Simplified diagram of the structure of a heterogeneous nuclear reactor on thermal neutrons (1 – control rod, 2 – massive radiation protection, 3 – heat-insulating housing, 4 – neutron moderator, 5 – nuclear fuel, 6 – liquid coolant) [2]

The current state of any nuclear reactor is characterized by two factors [2]: the multiplication factor k_p of neutrons in its core and the reactivity ρ_p. At $k_p \approx 1$ and $\rho_p \approx 0$, the number of fissions of the uranium isotope nuclei ${}_{92}{}^{235}\mathrm{U}$ in the reactor core is constant and the nuclear reactor is in a *stable critical state*. The conversion of the multiplication factor k_p of neutrons to unity is achieved by balancing the process of neutron multiplication in the reactor core and their losses. There are two main causes of neutron loss in a nuclear reactor [2, 8]: the first is the capture of neutrons by uranium nuclei without their fission; the second is the neutron escape from the reproduction zone. Control of the nuclear chain reaction of fission of uranium isotope nuclei k_p in fuel assemblies is provided by «retarded» neutrons. It is due to the considerable time of «life» in the active zone of the reactor of «delayed» neutrons that its control system manages to move the control rod-absorbers (usually made of boron or cadmium) and thereby select for the nuclear reactor the necessary multiplication factor k_p of neutrons and accordingly its reactivity ρ_p. Note that one important circumstance is that in the described nuclear reactor on thermal neutrons the nuclei of natural uranium ${}_{92}{}^{238}\mathrm{U}$, capturing fast neutrons from fission of uranium isotope nuclei ${}_{92}{}^{238}\mathrm{U}$ or neutrons in the process of their deceleration, do not test their division. Such excited uranium nuclei ${}_{92}{}^{238}\mathrm{U}$ in the process of a long chain of nuclear transformations (for a time of up to 2.3 days) pass to the stable nuclei of the weapon isotope of plutonium ${}_{94}{}^{239}\mathrm{Pu}$, which, like the nuclei of the uranium isotope ${}_{92}{}^{238}\mathrm{U}$, can be divided in the uranium assemblies of the reactor fuel assembly thermal neutrons [1, 3].

1.1.1. Classification of nuclear reactors. According to the design, modern nuclear reactors of nuclear power plants are divided into two large groups [11]:

- channel reactors (fuel assemblies in them are placed in separate channels that penetrate its active zone and are made in graphite blocks of neutron moderators, assemblies with each other can be swapped and flowed by the flow of a liquid heat carrier);
- hull reactors (fuel assemblies in them are permanently located inside a massive metal casing, and the active zone is washed by an intensive flow of liquid heat carrier).

Fig. 7, 8 show the general views of the channel and hull types of nuclear reactors used at Ukrainian NPPs, respectively [2, 9, 12].

Fig. 7. General view of a powerful nuclear reactor of the RBMK-1000 type installed in the reactor plant of one of the 4 operated power units of the Chernobyl nuclear power plant (before the catastrophe in 1986) from its assembled of separate lead blocks of the upper protective cover [2, 9]

As is known, in April 1986 on the 4th power block of the Chernobyl NPP, it was exactly on the RBMK-1000 nuclear reactor of high power of the channel type with thermal power of 1000 MW that the most serious accident in the world nuclear power history took place which undermined people's confidence in the safety of nuclear reactors. Some countries (for example, Italy) after the catastrophe at the Chernobyl nuclear power station passed laws prohibiting the location of nuclear power plants on its territory (the existing nuclear power plants were stopped and their nuclear reactors conserved) [8]. In Germany, government decisions have been taken to reduce the number of nuclear power plants operating on its territory [2, 8].

At present, the most secure design of a powerful nuclear reactor on thermal neutrons used in modern nuclear power plants is shown in Fig. 8 design of the WWER-1000 reactor [9, 12]. The overall dimensions of such a nuclear reactor are [9]: the height is up to 20 m and the hull diameter is up to 4.5 m. Control and regulation of the process of the chain nuclear reactions in the assemblies of fuel assemblies filled with uranium fuel elements of plate or cylindrical shape, and the process of heating the water coolant of a nuclear reactor of the WWER-1000 type is carried out with the help of rods of the control and protection system (CPS) and a block of protective tube (BPT). The housing of such a reactor is

calculated for the maximum pressure of an overheated mixture of its water coolant which is about 160 atm [8].

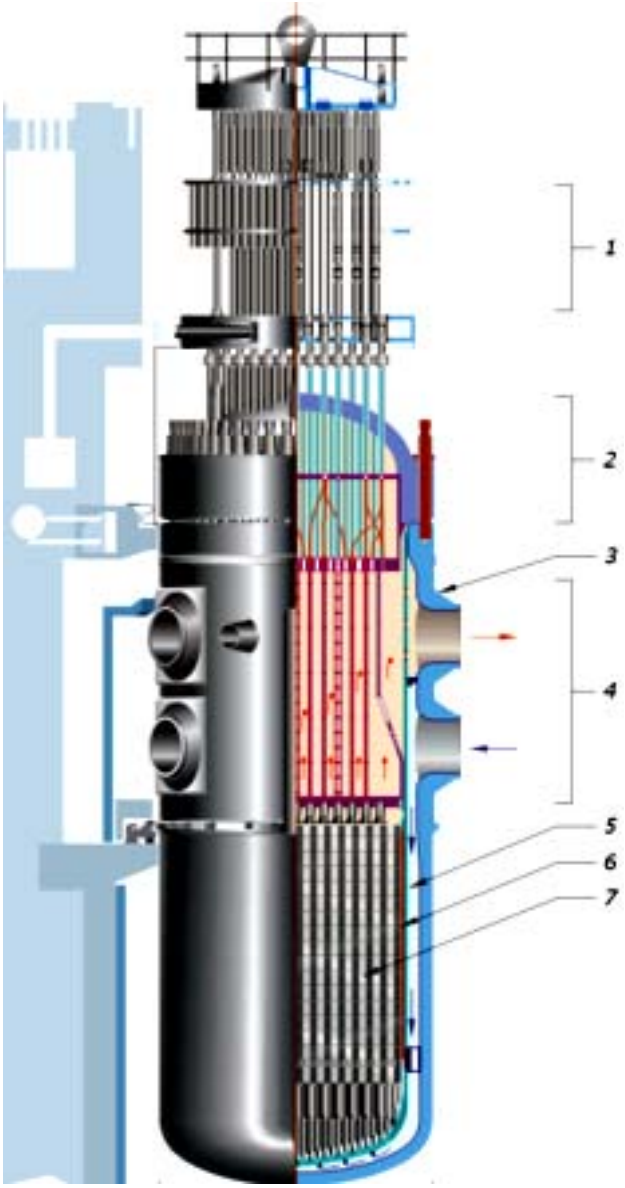

Fig. 8. The scheme of the structure of a powerful nuclear reactor of the WWER-1000 type (1 – drive of the CPS, 2 – protective cover of the reactor, 3 – reactor housing, 4 – block of the BPT, 5 – water shaft, 6 – core fence, 7 – fuel assemblies) [9]

It is interesting that the geometric shape of a nuclear reactor is chosen from the condition of a minimum ratio of the area of its massive radiation-resistant enclosure to the volume it occupies. This condition corresponds to the shape of a sphere, a short cylinder, and a cube [1]. This is done to minimize the leakage of neutrons from the core of the nuclear reactor, which has a *critical volume* in the critical state of the reactor ($k_p \approx 1$; $\rho_p \approx 0$) (for modern nuclear reactors this volume can be hundreds of m^3 [2]). The critical volume of the reactor corresponds to the *critical mass* of the fissionable nuclear fuel. We note that nuclear reactors have the lowest critical mass, in which the water solutions of the salts of pure fissile radioactive isotopes with a water neutron reflector serve as fuel. For example, for the uranium isotope ${}_{92}{}^{235}U$, the lowest critical mass is 0.8 kg, and for the isotope of plutonium ${}_{94}{}^{239}Pu$ – 0.5 kg [2]. As the nuclear fuel «burns out», the reactivity ρ_p of the reactor under consideration decreases. In this regard, its assembly of fuel assemblies is required to be changed. In WWER-1000 reactors, replacement of «burnt out» nuclear fuel is produced immediately from their entire core, and in RBMK-1000 reactors such a replacement is carried out gradually with the remaining fuel assemblies of different «ages» in operation. We recall that under the *active zone* of the reactor is meant the zone where the nuclear fuel is located, the controlled chain nuclear reaction of fission of its nuclei proceeds and where the intranuclear energy is allocated. Fig. 9 shows the time of replacement of nuclear fuel in a reactor of the WWER-1000 type.

Nuclear reactors according to the type of nuclear fuel used in their core are divided into [2, 11]:

- reactors with fuel assemblies based on such isotopes of uranium as ${}_{92}{}^{238}U$, ${}_{92}{}^{235}U$ and ${}_{92}{}^{233}U$;
- reactors with fuel assemblies based on the isotope of plutonium ${}_{94}{}^{239}Pu$, a whole family of plutonium isotopes ${}_{94}{}^{239\text{-}242}Pu$ in a mixture with natural uranium ${}_{92}{}^{238}U$;
- reactors with fuel assemblies based on the thorium isotope ${}_{90}{}^{232}Th$ (with further conversion when staying in the core in the uranium isotope ${}_{92}{}^{233}U$).

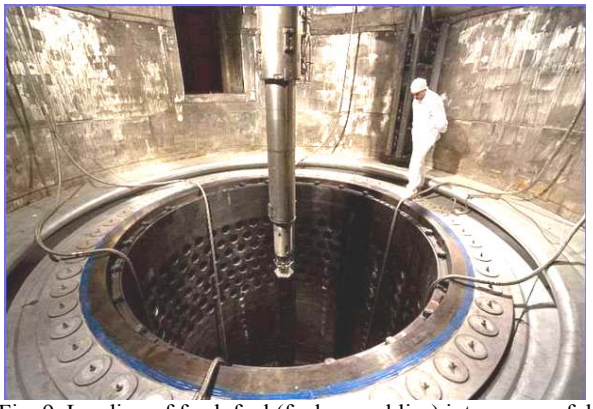

Fig. 9. Loading of fresh fuel (fuel assemblies) into a powerful water-water nuclear reactor of the WWER-1000 type (the upper hermetic protective cover of the reactor was removed) [2, 9]

Nuclear reactors according to the nature of the location of fuel in the core are classified into [2]:

- heterogeneous reactors (fuel in their zone is placed discretely in the form of blocks (fuel assemblies streamlined by the coolant), between which there is a neutron moderator);
- homogeneous reactors (fuel and neutron moderator represent a homogeneous mixture).

Nuclear reactors differ in the degree of enrichment of their nuclear fuel in fuel elements by [2, 11]:

- reactors with fuel assemblies based on the isotope of unprocessed natural uranium ${}_{92}{}^{238}U$;
- reactors with fuel assemblies based on the isotope of poorly enriched natural uranium ${}_{92}{}^{238}U$;
- reactors with fuel assemblies based on the isotope of highly enriched natural uranium ${}_{92}{}^{238}U$.

Nuclear reactors for the chemical composition of fuel in the core are divided into [2, 11]:

- reactors with metal isotopes of uranium, plutonium and thorium;

- reactors with uranium dioxide UO_2;
- reactors with uranium carbide UC.

Nuclear reactors in the energy spectrum of neutrons in the core are divided into [2, 11]:

- reactors on thermal (slow) neutrons called «thermal reactors»;
- fast neutron reactors called «fast reactors»;
- reactors on intermediate neutrons;
- reactors on neutrons with a mixed energy spectrum.

Nuclear reactors by type of coolant in their core are divided into [2, 11]:

- reactors with light water H_2O called «water-water nuclear reactors»;
- reactors with heavy water D_2O called «heavy water nuclear reactors»;
- reactors with gas in the core called «graphite-gas nuclear reactors»;
- reactors with a liquid-metal coolant (for example, with sodium, a liquid mixture of lead with bismuth);
- reactors with organic coolant;
- reactors with solid coolant;
- reactors on melts of a number of salts (for example, uranium fluorides).

Nuclear reactors according to the type of neutron moderator used in their zone are divided into [2, 11]:

- reactors with graphite *C* designed as «graphite-water and graphite-gas reactors»;
- reactors with light water H_2O designed as «light water and water-water reactors»;
- reactors with heavy water D_2O designed as «heavy water reactors»;
- reactors with metallic beryllium Be (can be made with beryllium oxide BeO);
- reactors with hydrides of a number of metals;
- reactors without moderator called «fast neutron reactors».

Nuclear reactors differ in the way they generate heat carrier vapor in [2, 11]:

- reactors with an external steam generator designed as «water-water reactors» (for example, two-circuit reactors of the WWER-1000 type);
- reactors with internal generation of steam, performed as «boiling reactors» (for example, RBMK-1000 single-loop reactors).

Nuclear reactors, according to the nature of their purpose and use, are divided into [2, 11]:

- power reactors used to generate electricity and heat (these reactors are installed at NPPs);
- transport reactors placed on vehicles (for example, on military submarines);
- industrial reactors used for the production of the weapon isotope of plutonium $_{94}{}^{239}Pu$ and the production of radioactive isotopes used in various fields (for example, in medicine);
- research reactors in which neutron and gamma-ray fluxes generated in their active zones are used to study the behavior of various substances with respect to the problems of nuclear physics, solid state physics, radiation chemistry, radiobiology, and radiology;
- experimental reactors designed to determine in the conditions of intensive neutron and thermal fields of various physical and technical properties of structural materials necessary for the design and operation of new designs of nuclear reactors at NPPs and nuclear special purpose plants.

As we can see, nuclear reactors are characterized by a wide range of their classification. The International Atomic Energy Agency (IAEA) uses the following classification of the main types of nuclear power reactors at nuclear power plants [2, 12]:

- PWR – pressurized water reactor in which light water H_2O is both a coolant and a retarder (for example, a WWER-1000 water-water reactor);
- LWGR – light water graphite reactor - reactor with light water H_2O as a coolant and with graphite as a moderator (for example, «graphite-water reactor» type RBMK-1000);
- BWR – boiling water reactor in which the formation of steam from a single-circuit circuit to a steam turbine occurs directly in the reactor;
- GCR – gas-cooled reactor in which gas is used as the heat carrier, and moderated block graphite;
- FBR fast breeder reactor which does not require the presence of a moderator in the core, and uses a liquid metal coolant (usually sodium) in the primary circuit, and in the second circuit – light water H_2O;
- HTGR – high-temperature gas-cooled reactor;
- PHWR – pressurized heavy water reactor – D_2O heavy water reactor as a moderator and coolant;
- HWGCR – heavy-water-moderated gas-cooled reactor – reactor in which gas is used as a coolant, and heavy water D_2O as a retarder;
- HWLWR – heavy-water-moderated boiling light-water-cooled reactor – reactor in which heavy water D_2O is used as a retarder and boiling coolant;
- PBMR – pebble bed modular reactor – modular reactor with spherical structures of its fuel assemblies.

In the nuclear power industry and in powerful nuclear power plants of various countries, the most widespread are «water-water nuclear reactors» (up to 62 %) and «boiling nuclear reactors» (up to 20 %) [2, 8].

1.1.2. Fuel for nuclear reactors of Ukrainian NPPs. Until 2011, nuclear fuel (uranium fuel assemblies) for all Ukrainian NPPs was supplied by the Russian company TVEL [13]. In 2008, our country set a course for diversifying nuclear fuel supplies for its nuclear power plants. To this end, in the same year, an agreement was concluded with the Westinghouse Electric Company (USA) to supply it to Ukraine during 2011-2015. 630 pieces of uranium assemblies for 3 powerful power units of domestic NPPs with nuclear reactors of WWER-1000 type [13]. In April 2012, the experimental operation of uranium fuel assemblies produced by the American company Westinghouse Electric Company at the 3rd power unit of the South Ukrainian Nuclear Power Plant revealed a number of serious design errors in these fuel assemblies that caused damages to the Ukrainian side amounting to about USD 175 million [13] . The operation of this unit of the South Ukrainian NPP was continued only after the installation of new assemblies of fuel

assemblies produced by the RF instead of damaged American nuclear fuel assemblies. According to the State Statistics Committee of Ukraine, during the period January-October 2015, the volume of nuclear fuel imports to our country amounted to USD 504 million including supplies from Russia in the amount of USD 471 million (94 %) and Sweden (from the US supplier Westinghouse Electric Company) for the amount of USD 33 million USA (6 %) [13]. Currently, the world-famous Russian company TVEL remains the main supplier of nuclear fuel for our nuclear power plants, providing at least 90 % of the necessary needs of Ukraine for this fuel. As of December 2016, Westinghouse Electric Company (USA) supplied nuclear fuel to a limited extent only for the 3rd power unit of the South Ukrainian Nuclear Power Plant and the 5th power unit of the Zaporizhzhya NPP [13].

1.1.3. Utilization and storage of spent nuclear fuel at Ukrainian NPPs. During the operation of the nuclear reactor, because of the accumulation of fission fragments in its uranium fuel, its isotopic and chemical composition changes and the formation of transuranium elements (mainly plutonium isotopes $_{94}^{244}$Pu) occurs [2, 11]. The spent nuclear fuel (SNF) in the core of the reactor at nuclear power plants is due to its residual heat release to relatively long storage. This residual heat release in SNF is a consequence of gamma and beta decays in radioactive fission products of nuclear fuel accumulated in assemblies during the operation of the nuclear reactor. In SNF, the excited nuclei of these fission products, due to their radioactive decay, become more stable or completely stable, with significant thermal energy released. In this connection, the residual heat generation in SNF is an important problem for working NPPs, directly related to their nuclear safety. To solve this unavoidable problem, special dry or wet SNF storage facilities should be located at the nuclear power plant, in which the latter, under a certain temperature regime, must remain for a sufficiently long time (for example, up to 3-4 years in their water-holding basins) [2]. Since 2001, Ukraine has only one dry SNF storage facility at Zaporizhzhya NPP. We also have one wet SNF storage in the exclusion zone of the Chernobyl nuclear power plant, which is unable to take SNF even from its nuclear power plants for long-term storage [2]. Currently, only two countries in the world – Russia and France possess SNF reprocessing technologies. Therefore, now SNF from Khmelnitsky, Rivne and South-Ukrainian NPPs is exported for storage and processing in Russia. Such technological procedures cost Ukraine annually USD (150-200) million [13].

Due to the high cost of SNF storage in the territory of the Russian Federation and the Ukraine's obligations to the IAEA in the zone of alienation of the Chernobyl nuclear power plant, the construction of the Central SNF storage facility is planned [13]. Since September 2016, technical documentation for the construction in Ukraine of such a dry large SNF storage facility is undergoing international expertise. The creation of such a SNF storage will allow domestic nuclear power plants to diversify the utilization of radioactive waste from their reactors.

1.1.4. Safety of nuclear power plants and their nuclear reactors. At present, the high degree of safety of nuclear power plants in many countries of the world is provided by the following basic protective factors [13, 14]:

- the principle of self-protection of the nuclear reactor of nuclear power plants (the composition of the reactor core and the physics of the nuclear processes taking place in it on the basis of natural feedbacks due to the appearance of the effect of «negative reactivity» should ensure its self-regulation);
- availability of emergency protection at nuclear reactors and a number of radiation safety barriers;
- multiple duplication of safety channels at nuclear power plants and the use of protective systems, both active (requiring intervention of maintenance personnel and the availability of a power supply source) and passive (not requiring intervention by maintenance personnel and the availability of a power source) of a protective nature;
- using materials that are highly resistant to the effects of intense radiation and thermal fields, electrical devices, technological systems and control systems (including their apparatus and cable-conductor products);
- introduction of a safety culture (from the moment of choosing a site for NPP construction up to the period of its launch and during its operation).

Nuclear reactors that remain at the operating power units of Ukrainian NPPs belong to WWER reactors, of which two are WWER-440 type (with installed power of 440 MW) and 13 WWER-1000 type (with installed power of 1000 MW) [13]. These reactors have two-circuit circuits (see Fig. 2) which are fundamentally more safe than the single-loop reactor scheme of the Japanese NPP «Fukushima-1» [8]. In the first circuit of the WWER-type reactor, because of the high pressure in it, there is no saturated vapor. Therefore, the risk of «denuding» (leaving without a coolant) and overheating of its nuclear fuel is fundamentally lower than in a single-loop reactor. The radiation safety system of modern NPPs in Ukraine and Russia (it is necessary not to lose sight of the fact that domestic nuclear power plants and their nuclear reactors are Russian developments) includes four main barriers to the spread of ionizing radiation and radioactive substances into their environment [13, 14]:

- a fuel matrix that prevents the release of fission products under the sheath of fuel assembly;
- a zirconium-steel sheath of fuel assembly which does not allow the products of fission of fuel to enter the coolant of the main circulation circuit;
- the main circulation circuit (1st circuit) which prevents the fission products from escaping under the protective hermetic shell of the reactor;
- a system of protective hermetic shells («*containment*») of the reactor excluding the release of nuclear fission products into the environment.

Fig. 10 shows a simplified scheme for the containment of a nuclear reactor of the WWER-1000 type [14].

We point out that the containment of a nuclear reactor of the WWER-1000 type with a volume of up to 75000 m^3, made of prestressed concrete with metal cables, is mechanically designed as an external force (for example, to drop an aircraft at speed of up to 200 m/s and a mass up to 5 tons), and on the internal action of gases

accumulated in an emergency mode in the reactor zone with an excess pressure of up to 5 atm [14]. In addition, this container of a nuclear reactor of the WWER type is able to withstand the impact of an air shock wave with a pressure up to 30 kPa on its front, a seismic effect from a calculated earthquake with an intensity of up to 8 points on the MSK-64 scale and hurricane impact with wind speed of up to 56 m/s [14].

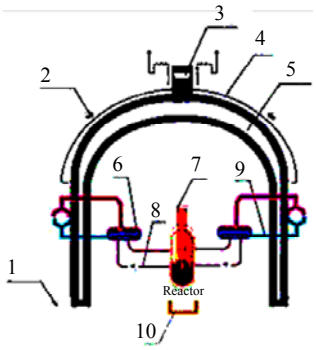

1 – atmospheric air
2 – hot air
3 – filter
4 – passive filtration traction tubes
5 – interblock space
6 – steam generator
7 – rods with absorber
8 – the first loop
9 – the second loop
10 – melt trap

Fig. 10. Scheme of protective hermetic shells of a nuclear reactor of WWER-1000 type at domestic NPPs [14]

In the event of a severe accident (for example, breaking the pipeline of the first cooling circuit of its core) on the nuclear reactor of the WWER-1000 type, its containment and liquidation, there is an emergency core cooling system (ECCS), containing special tanks with boric acid over the reactor [14]. Each 60 m^3 vessel of the ECCS system of the reactor is a thick-walled (90 mm thick) cylindrical vessel of bilayer clad steel with a diameter of up to 3175 mm, operating under a pressure of 60 atm [14]. Rapid delivery of the contents of the above-mentioned capacitances of the ECCS to the inside of the core of the nuclear reactor results in the quenching in it of a large amount of boron-containing material that absorbs fast and slow neutrons, chain nuclear reactions in the fuel assemblies, and the removal of the reactor to a minimum thermal power. In the future, according to the rules at NPP, a system for its emergency cooling should be connected to the cooling of the core of the emergency reactor [14]. The principle of deep defense of its nuclear reactors used at nuclear power plants also presupposes the existence of such a concept of nuclear safety, which provides not only means for preventing accidents, but also means for managing the consequences of beyond design basis accidents ensuring the localization of radioactive substances within the confinement. Such means include [14]:

- a hydrogen removal system (with passive recombiners) accumulated in the volume occupied by protective hermetic shells;
- a system for protecting the first circuit of the reactor from exceeding the pressure in its pipelines;
- a system of heat removal from steam generators;
- a system of heat removal from the designs of the protective hermetic shells of the nuclear reactor;
- a device for localization of the core melt («trap»), placed under the reactor.

The emergency protection of the nuclear reactor of the nuclear power plant consists of a set of devices designed to quickly stop the nuclear chain reaction in the reactor core. This protection automatically works when one of the parameters of the nuclear reactor reaches a value that could lead to its failure. [2]: temperature, pressure and flow rate of the heat carrier (in the first radioactive circuit of the WWER-type reactor), the level and rate of increase in the reactor power. In most cases, active elements of the active emergency protection of a nuclear reactor at nuclear power plants are rods with a substance that absorbs neutrons well (for example, boron or cadmium). Sometimes a liquid absorber injected under pressure into its radioactive coolant circuit is used to stop a nuclear reactor. In addition to active emergency protection, modern nuclear reactors also provide systems for their passive emergency protection (for example, the indicated ECCS system) [14].

In accordance with the «Rules of Nuclear Safety of Nuclear Plant Reactor Systems» in force in Ukraine and the Russian Federation, at least one of the envisaged reactor shutdown systems should perform the function of emergency protection of the nuclear reactor of nuclear power plants [12-16]. The emergency protection equipment for a nuclear reactor of a nuclear power plant must at the same time consist of at least two independent staffing sets. Each set of emergency protection equipment of the reactor should be designed in such a way that in the entire range of technological parameters set in the reactor plant design, an emergency protection is provided by at least three independent channels for each process parameter to be protected [15, 16].

It is important to note that at all NPPs in Ukraine and the Russian Federation, automatic radiation monitoring systems (ARMS) have been installed that fix the radiation level around radiation-hazardous NPP facilities in real time using a sensor network. The readings of the ARMS devices are transmitted to a special website in Internet.

1.2. The world's largest nuclear power plants. It should be noted that in 1978 in the world around a hundred nuclear reactors of various types and capacities operated in the nuclear power plant, in April 2017, the number of nuclear power units operating in the industrialized countries of the world (including temporarily suspended) was 451 [2]. The largest operating NPP in Europe is the Zaporizhzhya NPP (Energodar, Zaporizhzhya region, Ukraine) with installed power of 6000 MW, the construction of which began in 1980 [8]. Since 1996, six powerful dual-circuit power units with «water-water nuclear reactors» of the WWER-1000 type have been operating in the structure of this NPP (see Fig. 8). The world's largest nuclear power plant with installed power of 8212 MW is located in Kashiwazaki (Niigata prefecture, Japan) [8]. It has five «boiling nuclear reactors» (BWR type according to the IAEA classification) and two improved «boiling nuclear reactors» of the ABWR type [2, 8]. However, since 2011 this NPP does not generate electricity to the grid. Therefore, today the world's largest operating nuclear power plant is the South Korean nuclear power plant «Corey» which has seven powerful power units with «water-water reactors» (type PWR on the IAEA scale) with installed power of 6862 MW [8].

1.3. Generation of electricity at nuclear power plants in the world. As of December 31, 2015, nuclear power plants of the world in total produced about 2477 TWh of electricity per year, which amounted to about 10.7 % of the world's electricity generation [8]. The annual «peak» of electricity production at nuclear power plants around the world was recorded in 2006, amounting to 2660 TWh. The share of nuclear power in global annual production on our planet of electricity in 2015 compared with 1996 decreased from 17.6 % to 10.7 %. The world leaders in terms of the production of electricity at nuclear power plants for 2016 were [8]:

- the USA (805.3 billion kWh/year, 99 nuclear reactors operated at the NPP, generating up to 19.7 % of the electricity generated in the country);
- France (384 billion kWh/year, 58 reactors operating at nuclear power plants, generating up to 72.3 % of the country's electricity);
- China (210.5 billion kWh/year, 36 nuclear reactors operating at nuclear power plants generating up to 3.6 % of the country's electricity), which is currently implementing the world's largest program for the construction of new nuclear power plants;
- Russia (179.7 billion kWh/year, 37 nuclear reactors operated at nuclear power plants, generating up to 17.1 % of the country's electricity);
- South Korea (154.3 billion kWh/year, there were 25 nuclear reactors operating at nuclear power plants generating 30.3 % of the total amount of electricity generated in the country);
- Canada (97.4 billion kWh/year, 19 nuclear reactors, generating up to 15.6 % of the country's electricity);
- Ukraine (81 billion kWh/year, 15 powerful WWER (PWR) reactors operating at nuclear power plants, generating up to 52.3 % of the country's total electricity generation);
- Germany (80.1 billion kWh/year, 8 nuclear reactors operating at nuclear power plants, generating up to 13.1 % of the country's electricity);
- Great Britain (65.1 billion kWh/year, 15 powerful nuclear reactors that generate up to 20.4 % of the country's total electricity production);
- Sweden (60.6 billion kWh/year, 10 nuclear reactors, generating up to 40 % of the country's electricity, and the state program for the abandonment of nuclear power in the country was suspended).

From the above quantitative data for nuclear power plants in a number of countries, it can be seen that almost half of the world's annual electricity generation at nuclear power plants falls on only two countries – the United States and France. Now 31 countries of the world are using NPPs [8]. The overwhelming number of operating nuclear power plants are located in Europe, North America, Far East Asia and in the territory of independent countries formed from the collapse of the former USSR in 1991 [2, 8].

1.4. Nuclear energy of Ukraine. At present, 15 power units of four powerful NPPs with nuclear reactors of the WWER-440 and WWER-1000 type [13] are producing electricity in Ukraine: 13 Zaporizhzhya, Rivne, Khmelnitsky and South-Ukrainian NPPs (four powerful power units with RBMK-1000 reactors of the Chernobyl nuclear power plant completed their work: in 1986 – the 4th power unit, in 1991 – the second power unit, in 1996 – the first power unit, and in 2000 – the third power unit). In terms of the number of nuclear power reactors (all WWER-type «water-water reactors» or PWR type according to the IAEA classification) Ukraine ranks 5th in Europe and 10th in the world [13]. We point out that Ukraine inherited 12 power units at its nuclear power plants from the former USSR. During the independence of our country, three power units of nuclear power plants (in 1995 and 2000) were completed and put into operation, which were more than 80 % ready for the former USSR. The total electrical power of all NPPs in Ukraine in 2016 was about 130 TW. As indicated above, the contribution of Ukraine's nuclear power in 2016 to the annual energy balance amounted to about 52.3 % of the total electricity production in the country. Since autumn 2014, the generation of electricity at nuclear power plants in Ukraine has exceeded 50 % of its total output, which was due to a decrease in the capacity of domestic power engineering because of the fighting in the antiterrorist operation zone in the Donbass and the shortage of coal needed for thermal power plants (TPP) of the country [13].

Table 1 shows the main data on domestic nuclear power plants that produce electricity.

Table 1

Data on powerful nuclear reactors and power units of Ukrainian NPPs [13]

NPP name	Power unit	Reactor type	Power, MW	Fuel
Zaporizhzhya	1	WWER-1000	1000	TVEL
	2	WWER-1000	1000	TVEL
	3	WWER-1000	1000	TVEL
	4	WWER-1000	1000	TVEL
	5	WWER-1000	1000	TVEL +WH*
	6	WWER-1000	1000	TVEL
Rivne	1	WWER-440	440	TVEL
	2	WWER-440	440	TVEL
	3	WWER-1000	1000	TVEL
	4	WWER-1000	1000	TVEL
Khmelnitsky	1	WWER-1000	1000	TVEL
	2	WWER-1000	1000	TVEL
	3	WWER-1000	Conserv ated	TVEL
	4	WWER-1000	Conserv ated	TVEL
South-Ukrainian	1	WWER-1000	1000	TVEL
	2	WWER-1000	1000	TVEL
	3	WWER-1000	1000	TVEL +WH*
	4	WWER-1000	Conserv ated	TVEL

Note*. In Table 1 in the column «Fuel», the WH symbols denote the partial use of the US Westinghouse Electric Company's uranium assemblies at the same time as assemblies of TVEL, Russia [13].

From the data of Table 1 it can be seen that at present two powerful power units of Khmelnytsky (No. 3

and No. 4) and one powerful power unit (No. 4) of the South-Ukrainian NPP are suspended and all construction work on them is «frozen». I would like to hope that with the creation in a number of years in the zone of alienation of the Chernobyl nuclear power plant of the Central dry storage of SNF, a certain part of Ukraine will not turn into a large radioactive «dump» of both its own nuclear waste and nuclear waste from nuclear power plants supplied to Ukraine from Europe and North America.

Fig. 11-13 present, respectively, the general views of the South-Ukrainian NPP, the power plant hall of one of its powerful power units and one of its block control panels (BCP) [17]. This domestic nuclear power plant located on the picturesque bank of the Southern Bug river at altitude of 130 m above the level of the Baltic Sea is not threatened by strong earthquakes or tsunamis. The design of the technical facilities of this domestic nuclear power plant and its nuclear facilities provides protection from all sorts of natural disasters and shock effects of various external factors (for example, a falling aircraft) [17].

The leakage of nuclear chain reactions in uranium fuel assemblies with TVEL and, in part, with the uranium elements of the US Westinghouse Electric Company (at the 3rd power unit of the station) of each of the three operating power units with powerful WWER-1000 reactors at this nuclear power plant of Ukraine is clearly controlled with the BCP (see Fig. 13) using the CPS.

Fig. 11. General view of the fragment of the South-Ukrainian NPP with the total installed power of 3000 MW (Yuzhnoukrainsk, Mykolayiv region, Ukraine) [17]

Fig. 12. General view of the power plant hall of the power unit with the thermal power of 1000 MW of the South-Ukrainian NPP [17]

Fig. 13. General view of the block control panel (separate specific «command post») of one of the power units with thermal power of 1000 MW at the South-Ukrainian NPP [17]

Omitting and raising with the help of the CPS system special boron rods that actively absorb neutrons in the active zone of a nuclear reactor of the WWER-1000 type, the operational personnel of the power units of this NPP can slow down or accelerate the chain nuclear reactions in its uranium fuel assemblies. A highly reliable CPS system at each powerful power unit of the domestic NPP under review allows the reactor shutdown to stop the operation of the appropriate nuclear reactor («shut down» the reactor) [2, 17]. The reader needs to remember that the withdrawal of a nuclear reactor to a minimum thermal power (its stop) leads to its «poisoning».

In nuclear physics, the state of the nuclear reactor after its shutdown and «poisoning» was called «*iodine well*» [2]. This abnormal state of the reactor is characterized by the accumulation in its active zone of the short-lived radioactive isotope of xenon ${}_{54}{}^{135}\mathrm{Xe}$ (with a half-life of 9.2 hours), which in turn is the product of the radioactive decay of the intermediate isotope of iodine ${}_{53}{}^{135}\mathrm{I}$ (with a half-life of 6.8 hours) [2, 11]. Because the ${}_{54}{}^{135}\mathrm{Xe}$ xenon isotope has the largest neutron absorption cross section (up to $2.6 \cdot 10^6$ barn [1, 2]), the nuclear reactor in the «iodine well» state loses its reactivity ρ_p (it becomes negative) and, correspondingly, the thermal power. This makes it difficult to bring the reactor to its designed capacity for a time measured by (1-2) days [2, 8]. In this regard, such conditions for the nuclear reactor of nuclear power plants are undesirable. Therefore, short-term reactor shutdown at nuclear power plants and fluctuations in its output thermal power can not be made. It is allowed to stop the nuclear reactor only in the event of an emergency regime provided for by the relevant Rules (see 1.1.4).

1.5. The harmful effect of nuclear power plants on the environment. For a better understanding of the relevant environmental issue related to nuclear energy, the reader needs to be reminded that, for example, each powerful WWER-1000 reactor at domestic nuclear power plants with its full nuclear fuel loading contains 54 uranium fuel assemblies with a total mass of 41 tons at the total number of TVELs in them is 48 thousand pieces [8]. In a nuclear reactor of a modern nuclear power plant, about 300 kinds of radionuclides are formed from uranium fuel through nuclear transformations, of which

more than 30 as gas-aerosol emissions from the volume of its containment, in spite of the corresponding protective filters available in it, can enter the air atmosphere [8]. Among them, radioactive substances such as [11]: the cesium isotope $_{55}^{137}Cs$ (with a half-life of 30 years), the iodine isotope $_{53}^{131}I$ (with a half-life of 8 days), the iodine isotope $_{53}^{133}I$ (with a half-life of 20.8 hours) and the xenon isotope $_{54}^{138}Xe$ (with a half-life of 17 minutes). It should be noted that the operational regulations in force at the nuclear power plants of Ukraine and the Russian Federation permit the presence of up to 1 % of TVEL with a damaged protective zirconium-steel shell in the core of a nuclear reactor (for a two-circuit water-water power reactor of the WWER-1000 type this amounts to about 480 TVEL) [2, 8]. Through microcracks in TVEL and in the process of recovery of fuel from the reactor during their periodic replacement, radionuclides can enter the water coolant of the primary circuit and into the air under the dome of the containment. Therefore, the above-mentioned the safest powerful nuclear reactor of the WWER-1000 type forms about 40 thousand Curies per year (the activity in 1 Curie (Ci) is equal to $3.7 \cdot 10^{10}$ Becquerels (Bq) which is its unit of calculation in the SI system [1]) of gaseous radioactive emissions [8]. Most of them quickly disintegrate and are retained by protective filters of the contaminant. We note that the activity of a radioactive substance in atomic physics is the number of decays of its nuclei in one second. For comparison, it should be noted that single-circuit power reactors of the RBMK-1000 type produce radioactive gaseous emissions at NPPs by almost an order of magnitude compared to two-circuit high-power reactors of the WWER-1000 type [8]. The average daily release of radioactive gases and aerosols at Kursk NPP, still using RBMK-1000 reactors, was in the period 1981-1990 up to 750 Curies per reactor unit (with an annual radioactive indicator of such emissions reaching a level of up to 274 thousand curies) [8]. We point out that most of the radioactivity of gas-aerosol emissions at nuclear power plants is generated by short-lived radionuclides and disintegrates without much damage to the environment in a few hours or days. It should also be pointed out that, in addition to the usual gaseous emissions, nuclear power plants occasionally fill up the air atmosphere surrounding them and further pollute nearby areas with a small amount of radionuclides hazardous to human health - products of corrosion of the reactor vessel and its primary circuit, as well as fission fragments of uranium isotope nuclei $_{92}^{235}U$. These radionuclides can be traced for several tens of kilometers around any nuclear power plant.

1.6. Advantages and disadvantages of nuclear power. The main advantages of nuclear power plants over other competing powerful industrial sources of electrical and thermal energy for humanity today are [8]:

- practical independence from fuel sources due to the relatively small volume of nuclear fuel consumed by any nuclear power plant (for example, for a WWER-1000 reactor for 1.5 years of operation as part of a powerful power unit, only about 41 tons of uranium dioxide UO_2 inside fuel assemblies are required, at the same time, for example, for the Zmiev TPP with installed power of 2200 MW, two railway coal trains are required for only 1 day [7]);
- relative ecological cleanliness in comparison with TPPs (total annual emissions to the environment of such harmful substances as sulfur dioxide, nitrogen oxides, carbon oxides, hydrocarbons, aldehydes and dust per 1000 MW of installed power at pulverized coal-fired power plants are about 165 thousand tons; 1000 MW of its power consumes about 8 million tons of oxygen O_2 from the atmosphere per year, while the NPP does not consume O_2 during its operation of atmospheric oxygen at all);
- higher ability to confront energy crisis situations in society and, accordingly, to keep the volume and cost of electricity produced at a level acceptable to its consumers (increase in the world prices for coal, gas and oil increases the competitiveness of nuclear power plants).

The main disadvantages of nuclear power plants are [8]:

- severe consequences for the environment and the population from major accidents and catastrophes on powerful nuclear reactors of nuclear power plants (to exclude such situations, modern nuclear power plants are equipped with complex nuclear and radiation safety systems for their nuclear facilities with redundancy and multiple reserves of resistance of their structures to high radiation and temperature providing exclusion of reactor core meltdown even in the event of a maximum design accident);
- large expenditures of financial resources for the liquidation of technical facilities of nuclear power plants and its power units after the end of their working life by nuclear reactors (according to expert estimates, these costs amount to 20 % of the NPP construction cost, the problem of extending the life of nuclear power units is acute not only for nuclear power in Ukraine, but also of all other countries of the world using nuclear power plants to generate electricity [18]);
- the inability of maneuvering modes of operation of nuclear power reactors of nuclear power plants covering emerging «peaks» and smoothing «dips» on the graphs of their electrical load;
- higher financial costs for NPP construction compared to TPPs of similar installed power (for example, for NPPs, these costs are about USD 2300 per 1 kW of electric power of their power units, and for pulverized coal-fired TPPs – about USD 1200 per 1 kW of electric power of power units of such stations).

2. The main problems, trends and prospects for the development of nuclear power plants in the world and Ukraine. The current problems in the field of world nuclear power which are actively engaged in the industrial production of electricity and thermal energy by means of a complex and dangerous for human life technological use of atomic energy of a number of fissile radioactive materials (for example, the uranium isotope $_{92}^{235}U$ and the isotope of plutonium $_{94}^{239}Pu$ [1]), can be reduced to the following [2, 8]:

- the problem of developing and creating for NPPs of more advanced by their power efficiency, nuclear power and radiation safety powerful nuclear units with more than 35 % efficiency;
- the problem of minimizing the occurrence of accidents at nuclear power plants of nuclear power plants

which lead to serious consequences for entire regions of the country and the peoples of neighboring countries;

- the problem of SNF utilization and reprocessing from powerful nuclear reactors of nuclear power plants in the territories of those countries where these nuclear wastes were produced;
- the problem of the presence of a closed nuclear cycle in the territories of those countries that actively use powerful nuclear facilities for the industrial production of electricity and heat in large amounts commensurate with the volumes of generation of these types of energy by their heat power engineering using organic fuels (this problem is especially relevant for Ukraine which due to its limited financial resources is trying to gradually approach it from year to year using even such a difficult path as avoiding direct bonded dependence from the Russian Federation in matters of preserving and further developing its own nuclear power and diversifying supplies to domestic NPPs of uranium fuel assemblies with TVEL from other countries of the world);
- the problem of extending the life of power units of NPPs and, accordingly, the resource of nuclear reactors.

In the world nuclear power industry there is a tendency of aging of nuclear reactors. According to the IAEA, the average «age» of operating nuclear reactors at nuclear power plants in the world is 29 years [8]. The world's «oldest» existing reactor is now in Switzerland which has been working reliably for 47 years. It should be noted that the regulatory life of nuclear power units of NPPs is set by the government of a particular country on the basis of the design life of their reactors of one type or another. Usually this period is from 30 to 40 years [8]. In Ukraine and the Russian Federation, the standard operating life of most types of NPP power units is 30 years [8, 18]. It is known that extending the life of the power unit of the nuclear power plant is a very cost-effective measure. Thus, with a financial cost to extend the life of a powerful nuclear «water-water reactor» of the WWER-1000 type (PWR type according to the IAEA scale) for about 20 years at about USD 90 million, the possible profit from its operation at a NPP for such an additional period may to make about USD 1.3 billion [8, 19]. In Ukraine and the Russian Federation, the operation of two-loop water-water nuclear reactors of the first-generation of WWER type and single-loop nuclear reactors of the RBMK type has already been extended to 45 years, and nuclear reactors of the WWER type of the second generation up to 55 years [2, 8, 19].

In conditions of a relatively fast approaching energy «hunger» in the world and the depletion of hydrocarbon fuel in the earth's crust (according to expert estimates of hydrocarbons for TPPs, the world will suffice only for the next 50-100 years [6]) and the practical inexhaustibility of radioactive uranium nuclear power has real prospects for its further development. Alternative energy (wind energy, solar energy, hydrogen power, geothermal energy, biogas power and small hydropower) has not yet been able to seriously compete with traditional energy (heat power, nuclear power and hydropower). Taking into account a number of the above obvious advantages of nuclear power over other well-known types of modern technologies for generating electricity and heat, at present, despite the existing limitation of peaceful use of atomic energy in several countries of the world (for example, in Italy, Germany, Sweden and the USA [20]), we can reasonably say that in the near future, mankind will continue to actively use the possibilities of nuclear energy for the purpose of generating electricity and heat on an industrial scale.

Conclusions. The presented brief analytical scientific and technical review of the retrospective, current state, major achievements, trends and prospects for the development of world nuclear power indicates a tremendous breakthrough in knowledge of mankind about the structure of the microworld of matter and its limited possibilities for peaceful use of the inexhaustible reserves of its intranuclear energy. The world nuclear power is now on the difficult and complex scientific and technical way of its «growing up» (it was only a little more than 60 years since the world's first nuclear power plant was put into operation) and the demonstration of the energy potential of this new for the people progressive industrial technology for obtaining electrical and thermal energy in huge volumes.

Nuclear power, like any other progressive industrial technology, has its own «pluses» and «minuses» for human society and earthly nature in general. Despite its latent radiation danger, with a mortal threat to everything living and existent on Earth, more than once in the modern history of the development of human civilization «bursting out» with the infliction of large human casualties and financial losses on its society, nuclear power engineering with several hundred powerful nuclear power units at the NPPs around the world occupies serious advanced positions in the volumes of annual production of electrical and thermal energy. In Ukraine, these volumes of electricity since 2014 for a number of objective reasons account for at least 50 % of the country's annual energy balance.

Taking into account the limited reserves of organic hydrocarbon fuel for TPPs on the Earth and the practical inexhaustibility of natural radioactive uranium (nuclear) fuel for NPPs on our planet, the world nuclear power has all the possibilities for its further development aimed at meeting the ever growing needs of human society for electricity and thermal energy.

REFERENCES

1. Kuz'michev V.E. *Zakony i formuly fiziki* [Laws and formulas of physics]. Kiev, Naukova Dumka Publ., 1989. 864 p. (Rus).

2. Available at: https://en.wikipedia.org/wiki/Nuclear_reactor (accessed 09 August 2017).

3. Baranov M.I. *Izbrannye voprosy elektrofiziki: Monografija v 3-h tomah. Tom 1: Elektrofizika i vydajushhiesja fiziki mira* [Selected topics electrophysics: Monographs in 3 vols. Vol.1: Electrophysics and outstanding physics of the world]. Kharkov, NTU «KhPI» Publ., 2008. 252 p. (Rus).

4. Baranov M.I. *Antologiia vydaiushchikhsia dostizhenii v nauke i tekhnike: Monografiia v 3-h tomakh. Tom 1.* [An anthology of outstanding achievements in science and technology: Monographs in 3 vols. Vol.1]. Kharkov, NTMT Publ., 2011. 311 p. (Rus).

5. Baranov M.I. An anthology of the distinguished achievements in science and technique. Part 40: The scientific opening of the method of explosive implosion for the obtaining

above critical mass of nuclear charge and Ukrainian «track» in the «Manhattan» American atomic project. *Electrical engineering & electromechanics*, 2017, no.5, pp. 3-13. **doi: 10.20998/2074-272X.2017.5.01.**

6. Baranov M.I. *Antologija vydajushhihsja dostizhenij v nauke i tehnike: Monografija v 3-h tomah. Tom 3* [An anthology of the distinguished achievements in science and technique: Monograph in 3 volumes. Volume 3]. Kharkiv, PhPB Panov A.N. Publ., 2016. 415 p. (Rus).

7. Available at: http://dic.academic.ru/dic.nsf/bse/156142/Атомная_электростанция (accessed 25 May 2017). (Rus).

8. Available at: https://en.wikipedia.org/wiki/Nuclear_power_plant (accessed 19 September 2017).

9. Available at: https://www.google.ru/search?q=аэс+принцип+работы&newwindow (accessed 12 October 2016). (Rus).

10. Frish O. *Niels Bohr*. New York, Publ. S. Rozental, 1967. 137 p.

11. Levin V.E. *Jadernaja fizika i jadernye reaktory* [Nuclear physics and nuclear reactors]. Moscow, Atomizdat Publ., 1979. 420 p. (Rus).

12. Andrushechko S.A., Aforov A.M., Vasilyev B.Yu., Generalov V.N., Kosourov K.B., Semchenkov Yu.M., Ukraintsev V.F. *AES s reaktorom tipa WWER-1000. Ot fizicheskih osnov ekspluatacii do evoljucii proekta* [AES with a reactor of the WWER-1000 type. From the physical foundations of exploitation to the evolution of the project]. Moscow, Logos Publ., 2010. 604 p. (Rus).

13. Available at: https://en.wikipedia.org/wiki/Nuclear_power_in_Ukraine (accessed 20 August 2016).

14. Available at: http://energ2010.ru/Stati/Elektrostanciya/AES/Bezopasnost_aes.html (accessed 10 June 2016). (Rus).

15. Available at: https://ria.ru/eco/20090426/169135271.html (accessed 18 November 2016). (Rus).

16. Available at: https://ru.wikipedia.org/wiki/Аварийная_защита_ядерного_реактора (accessed 12 March 2016). (Rus).

17. Available at: https://www.segodnya.ua/ukraine/rabotniki-juzhno-ukrainckoj-aec-nash-reaktor-vyderzhit-dazhe-padenie-camoleta.html (accessed 15 May 2017). (Rus).

18. Domashev E.D., Zenyuk A.Yu., Reisig V.A., Kolesnichenko Yu.M. Some approaches to the solution of the problem of prolonging the resource of power units of Ukrainian AES. *Industrial heat engineering*, 2001, vol.23, no.6, pp. 108-112. (Rus).

19. Favorskiy O.N. On the energy industry of Russia in the next 20-30 years. *Herald of the Russian Academy of Sciences*, 2007, vol.77, no.2, pp.121-127. (Rus).

20. Available at: http://economics.studio/kniga-ekonomika-prirodopolzovaniya/plyusyi-minusyi-atomnoy-energetiki-76786.html (accessed 14 April 2017). (Rus).

Received 19.12.2017

M.I. Baranov, Doctor of Technical Science, Chief Researcher,
Scientific-&-Research Planning-&-Design Institute «Molniya»
National Technical University «Kharkiv Polytechnic Institute»,
47, Shevchenko Str., Kharkiv, 61013, Ukraine,
phone +380 57 7076841,
e-mail: baranovmi@kpi.kharkov.ua

How to cite this article:
Baranov M.I. An anthology of the distinguished achievements in science and technique. Part 44: Traditional power engineering. Nuclear power stations: retrospective view, state and prospects of their development. *Electrical engineering & electromechanics*, 2018, no.3, pp. 3-16. **doi: 10.20998/2074-272X.2018.3.01.**

UDC 621.313.333 **doi: 10.20998/2074-272X.2018.3.02**

K.M. Vasyliv

REGULARITIES OF ELECTROMAGNETIC PROCESSES OF A CONTACTLESS EXCITATION SYSTEM OF AN ASYNCHRONIZED GENERATOR BASED ON A CASCADE THREE-PHASE-THREE-PHASE VOLTAGE MODULATOR IN A SINGLE-STAR CIRCUIT

The regularities of electromagnetic processes occurring in a noncontact excitation system of an asynchronized generator based on a cascade three-phase - three-phase voltage modulator in a single-star circuit for the possibility of expanding the range of a two-zone slip of a generator are established. A method for correcting the parameters of the machines' rotors of modulator and generator is proposed which makes it possible to stabilize the operation of the switch for the slip range from minus one to plus five tenths with maintaining the performance of the asynchronized generator. References 3, figures 8.
Key words: **asynchronized generator, voltage modulator, switch, contactless excitation system, slip.**

Установлено закономерности электромагнитных процессов, протекающих в бесконтактной системе возбуждения асинхронизированного генератора на базе каскадного трехфазно-трехфазного модулятора напряжения по схеме в одну звезду на предмет возможности расширения диапазона двухзонного скольжения генератора. Предложено способ корректировки параметров роторов машин модулятора и генератора, позволяющий стабилизировать работу коммутатора для диапазона скольжения от минус единицы до плюс пяти десятых с сохранением работоспособности асинхронизированного генератора. Библ. 3, рис. 8.
Ключевые слова: **асинхронизированный генератор, модулятор напряжения, коммутатор, бесконтактная система возбуждения, скольжение.**

Introduction. The basic structural elements of the current stationary power systems are thermal and nuclear power plants. At the same time, it is practicable to use a fairly large number of different autonomous electric power plants (AEPPs), both in industry and in other sectors, in particular, in transport and agricultural complex. There is a need for AEPPs also at the trenches of transport of organic energy (oil and gas pipelines). Promising is the use of wind power plants which can work in parallel with the stationary power system, and in the autonomous mode. At the moment, AEPPs have become a significant part of the generation and consumption of electrical energy in general. Therefore, attention to them, from the point of view of scientific research both in the theoretical and practical aspects in order to improve them, is sufficiently argued and logical.

For consumers of electrical energy, it is necessary to have not only reliable power supply, but also to receive high-quality electric power, one of the most important indications of which is the frequency of voltage. The stability of the voltage frequency is principally unnecessary both for stationary power systems and for autonomous power supply sources (APSS) because reducing the frequency of voltage in stationary power systems leads to loss of stability of their work and, consequently, to collapse.

For APSS, certain features are characteristic of the most significant of which it is logical to include such. The first is the probability of the necessity of operation in the mode of limiting loads which makes an actual problem of the reliability of their operation in general. The second peculiarity of such installations is the substantial volatility and wide range of changes in the frequency of the rotation of the drive of the autonomous generator, for example, wind turbine installations (WTI), which causes another problem of the volatility of the voltage frequency.

The analysis of scientific literature and practical solutions shows that these complex and actual problems can be effectively solved by the use in the APSS of asynchronized generators (ASGs) with contactless valve excitation system (CLVES) based on a cascade voltage modulator (CVM) [3]. From the point of view of the circuit decision, asynchronous generators with CLVES based on CVM can be implemented in many variants (of the order of 16 circuits). All such generators operate according to the same principle but each circuit decision of the electric circuit of the modulator, the switch and the generator itself introduces its specific features from the point of view of the physics of processes. Therefore, in scientific research, it is necessary to analyze each of these circuits separately. Proceeding from this, the object of the study in the paper is the contactless valve system of excitation of the asynchronized generator on the basis of a cascade three-phase three-phase voltage modulator (C T-T VM) according to the circuit of single star. The circuit of a power electric circuit of such a system of excitation is shown in Fig. 1. From this figure it can be seen that C T-T VM consists of two asynchronous machines AM1 and AM2, phase windings of which rotors are split into three branches and are interconnected one-to-one by intersecting bonds, and at the input split phase segments can have a potential combined connection or can be connected to a single joint node. The options of these connections are determined by the positions of the key K. When the key K is open (identifying its state as K=1) this is the first option, and when the key K is locked (K=2) this is the second one. Stator windings of modulator machines AM1 and AM2 are powered by two three-phase power sources E1 and E2 which have a mutually opposite sequence of phases. Here it is a priori assumed that such sources are accumulator batteries with controlled voltage inverters.

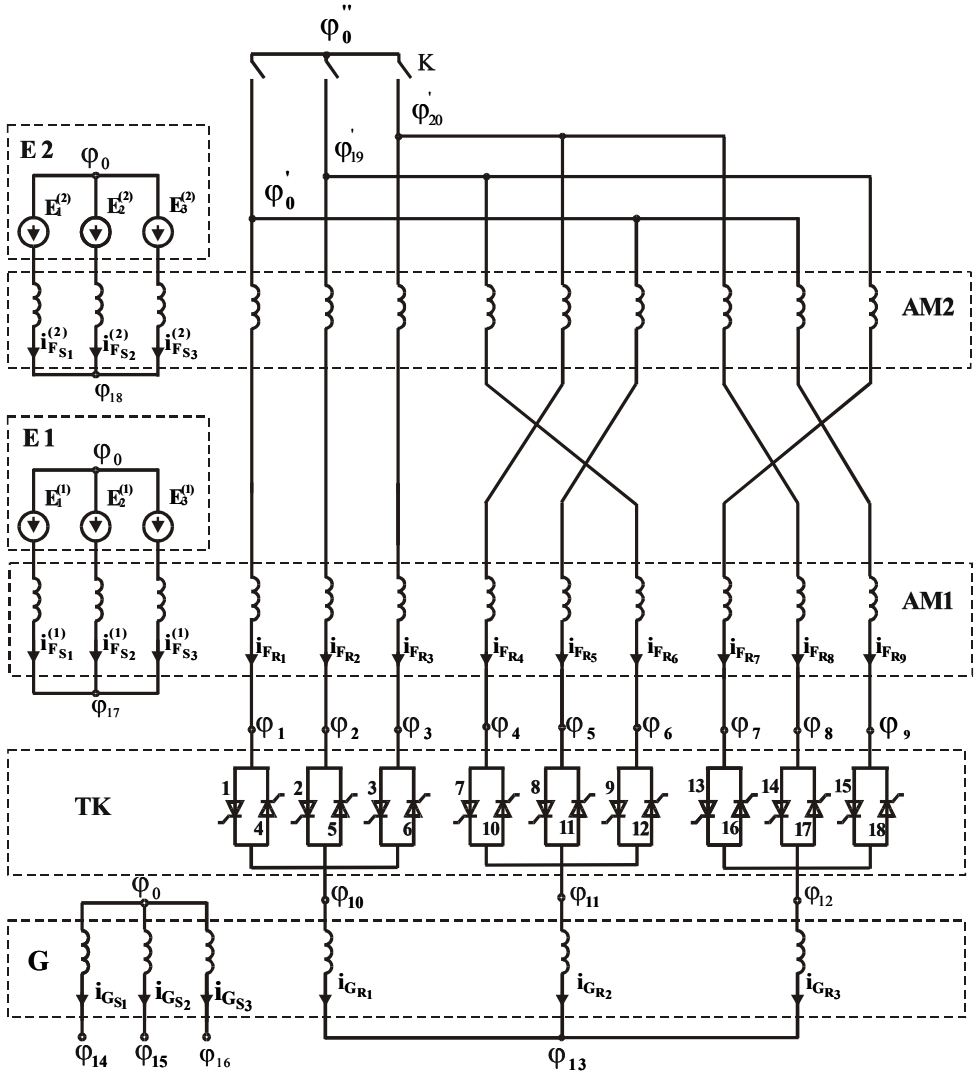

Fig. 1. Power electric circuit of asynchronized generator

The rest of the structural elements of the circuit (Fig. 1) include: TK – a thyristor switch of a cycloconverter type with natural switching as which a direct thyristor frequency converter (DTFC) serves, G – asynchronized generator as which as a three-phase asynchronous machine with a phase rotor, the coils of which the rotor phases are connected in a star serves. All other indications on this circuit are generally accepted: by the letters *E*, *φ* and *i* the electromotive forces, the electric potentials in the nodes, and the currents of the electric circuit branches are indicated. By the letters *F*, *G* in the lower indices the affiliation of the coordinates (of currents, voltages, etc.) to the modulator machines and ASG are indicated, and by the letters *S*, *R* in the lower indices *i* the affiliation of the coordinates to stator and rotor of electric machines are indicated, respectively. Thyristors of DTFC are numbered. Numbers 1 and 2 in brackets in the upper indices indicate the relevance to the first E1 and the second E2 sources, respectively.

In the opinion of the author, in order to facilitate the adoption of the main provisions of the paper, it is logical to briefly describe the principle of the operation of the ASG of this type. It is based on the fact that the voltage modulator by the way of adding the voltages and frequencies of the phase branches of the rotors of the machines of the modulator forms the total voltage of the modulus form, the filling frequency of which is proportional to the frequency of rotation of the rotors of the modulator machines and the number of their pairs of poles (rotors of AM1 and AM2 are placed on one shaft with ASG), and the modulation frequency is determined by the frequency of two-zone slip. The linearly coupled winding of the rotors of the modulator, the cycloconverter type switch decodes the modulated voltage resulting in the formation of a three-phase system at its output (on the winding of the generator's rotor) slip times. This provides a stable time for rotating the magnetic field of the generator in relation to its stator winding, which, in turn, forms the frequency of the generator voltage which is equal to the frequency of the supply networks of E1 and E2. Thus, theoretically, the frequency of the ASG voltage should be equal to the frequency of the supply networks of E1 and E2 of the asynchronous machines of the modulator AM1 and AM2 and not to depend on the rotational speed of the ASG rotor.

Analysis of publications and the goal of investigations. The ideology of generators of a stable frequency (GSF) with a contactless valve excitation system based on the CVM was introduced in [3]. On the coincidence of the issues on scientific research and

development of automotive electrical power systems (AEPS) on the basis of ASG with CLVES a rather narrow circle of scientists and engineers is working, and therefore the essential share of publications aimed at researching these systems of power supply through mathematical modeling belongs to the author of this paper. The appearance of a number of publications aimed at the development of methods and mathematical models as well as the study of the laws of the course of electromagnetic and electromechanical processes occurring in the above-mentioned AEPS is due to the presence in them of various types of elements – asynchronous machines and DTFC on a number of circuits of their power electrically circles as well as the presence of a control system of the switch and automatic control system of individual coordinates (in particular, voltage) which causes the complexity of electromagnetic and electromechanical processes which occur in these AEPSs.

One of the main scientific works related to the research of the AEPS on the basis of ASG with CLVES is the publication [1]. It is aimed at the development of mathematical models and corresponding software complexes as a means for studying the regularities of the flow of electromagnetic and electromechanical processes occurring in AEPS on the basis of ASG with CLVES in three-phase - three-phase circuit of the voltage modulator. Mathematical models and corresponding software complexes allow to study electromagnetic and electromechanical processes that occur in the auto-nominal system of electric power supply during operation of ASG on typical load such as asynchronous motors, active-inductive and active-inductive-capacitive loads.

In the publications which are the researches of electromagnetic and electromechanical processes in the AEPS on the basis of ASG with CLVES, it is considered that asynchronous machines of the voltage modulator and the generator have a typical design. Proceeding from this, the two-zone slip diapason which ensures the normal operation of the AEPS is $S = -0.06 \div +0.06$. This indicates that in general, AEPS on the basis of ASG with CLVES is operational. But such a range of slip is being developed too narrowly to argue about the feasibility of practical application of such asynchronous generators in the AEPS. Therefore, the research proceeds with the goal of achieving the expansion of the slip diapason to the limits that would allow the practical use of this class of ASG, even in such electric power plants as WTI.

Taking into account the fact that the performance of ASG with CLVES is largely determined by the proper operation of the switch, all attention should be concentrated on the processes occurring precisely in the CLVES and its separate structural elements which include the modulator machines, the thyristor switch itself and the excitation winding of the ASG (its rotor winding).

The first piece aimed at solving this problem was the publication [2] concerning the contactless excitation system of ASG on the basis of a cascade three-phase - three-phase voltage modulator in the circuit of two stars (when each of the phases of the rotor winding of the generator is split into two branches, and the 6 branches thus formed are connected in two separate three-phase stars). In [2] one modulator circuit is considered in which split phases of rotors of machines of the modulator on the input are connected to a single joint node (for the circuit of Fig. 1 this is K = 2). According to the research [2], it was suggested that the slip range may be expanded from $S = -0.06$ to $S = +0.2$ by increasing the ratio of the number of turns of the stator winding to the number of turns of the rotor winding of the modulator machines.

Taking into account the specificity of each of the circuits of the thyristor switch and modulator, it is clearly evident that the practical need to perform a similar study of the contactless switch excitation system of the ASG on the basis of a three-phase - three-phase cascade voltage modulator according to the circuit of single star which is characterized by a doubly smaller number of thyristors than a two-star circuit which qualifies as an advantage in terms of practical application.

Thus, the purpose of the study is to establish the laws of the course of electromagnetic processes that occur in the contactless valve system of excitation of ASG on the basis of a cascade three-phase - three-phase voltage modulator in the circuit of single star for the possibility of expanding the working range of dual-zone slip.

Presentation of main material. The results of preliminary investigations [1, 2] indicate that the operation of the switch is significantly determined by the ratio of the parameters of windings of stators and rotors of the modulator machines. The huge values of the parameters of the rotors causes the inertia of the electromagnetic processes in the circuit of the modulator and generator exciter which results in disturbed normal operation of the switch which does not permit to form the three-phase voltage of the slip frequency in the winding of the rotor of the generator, and therefore, to form the voltage of the stable frequency in the stator winding of the ASG.

In order to create favorable conditions for the operation of the switch based on the positive result of the investigation obtained in [2], it is proposed to reduce the inductive resistances of rotor windings not only of the modulator machines but also of the generator by increasing the ratio between the number of turns of the stator and rotor windings (that is, an increase in their coefficients of transformation). The verification of the effect of changing the coefficients of the transformer-mass on the efficiency of the CLVES of the asynchronized generator is made by analyzing the functions of the currents and voltages of the phase branches of the rotors of the modulator and generator machines. The dependences of currents and voltages are obtained by calculating the electromagnetic processes of the CLVES of Fig. 1 using the mathematical model and software developed in [1]. Simulation is used for ASG of 100 kW power, the input data of which have the following values: $L_{G_m} = 0.1$ H – the operating inductance (from the stator side); $L_{G_S} = 0.005$ H – the inductance of scattering of the stator; $L_{G_R} = 0.005$ H – the reduced to the stator winding inductance of scattering of the winding of the rotor; $K_{G_i} = 10$ – the coefficient of transformation of the generator; $P_{G0} = 2$ – the number of pairs of poles of

the generator; $R_{GS} = 0.01$ Ω – the active resistance of the phases of the stator winding; $R_{G_R} = 0.05$ Ω – the active resistance of the rotor winding phases.

In order to avoid overloading the volume of input data, for modulator machines we present only the most important data, which include: $K_i^{(1)} = 20$ – the coefficient of transformation of AM1; $P_0^{(1)} = 2$ – the number of pairs of poles of AM1; $K_i^{(2)} = 20$ – the coefficient of transformation of AM2; $P_0^{(2)} = 6$ – the number of pairs of pole of AM2.

It is fundamentally important to note that, in accordance with the theory of ASG with CLVES on the basis of a cascade voltage modulator [3], to form the modulated voltage of the slip frequency at the output of the modulator, the ratio of the number of pairs of poles of the generator and the modulator machines must satisfy the following condition:

$$(P_0^{(1)} + P_0^{(2)})/2 = 2 \cdot P_{G0}. \qquad (1)$$

The above numerical values of the number of pairs of poles of the generator and the asynchronous machines of the modulator AM1 and AM2 satisfy the condition (1).

According to [2], the maximum slip value at which it was possible to achieve the performance of ASG with CLVES on the basis of CVM is 0.2 (S = +0.2). Therefore, for a benchmark to study the operation of ASG with a contactless valve system of excitation according to the circuit into a single star, we take precisely this value of slip. Proceeding from this, at the beginning of the study, we consider the calculating dependences of the voltages and currents of the phase branches of the rotor windings of the modulator machine and the phase currents of the rotor winding of the generator for two values of the double-zone slip S = –0.2 and S = +0.2.

Fig. 2 shows the calculated dependences on e time of voltages of the phase branches of modulator machine rotors.

In particular, Fig. 2,*a* illustrates the voltages of the first three split phase branches of the rotors of the modulator machines $u_{F_{R1}}, u_{F_{R2}}, u_{F_{R3}}$ (see Fig. 1). Each of these curves is formed by the sum of the electromotive forces of the interconnected split phase branches of the machine rotors of the modulator AM1 and AM2 which, in turn, are induced separately for each of machines AM1 and AM2 by winding currents of their stators. Similarly, Fig. 2,*b* illustrates the voltages $u_{F_{R4}}, u_{F_{R5}}, u_{F_{R6}}$ of the second three, and Fig. 2,*c* – the voltages $u_{F_{R7}}, u_{F_{R8}}, u_{F_{R9}}$ of the third three split phase branches of the rotors of the modulator machines (Fig. 1).

From Fig. 2 it can be seen that the voltages of the successively connected phase branches of the rotors of the cascade modulator machines have a modulated form with a sliding frequency (here the slip is S = +0.2) which corresponds to the period $T = 0.1$ s. At the same time, each of the three voltage systems, depicted in Fig. 2,*a*-*c* are shifted in phase by a $2\pi/3$ angle over the slip frequency which is achieved by cross-connecting the split phase branches of the modulator machines (see Fig. 1). Modulated voltages with the slip frequency give reason to expect the formation of a system of three-phase voltages of the slip frequency in the rotor winding of the generator. The fact of the mutual displacement of the voltages of all three groups of phase branches with a slip frequency of $2\pi/3$ provides an appropriate shift of phase voltages and currents of the rotor winding of the generator.

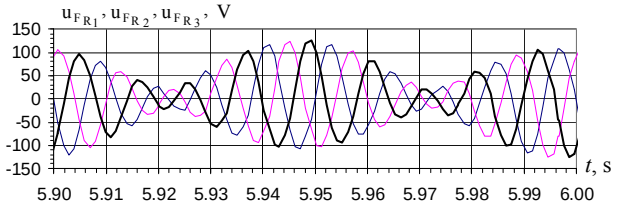

a

($u_{F_{R1}}, u_{F_{R2}}, u_{F_{R3}}$ – the voltages of I, II, III phase branches)

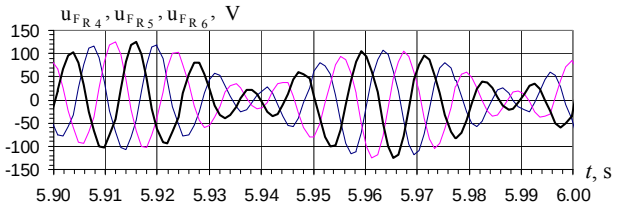

b

($u_{F_{R4}}, u_{F_{R5}}, u_{F_{R6}}$ – the voltages of IV, V, VI phase branches)

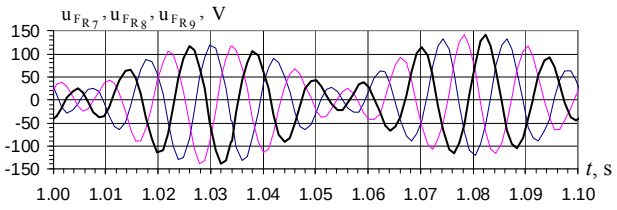

c

($u_{F_{R7}}, u_{F_{R8}}, u_{F_{R9}}$ – the voltages of VII, VIII, IX phase branches)

Fig. 2. Calculated dependencies on time of instantaneous voltages of the phase branches of the rotors of the modulator machines

For a more complete understanding of the electromagnetic processes occurring in the ASG excitation system, consider the curves of the instantaneous values of the phase currents of the rotors of the modulator machines. They are pictured in Fig. 3.

A positive half-wave of currents in Fig. 3,*a* is formed by thyristors 1, 2, 3, and negative – by thyristors 4, 5, 6 (see the circuit in Fig. 1). Similarly, the currents of two other groups of phase branches of the Fig. 3,*b* and Fig, 3,*c* are formed, respectively.

In the context of the analysis of the processes occurring in the CLVES of the ASG, the essential characteristic of the phase voltages and currents of the generator rotor windings is of crucial importance because in order to obtain a stable voltage frequency of the winding of the stator of the generator, in the generator rotor winding there should be a three-phase system of currents of slip frequency. Therefore, consider the phase currents of the winding of the rotor of the ASG.

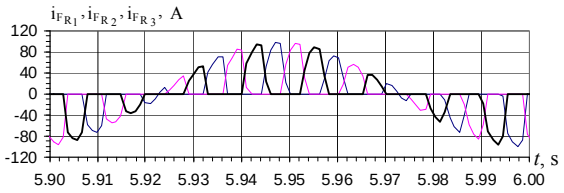

a

($i_{F_{R1}}$, $i_{F_{R2}}$, $i_{F_{R3}}$ – the currents of I, II, III phase branches)

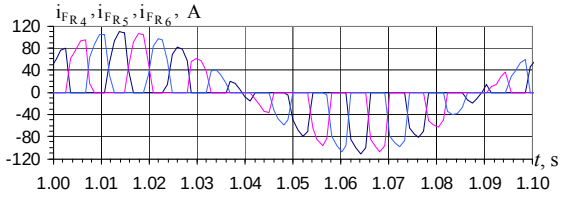

b

($i_{G_{R4}}, i_{G_{R5}}, i_{G_{R6}}$ – the currents of IV, V, VI phase branches)

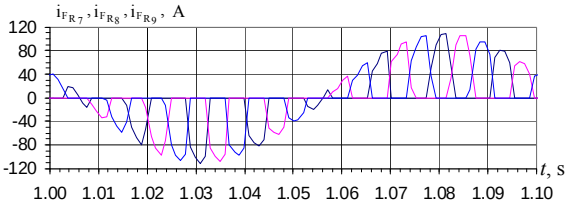

c

($i_{G_{R7}}, i_{G_{R8}}, i_{G_{R9}}$ – the currents of VII, VIII, IX phase branches)

Fig. 3. Calculated dependencies on time of instantaneous currents of the phase branches of the rotors of the modulator machines

Fig. 4 depicts the calculated dependences of the instantaneous values of the phase currents of the rotor winding of the asynchronized generator for slip S = +0.2. From this figure it is clear that three-phase currents are formed in the winding of the ASG rotor, the shape of which is close to the sinusoidal with slip frequency. The period of these currents corresponds the slip frequency (S = +0.2) and is T = 0.1 s. This shape of currents in the winding of the ASG rotor gives rise to the expectation that the frequency of the phase voltages of the stator winding will be equal to the voltage frequency in the stator windings of the modulator machines.

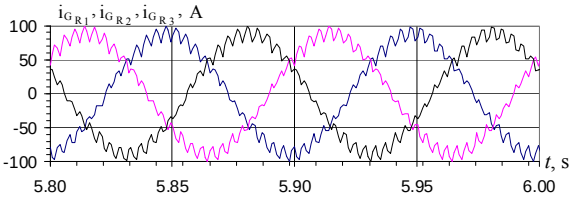

Fig. 4. Calculated dependencies of the ASG rotor phase currents $i_{G_{R1}}, i_{G_{R2}}, i_{G_{R3}}$

The above simulation results, as well as the results of research which are not presented here, give grounds to assert that for ASG slip which is equal to plus two tenths (S = +0.2), its CLVES is operational and provides the necessary frequency of the winding voltage of the stator of the generator which is the subject of research in this publication. And the analysis of the voltage curves of the stator windings of the generator forms the subject of separate studies on the fact that the shape of these curves is influenced by other factors which are not sufficiently thoroughly studied yet but from already existing research results it is known that they change the harmonic spectrum of phase voltages of the generator.

To determine the extreme limit of the operating range of the positive slip zone of the asynchronized generator with contactless valve system, it is necessary to have information on the nature of the currents of the rotor winding of the generator for other larger values of slip. Therefore, below we give the calculating dependence of these currents for a series of values of positive slip. The shape of these curves will provide information for understanding the laws of the flow of electromagnetic processes that occur in the contactless valve system of the asynchronized generator excitation and, as a result, will give a basis for the determination extreme allowable operating slip in its positive area.

Fig. 5 shows the calculated dependencies of the phase currents of the generator rotor winding for slip S = +0.5.

From Fig. 5 it is seen that the curves of the phase currents of the rotor of the generator have a quasi-sinusoidal shape with a period of the fundamental harmonic equal to 0.04 (T=0.04) s corresponding to the slip frequency F_k=25 Hz (F_k=50·S=50·0.5=25). This shape of the curves of phase currents with a clearly defined frequency also ensures the stability of the generator voltage frequency, and therefore, for slip S =+ 0.5, the CLVES of the ASG is operational.

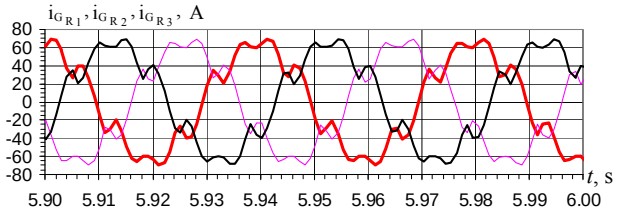

Fig. 5. ASG rotor phase currents $i_{G_{R1}}$, $i_{G_{R2}}$, $i_{G_{R3}}$ for slip S = +0.5

A further increase in slip in the positive region leads to a change in the shape of the curves of phase currents, as can be seen from Fig. 6 and Fig. 7. The first one depicts the calculated dependences of the phase currents of the rotor winding of the generator for slip S = +0.9, and on the second one – for slip S = +0.95. From these figures it is evident that phase currents in the shape are not sinusoidal. Instead, there is a tendency towards the formation of a voltage system of modulated shape, Therefore, the conclusion is unambiguous, its essence is that for a positive slip whose value exceeds S = +0.5, CLVES of the ASG loses efficiency. Thus, the extreme limit of the positive range of the operating slip of the ASG is slip with the value S = +0.5.

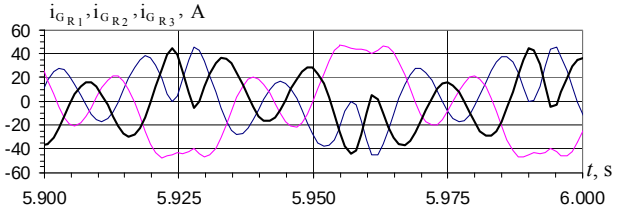

Fig. 6. ASG rotor phase currents $i_{G_{R1}}$, $i_{G_{R2}}$, $i_{G_{R3}}$ for slip S = +0.9

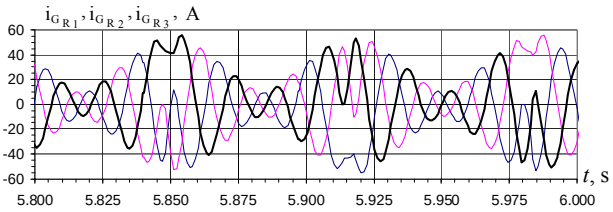

Fig. 7. ASG rotor phase currents $i_{G_{R1}}$, $i_{G_{R2}}$, $i_{G_{R3}}$ for slip S = +0.95

As already noted, the ASG with the CLVES on the basis of the cascade voltage modulator can operate in the mode of two-zone slip because the excitation here is executed from the side of the rotor, as in a synchronous machine. Therefore, it is fundamentally important to find out its functional possibilities for a negative slip range. To this end, research has also been carried out for a number of values of negative slip.

Fig. 8 depicts the calculated dependencies of phase currents of the rotor of the generator for the three values of slip: S = –0.2; S = –0.8 and S = –1.0. From Fig. 8 it is clearly visible that the phase currents of the rotor of the ASG have a shape close to the sinusoid with the frequency of the fundamental harmonic which is equal to the slip frequency. This gives grounds to argue that unlike the positive area of slip, in the negative one the CLVES is operable in its entire range from S = 0 to S = –1.0.

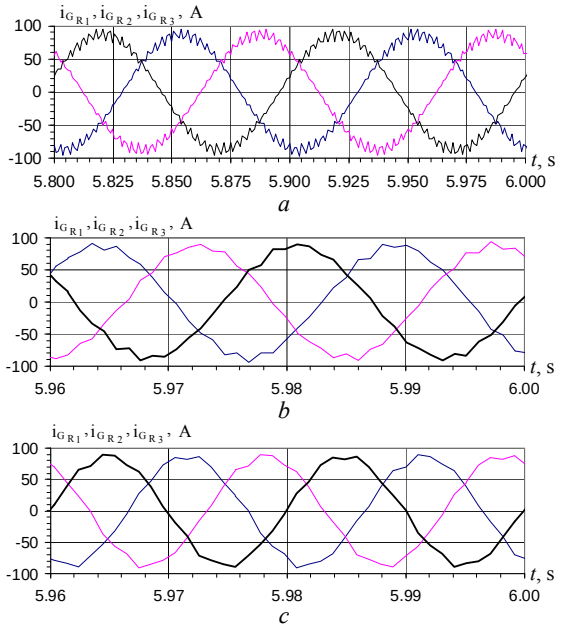

Fig. 8. ASG rotor phase currents ACГ $i_{G_{R1}}$, $i_{G_{R2}}$, $i_{G_{R3}}$ (*a* – for S = –0.2; *b* – for S = –0.8; *c* – for S = –1.0)

At this stage, with the help of the mathematical model developed in [1] and the corresponding program code, an analysis of the electromagnetic processes is carried out in the contactless valve excitation system of the ASG on the basis of a cascade three-phase - three-phase voltage modulator according to the circuit of a single star and established the laws of their course on the effect of the two-zone slip on the performance of the asynchronized generator.

In the context of the prospect of research in order to further develop the theory of asynchronized generators of this type, it seems necessary to perform an analysis of the electromagnetic processes occurring in such generators for the effect of the two-zone slip on the voltage quality of the ASG and on the frequency criterion, and by the criterion of the harmonic spectrum. In addition, the goal is to carry out similar studies for a modulator circuit with a common connection of split phase phase branches of the rotors of the modular machines when the key K is locked (Fig. 1) because here the circuit is considered with a potential combined connection when the key K is open.

Conclusions.

1. The narrow range of operating dual-zone slip of an asynchronized generator with contactless valve excitation system based on a cascade voltage modulator under the circuit of a single star which at the time of recent research was ±0.06 does not allow the practical application of such generators as autonomous sources of electric power supply.

2. In order to study the possibilities of expanding the range of two-zone slip of the ASG with CLVES, the study of electromagnetic processes occurring in this excitation system was performed. Based on the research carried out by mathematical modeling with the help of the developed by the author mathematical models and software complex, the laws of the flow of these processes depending on the value of the two-zone slip are established.

3. By changing the parameters of the rotors of the machines of the modulator and ASG due to an increase in the ratio of the number of turns of the stator winding to the winding of the rotor of the asynchronous machines of the modulator and the generator, an essentially expansion of the slip range of the asynchronized generator was achieved.

4. The area of negative slip is increased to the value S = –1, and the area of the positive one up to S = +0.5.

5. Extension of the range of working slip to the specified limits creates real opportunities for the practical application of generators of this class in autonomous power supply systems with a wide range of changes in the rotational speed of the drive.

REFERENCES

1. Vasyliv K.M. Mathematical model of dynamic processes of an autonomous electric power system on the basis of contactless asynchronized generator with a three-phase-three-phase cascade modulated exciter. *Technical electrodynamics*, 2004, no.5, pp. 50-55. (Ukr).

2. Vasyliv K.M. Regularities of electromagnetic processes in the contactless excitation system of an asynchronous generator following a two-star scheme based on a threephase-threephase voltage modulator. *Bulletin of NTU «KhPI»*, 2016, no.32(1204), pp. 48-52. (Ukr).

3. Galinovskiy A.M. Non-contact asynchronized generator with a modulated frequency converter. *Trudy I Mezhdunarodnoi (III Vserossiiskoi) konferentsii po Elektromekhanotronike* [Proceedings of the 1st International (III All-Russian) Conference on Electromechanotronics]. St. Petersburg, 1997, pp. 182-192. (Rus).

Received 25.02.2018

K.M. Vasyliv, Doctor of Technical Science, Professor,
Lviv Polytechnic National University,
28a, S. Bandera Str., Lviv, 79013, Ukraine,
phone +38 032 2226403,
e-mail: karl.vasyliv@gmail.com

How to cite this article:
Vasyliv K.M. Regularities of electromagnetic processes of a contactless excitation system of an asynchronized generator based on a cascade three-phase-three-phase voltage modulator in a single-star circuit. *Electrical engineering & electromechanics*, 2018, no.3, pp. 17-22. **doi: 10.20998/2074-272X.2018.3.02.**

UDC 621.771.06:233.2 **doi: 10.20998/2074-272X.2018.3.03**

I.N. Zadorozhniaia, N.A. Zadorozhniy

SYNTHESIS OF A TWO-MASS ELECTRIC DRIVE WITH AN ASTATIC SYSTEM OF SUBORDINATE REGULATION AT THE ACTION OF VARIABLE FRICTION FORCES

Purpose. *The solution of actual problem of active suppression of resilient electromechanical vibrations in an electric drive with the astatic system of automatic control is presented.* ***Methodology.*** *For research of damping properties of electrical drive according to a flow diagram from transmission functions on regulation and indignation a characteristic polynomial is got in the rationed form of parameters that takes into account the physical phenomena and sets intercommunications of parameters in the electromechanical system. As a result of it a characteristic polynomial at a successive dynamic decoupling appears separate interactive electromagnetic and mechanical subsystems. Thus, electromechanical interaction physically means complete extraction of energy of vibrations from a mechanical subsystem in electromagnetic with simultaneous transformation for minimum time. An electric drive for the case of realization of processes of electromechanical interaction is the dynamic extinguisher of vibrations.* ***Results.*** *The active resilient mechanical oscillation damping comes true due to optimization of dynamic inflexibility of mechanical description of electrical drive and as a result the required degree of stability is provided at minimum vibration and high exactness of working off indignations on loading.* ***Originality.*** *For the first time an electrical drive with the astatic system of automatic control at the action of variable forces of friction for the offered optimal parameters of dynamic inflexibility of mechanical description effectively damps vibrations. The synthesis of parameters of regulators according to correlations allowed to realize the maximum indexes of character of attenuation processes at a zero static error.* ***Practical value.*** *The synthesis method is approved in industrial conditions during the adjustment and modernization of the machine tool and is recommended for setting up automatic control systems for the operating and newly designed electric drives of technological machines.* References 13, figures 2.

Key words: **electromechanical system, damping, electric drive, interaction, regulation, speed controller, synthesis, variable friction forces.**

Получил дальнейшее развитие метод синтеза электропривода с астатической системой подчиненного регулирования при действии переменных сил трения с активным демпфированием упругих механических колебаний, что достигается выбором определенного соотношения динамических параметров. Показано, что параметры в электромеханических системах находятся во взаимосвязи, а реализация расчетных соотношений для регулятора скорости при оптимизации основана на компенсации влияния упругих сил инерционными и может быть использована для настройки систем управления технологических машин. Библ. 13, рис 2.

Ключевые слова: **электромеханическая система, демпфирование, электропривод, взаимодействие, регулирование, регулятор скорости, синтез, переменные силы трения.**

Introduction. The regulated automated electric drive (ED) of modern technological machines fulfills the functions of limiting dynamic loads of electrical and mechanical equipment; in theory, it provides a high static and dynamic accuracy of the reproduction of control laws and invariance to perturbations normalized rapidity [1, 2]. However, the practical implementation of the dynamic capabilities of ED is difficult due to the influence on the processes of regulation and control of elastic mechanical links of gears, the action of variable frictional forces on the shaft of working mechanisms [3, 4]. In the low-speed mode in ED with a wide range of regulation, variable friction forces in combination with elastic mechanical oscillations are the cause of self-oscillations and loss of stability [5, 6].

Problem definition. In published scientific research, the results of the analysis are presented and methods for synthesizing two-mass electromechanical systems (EMS) based on various optimization criteria are proposed, as a rule, without consideration of the interaction effects of subsystems [7-9], therefore it is of interest to investigate electric drives with an astatic system of automatic regulation and minimization of vibrational components of processes under the action of variable friction forces and optimal (limiting) electromechanical interaction.

The two-mass EMS with an astatic subordinate control system is represented by the structural circuit in Fig. 1. When describing the structural circuit, a relative form of writing of parameters is used, and the control object is characterized by the following parameters: $T_{M1} = J_1\omega_H/M_H$ is the mechanical time constant of the electric motor; $T_{M2} = J_2\omega_H/M_H$ is the mechanical time constant of the mechanism (the second mass reduced to the motor shaft); $\Omega_{12} = \sqrt{c_{12}(T_{M1}+T_{M2})/T_{M1}T_{M2}}$ is the frequency of free oscillations of a two-mass EMS; $c_{12} = C_{12}\omega_H/M_H$ is the coefficient of elasticity of mechanical transmission; $\beta_C = \pm B_C\omega_H/M_H$ is the coefficient of friction of the mechanical load for different parts of the characteristic; $\gamma = (T_{M1} + T_{M2})/T_{M1}$ is the coefficient of distribution of inertial masses of the motor and the mechanism.

At tuning the current (torque) loop to the maximum speed, the influence of elastic mechanical oscillations on it for the integration constant of the current loop $T_T << T_y$ ($T_y = 1/\Omega_{12}$) and $\gamma = 1.01 – 1.5$ is considered insignificant [7] which allows the transfer function to be adopted after conversion as $W_{KT}(p) \approx 1.0$. The speed controller is proportional-integral with the transmission coefficient K_R and the integration constant τ provides zero static error when the load m_C changes on the shaft of the mechanism.

Investigations of the influence of variable friction forces are performed for individual (linearized) sections of the load characteristic. Under the influence of elastic links in combination with the manifestation of «negative» viscous friction ($\beta_C < 0$), vibrations are excited in EMS with destabilization of the control processes and loss of stability [10]. There are also problems of stability of EMS with a doubly integrated automatic control system in the low-speed mode and with the action of friction forces on the increasing section of the load characteristic ($\beta_C > 0$).

The goal of the investigation is solution of the actual problem of active suppression of elastic electromechanical oscillations in EMS with an astatic system of automatic regulation. If the damping of the elastic mechanical oscillations is carried out by optimizing the dynamic stiffness of the mechanical characteristic of the ED [11], then it is possible to provide the required degree of stability with minimal EMS vibrations and high accuracy of working out the load perturbations.

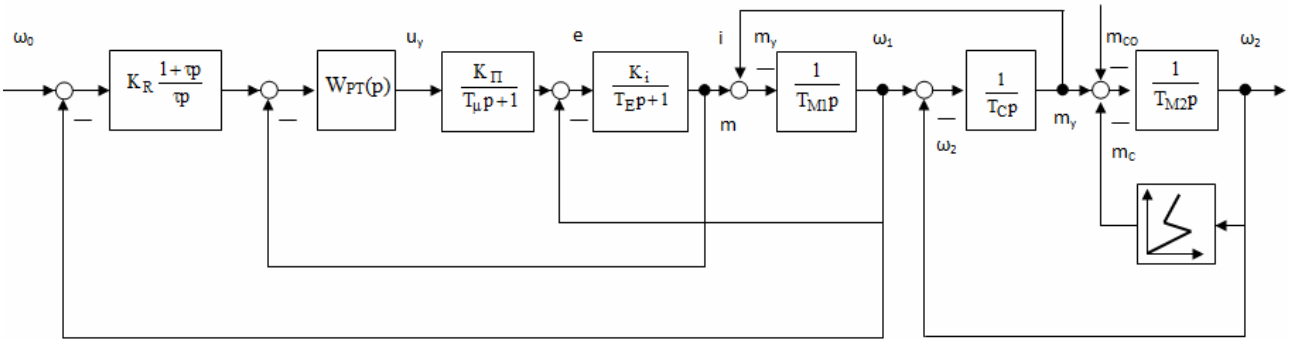

Fig. 1. Structural circuitf a two-mass electromechanical system with nonlinear mechanical loading at astatic regulation

To study the damping properties of EMS on the basis of the structural circuit, the transfer functions are obtained for the control and disturbing actions, of which, as in the source [10], the characteristic polynomial (CP) is used:

$$\begin{aligned} Q(p) &= \gamma T_{M1}\tau T_y^2 p^4 + (\gamma K_R \tau T_y^2 + T_{M1}\tau T_d)p^3 + \\ &+ (\gamma T_{M1}\tau + K_R \tau T_d + \gamma K_R T_y^2)p^2 + \\ &+ (K_R T_d + (K_R \pm \beta_C)\tau)p + K_R. \end{aligned} \quad (1)$$

Research materials. In CP (1), for convenience of writing and analysis, the following notations are accepted: $T_d = \pm\beta_C/c_{12}$ is time constant due to viscous friction; $T_y = 1/\Omega_{12}$ is the time constant of elastic vibrations.

If after the transformation of expression

$$K_R \pm \beta_C = K_R\left[1 \pm \frac{\beta_C}{K_R}\right]$$

we denote

$$1 \pm \frac{\beta_C}{K_R} = \varepsilon\,, \quad (2)$$

then the meaning of the coefficient «ε» becomes understandable – it characterizes the additional deviation in the dynamics of the velocity of the mechanism ω_2 under the action of the variable friction forces.

In the region of small deviations from the point of steady-state oscillation mode

$$\varepsilon > 1, \text{ if } \beta_C > 0,\ \omega < \omega_0,$$
$$\varepsilon = 1, \text{ if } \beta_C = 0,\ \omega = \omega_0,$$
$$0 < \varepsilon < 1, \text{ if } \beta_C < 0 \text{ and } |\beta_C| < K_R,\ \omega > \omega_0.$$

Then for the canonical form of the polynomial

$$\begin{aligned} Q(p) &= \gamma\frac{T_{M1}}{K_R}\tau T_y^2 p^4 + (\gamma\tau T_y^2 + \frac{T_{M1}}{K_R}\tau T_d)p^3 + \\ &+ (\gamma\frac{T_{M1}}{K_R}\tau + \tau T_d + \gamma T_y^2)p^2 + (T_d + \varepsilon\tau)p + 1. \end{aligned} \quad (3)$$

To analyze the active suppression of elastic vibrations with the development of destabilization processes in the case of astatic regulation in terms of CP (1) is difficult because of the many options for combining parameters and particular solutions. Therefore, we represent CP (3) in the normalized form taking into account generalized parameters

$$\left.\begin{aligned} K_B &= \frac{\Omega_{12}^2}{\Omega_E^2} = \frac{\tau T_{M1}}{K_R T_y^2};\\ \xi_D &= \frac{1}{2}\sqrt{\frac{\tau K_R}{T_{M1}}};\\ \xi_C &= \frac{T_d}{2\sqrt{\gamma}T_y};\\ \gamma &= \frac{T_{M1}+T_{M2}}{T_{M1}}. \end{aligned}\right\} \quad (4)$$

The proposed form of the normalization of the polynomials of electromechanical interaction processes [11] takes into account physical phenomena and establishes the interrelations of the EMS parameters.

According to (4), K_B is the interaction coefficient of electromagnetic and mechanical EMS subsystems; ξ_D is the coefficient of damping of the (separate) partial electromagnetic subsystem; ξ_C is the coefficient of damping of the (separate) partial mechanical subsystem, and

$$\xi_C > 0, \beta_C > 0, \varepsilon > 1,$$
$$\xi_C = 0, \beta_C = 0, \varepsilon = 1,$$
$$\xi_C < 0, \beta_C < 0, \varepsilon < 1, |\beta_C| < K_R.$$

In a joint consideration of relations (4) for K_B and ξ_D, we obtain the formulas for the relationship between the EMS parameters of the initial structural circuit with generalized exponents

$$\left.\begin{aligned} \frac{T_{M1}}{K_R} &= \frac{\sqrt{K_B}T_y}{2\xi_D}; \\ \tau &= 2\sqrt{K_B}\xi_D T_y. \end{aligned}\right\} \quad (5)$$

Taking the valuation form (5), we represent CP in the form

$$\begin{aligned} Q(p) &= \gamma K_B T_y^4 p^4 + 2(\gamma\sqrt{K_B}\xi_D + \sqrt{\gamma}K_B\xi_C)T_y^3 p^3 + \\ &+ \left(\gamma(1+K_B) + 4\sqrt{\gamma}\sqrt{K_B}\xi_D\xi_C\right)T_y^2 p^2 + \\ &+ 2(\varepsilon\sqrt{K_B}\xi_D + \sqrt{\gamma}\xi_C)T_y p + 1. \end{aligned} \quad (6)$$

ED at working out the speed deviation with zero static error under load action, variable friction forces and steady motion with damping of processes in the mechanical subsystem will be a dynamical vibration suppressor.

In this case, CP (6) with a successive dynamic decomposition is represented by separate interacting electromagnetic and mechanical subsystems with the description of the processes in the following form:

$$Q(p) = (T_0^2 p^2 + 2\xi_1 T_0 p + 1)(T_0^2 p^2 + 2\xi_2 T_0 p + 1) = 0. \quad (7)$$

The electromechanical interaction of the processes in the description in the form (7) physically means the complete extraction (retraction) of vibration energy from the mechanical subsystem to the electromagnetic one with simultaneous transformation at $\xi_2 \to \xi_1$ in the minimum time.

The CP (7) after conversion to the standard form is written as

$$\begin{aligned} Q(p) &= T_0^4 p^4 + 2(\xi_1 + \xi_2)T_0^3 p^3 + (2 + 4\xi_1\xi_2)T_0^2 p^2 + \\ &+ 2(\xi_1 + \xi_2)T_0 p + 1. \end{aligned} \quad (8)$$

The processes in EMS under the action of the variable friction forces and the excitation of elastic mechanical vibrations which are described in the normalized form (6) will correspond to processes (8) under the condition that the coefficients of the corresponding powers of the characteristic polynomial operator are equal which gives the following system of equations:

$$\begin{cases} \gamma K_B T_y^4 = T_0^4; \\ 2(\gamma\sqrt{K_B}\xi_D + \sqrt{\gamma}K_B\xi_C)T_y^3 = 2(\xi_1 + \xi_2)T_0^3; \\ (\gamma(1+K_B) + 4\sqrt{\gamma}\sqrt{K_B}\xi_D\xi_C)T_y^2 = (2 + 4\xi_1\xi_2)T_0^2; \\ 2(\varepsilon\sqrt{K_B}\xi_D + \sqrt{\gamma}\xi_C)T_y = 2(\xi_1 + \xi_2)T_0. \end{cases} \quad (9)$$

The system of equations (9) is solved taking into account physical considerations in a complete EMS at an optimal electromechanical coupling

$$\xi_1 \le \xi_2, \quad (10)$$

where $\xi_1 = \xi_E$ is the coefficient of damping of the processes of the electromagnetic subsystem in the composite EMS; $\xi_2 = \xi_M$ is the coefficient of damping of the processes of the mechanical subsystem in the composite EMS.

It is known that the ED may possess the damping properties of vibrations in an elastic mechanical subsystem with viscous friction under vibrational motion of an electromagnetic subsystem [12], then in a system with destabilization $\xi_1 < 1$. And, of course, the total effect of vibration damping in the mechanical subsystem can not be higher than the damping action of the electric motor. Such a restriction allows us to accept and express, in order to simplify the transformations when solving the system (9), the following notation

$$\xi_C = m\xi_D, \quad (11)$$

where m is the coefficient of weight (share) of damping by friction forces (in relation to ξ_D); $0 < m < 1$ is the viscous friction at moving with a speed corresponding to the positive section of the friction characteristic; $-1 < m < 0$ at vibrational motion with a speed corresponding to the negative section of the friction characteristic.

The processes (7) in the electromagnetic and mechanical subsystem will be equivalent, that is, they will proceed with a limiting degree of stability and minimum oscillation in the case of $\xi_2 = \xi_1$ for damping

$$\xi_D = \sqrt{\frac{\gamma(1+m)^2 - 2(1-m)(\varepsilon-m) + (\varepsilon-m)^2}{\varepsilon^2(1-m)^2 + 2m(1-m)(\varepsilon-2)(\varepsilon-m) + m^2(\varepsilon-m)^2}}$$

when performing the following relationships for generalized indices of electromechanical interaction of subsystems

$$K_B = \gamma\frac{(1-m)^2}{(\varepsilon-m)^2}; \quad \xi_C = m\xi_D. \quad (12)$$

The analysis of the obtained relations (12) shows that for the limiting degree of damping – the minimum of oscillation – the coefficient of the electromechanical interaction K_B and the damping coefficient ξ_D are determined by the mass distribution coefficient of the inertial masses γ and by the deflection coefficient of the speed ε and coefficient of weight «m». Assuming the absence of the action of variable friction forces on the shaft of the mechanism $\varepsilon = 1$ and $m = 0$, the following relationships are obtained:

$$K_B = \gamma; \quad \xi_D = \sqrt{\gamma - 1}, \quad (13)$$

which correspond to those given in [9] for the realization of processes in EMS with a limiting degree of electromechanical damping of elastic vibrations by an astatic automatic control system. Thus, if we perform the synthesis of the EMS parameters under astatic regulation, observing the relations (12), the processes in the dynamics will correspond to the reference one (7) and when the destabilizing factors are affected with the action of the «negative» viscous friction, the EMS will be stable for $\gamma > 1$, $0 < \varepsilon < 1$ and a positive frictional viscous for $1 < \gamma < 5$ и $\varepsilon > 1$. In the limiting case, the nature of the oscillatory damping processes in the EMS will correspond to the limiting damping with the indices:

$$\xi_0 = \sqrt{\frac{\gamma(1-m)^2 - 2(\varepsilon-m)(1-m) + (\varepsilon-m)^2}{4(\varepsilon-m)(1-m)^2} + m\xi_D^2};$$

$$\xi_E = \xi_M = \xi_0, \quad (14)$$

$$\Omega_E = \Omega_M = \Omega_{EM} = \Omega_0\sqrt{1-\xi_0^2}, \qquad (15)$$

where ξ_0 is the coefficient of vibration damping in EMS; $\Omega_0 = \frac{1}{T_0} = \Omega_{12}\sqrt{\frac{(\varepsilon - m)}{\gamma(1-m)}}$ is the natural frequency of undamped oscillations of a two-mass EMS in dynamics equivalent to a one-mass one.

Characteristics of the processes in ED (14), (15) with the limiting degree of damping of elastic vibrations under the action of variable friction forces are achieved by setting the current regulator according to the criterion «modular optimum», and the speed regulators of the system of subordinate regulation according to the ratios

$$K_R = \frac{2T_{M1}\xi_D}{\sqrt{K_B}T_y}; \quad \tau = 2\sqrt{K_B}\xi_D T_y, \qquad (16)$$

which are obtained from formulas (5) with subsequent substitution of optimal values of the parameters K_B, ξ_D, ξ_C from (12).

Fig. 2 shows the oscillogram of the motor torque variation $m(t)$ for small velocity deviations at a single step change in the load for a section of the characteristic with negative friction where the graph of the transient 1 is presented for the case of tuning to a symmetric optimum with typical parameters of the automatic control system in calculations without taking into account the properties of the elastic link and variable friction forces, and the graph of the transient 2 – for the case of tuning to a minimum of oscillation with optimal parameters of the automatic control system for the section of the characteristic with a «negative» friction. ED is effectively damping vibrations. In particular, the proposed method for synthesizing the parameters of the automatic control system was tested in industrial conditions while positive results were obtained when adjusting and modernizing the machine electric drive [13].

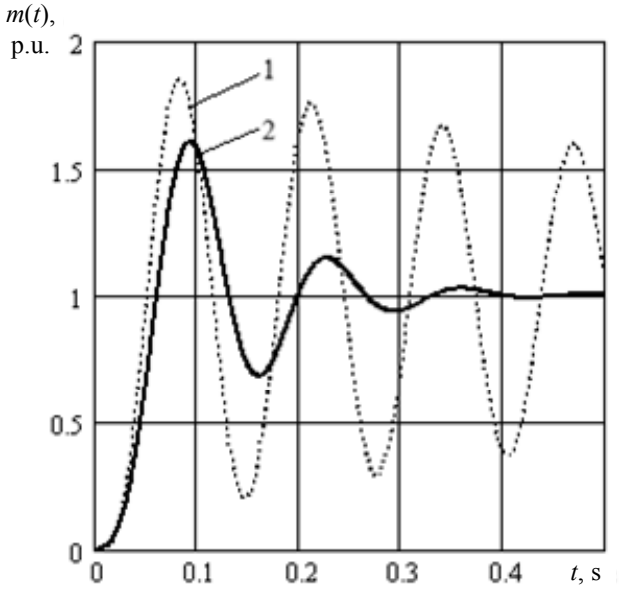

Fig. 2. Graphs of motor torque variation for small speed deviations at a single step change in load:
$1 - \gamma = 1.5$, $\Omega_{12} = 62.8$ s^{-1}, $K_R = 141.75$, $\tau = 0.02$ s;
$2 - \gamma = 1.5$, $\Omega_{12} = 62.8$ s^{-1}, $K_R = 65.227$, $\tau = 0.0273$ s, $\xi = 0.686$, $m = -0.5$, $\varepsilon = 0.98$

Conclusions.

1. A two-mass ED with an astatic regulation system under the action of variable friction forces effectively damps the oscillations at optimizing the parameters of the regulators.

2. Synthesis of the parameters of speed regulators by the relations for the transfer coefficient K_R and the integration constant τ makes it possible to realize the limiting indices of the nature of damped processes with zero static error.

3. The synthesis method based on the generalized parameters K_B, ξ_D, ξ_C and γ satisfies the requirements of system analysis, since it takes into account the measures of mechanical, constructive, electromechanical methods of suppressing elastic mechanical vibrations.

4. The method of synthesis is recommended for practical use for control systems for ED of metallurgical and lifting-transport machines, metal-cutting machines.

REFERENCES

1. Kliuchev V.I. *Teoriia elektroprivoda* [Theory of the electric drive]. Moscow, Energoatomizdat Publ., 2001. 704 p. (Rus).

2. Popovich M.G., Lozins'kii O.Iu., Klepikov V.B. *Elektromekhanichni sistemi avtomatichnogo keruvannia ta elektroprivodi : navch.posibnik dlia stud. vishch. navch. zakladiv, iaki navchaiut'sia za napriamom «Elektromekhanika»* [Electromechanical systems of automatic control and electric drives: a manual for students of higher educational institutions in the direction of «Electromechanics»]. Kyiv, Lybid Publ., 2005. 680 p. (Ukr).

3. Andriushchenko V.A. On the stability of the traction electric drive of low speeds with unlimited increase of some of its parameters. *Russian Electromechanics*, 1976, no.1, pp. 100-103. (Rus).

4. Ivanchenko F.K. *Mekhanika privodov tekhnologicheskikh mashin* [Mechanics of drives of technological machines]. Kyiv, Vishcha shk. Publ., 1986. 152 p. (Rus).

5. Besekerskii V.A. *Dinamicheskii sintez sistem avtomaticheskogo regulirovaniia* [Dynamic synthesis of automatic control systems]. Moscow, Nauka Publ., 1970. 576 p. (Rus).

6. Klepikov V.B., Osichev V.B. Determination of the stability limits of an electric drive with negative viscous friction taking into account the elasticity of the kinematic chain. *Electricity*, 1989, no.1, pp. 36-41. (Rus).

7. Bortsov Iu.A., Sokolovskii G.G. *Avtomatizirovannyi elektroprivod s uprugimi sviaziami* [Automated electric drive with elastic connections]. St. Petersburg, Energoatomizdat Publ., 1992. 288 p. (Rus).

8. Burgin B.Sh. *Analiz i sintez dvukhmassovykh elektromekhanicheskikh sistem* [Analysis and synthesis of two-mass electromechanical systems]. Novosibirsk, NETI Publ., 1992. 199 p. (Rus).

9. Samuelsson O. Load modulation at two locations for damping of electromechanical oscillations in a multimachine system. *Power Engineering Society Summer Meeting 2000*. IEEE, 2000, vol.3, pp. 1912-1917. **doi: 10.1109/pess.2000.868826**.

10. Zadorozhnii N.A., Marilov N.G., Kutovoi Iu.N., Arus Mokhammed. Analysis of electromechanical drive systems with elastic mechanical connections in the regime of low speeds and slippin. *Bulletin of NTU «KhPI». Series: Problems of automated electric drive. Theory and practice*. Kharkov, 1997, pp. 122-123. (Rus).

11. Zadorozhnii N.A., Zadorozhniaia I.N. Synthesis of parameters of an astatic automatic control system for two-mass

electric drives with a specified degree of stability and minimum oscillation. *Bulletin of NTU «KhPI». Series: Problems of automated electric drive. Theory and practice*, 2015, no.12(1121), pp. 155-159. (Rus).
12. Zadorozhnia I.M. Optimization of dynamic modes of drives of metallurgical machines with minimization of influence of elastic oscillations. *Electromechanical and Energy Systems, Modeling and Optimization Methods. Conference proceedings of the 11th International conference of students and young researches*. Kremenchuk, April 9-11, 2013, pp. 51-52. (Ukr).
13. Zadorozhnii N. A., Rebedak O. A., Zadorozhniaia I.N. Features of the work of the feed mechanism deep machine KZH-1910 in low speed mode. *Bulletin of NTU «KhPI»*, 2013, no.36(1009), pp. 209-210. (Rus).

Received 19.02.2018

I.N. Zadorozhniaia[1], *Candidate of Technical Science, Associate Professor,*
N.A. Zadorozhniy[1], *Candidate of Technical Science, Associate Professor,*
[1] Donbass State Engineering Academy,
72, Akademicheskaia Str., Kramatorsk, Donbass Region, 84313, Ukraine,
e-mail: zadorozhnyaya_in@ukr.net

How to cite this article:
Zadorozhniaia I.N., Zadorozhniy N.A. Synthesis of a two-mass electric drive with an astatic system of subordinate regulation at the action of variable friction forces. *Electrical engineering & electromechanics*, 2018, no.3, pp. 23-27. **doi: 10.20998/2074-272X.2018.3.03.**

UDC 681.513, 621.365, 62-83-52 **doi: 10.20998/2074-272X.2018.3.04**

O.Y. Lozynskyi, Y.S. Paranchuk, R.Y. Paranchuk, F.D. Matico

DEVELOPMENT OF METHODS AND MEANS OF COMPUTER SIMULATION FOR STUDYING ARC FURNACE ELECTRIC MODES

Goal. ***The purpose of the article is the creation of a three-phase instantaneous coordinates Simulink computer model of the power supply and automatic coordinates control system (ACS) of the DSP-200 type arc furnace electric mode (EM). The model has a convenient interface for changing the structure and parameters of the three-phase arcs power supply system, the structure and laws of the electric mode control system, as well as the stochastic characteristics of parametric and coordinate disturbances.*** ***Method.*** ***The provisions of the electric circuits theory, experimental study and mathematical and computer simulation in the Simulink system of the MatLAB computing environment were used for the research.*** ***Results.*** ***A high-precision instantaneous coordinates Simulink-model of the power supply system and electric mode coordinates ACS of the ER DSP-200 furnace was created. This model was used to study the EM and evaluate the performance of the arc furnace during various technological melting periods and with various structures of the automatic control system.*** ***Scientific novelty.*** ***For the first time, based on a combination of Simulink application library elements and SimPowerSystems standard library blocks of the MatLAB environment a complete high-precision three-phase instantaneous coordinate model of arc furnace DSP-200 power supply system and EM ACS was developed. The developed model has significant advantages in accuracy, performance and features compared to existing ones.*** ***Practical value.*** ***Possibility to run on the created Simulink-model mathematical experiments on the research of the electric mode coordinates control dynamic indices and electromagnetic compatibility indices of the electric arc furnace and the supply network under the influence of the deterministic and random perturbations.*** References 11, tables 3, figures 16.

Key words: **arc furnace, Simulink computer model, power supply system, automatic control system, electric mode, regulator, dynamic current-voltage arc characteristic, electromechanical circuit.**

Цель. ***Целью статьи является создание трехфазной в мгновенных координатах компьютерной Simulink-модели системы питания и системы автоматического регулирования (САР) координат электрического режима (ЭР) дуговой сталеплавильной печи типа ДСП-200, которая имеет удобный интерфейс для изменения структуры и параметров системы питания трехфазных дуг, структуры системы и законов управления электрическим режимом, а также стохастических характеристик параметрических и координатных возмущений.*** ***Методика.*** ***Для проведения исследований использовались положения теории электрических цепей, экспериментальные исследования и математическое и компьютерное моделирование в приложении Simulink программы Matlab.*** ***Результаты.*** ***Создана высокоточная компьютерная в мгновенных координатах Simulink-модель системы питания и САР координат ЭР ДСП-200 и с ее использованием проведены исследования ЭР и получены оценки показателей функционирования дуговой печи в различных технологических периодах плавления и при различных структурах системы автоматического управления (САУ).*** ***Научная новизна.*** ***Впервые на основе сочетания элементов библиотеки приложения Simulink и типовых библиотечных блоков SimPowerSystems программы Matlab составлена трехфазная в мгновенных координатах полная модель системы питания и САУ ЭР дуговой печи ДСП-200, которая имеет значительные преимущества по точности, быстродействию и функциональным возможностям по сравнению с известными моделями.*** ***Практическая ценность.*** ***Возможность выполнения на созданной Simulink-модели математических экспериментов по исследованию показателей динамики регулирования координат ЭР и показателей электромагнитной совместимости режимов ДСП и электросети при действии детерминированных и случайных возмущений.*** Библ. 11 табл. 3, рис. 16.

Ключевые слова: **дуговая сталеплавильная печь, компьютерная Simulink-модель, система питания, система автоматического регулирования, электрический режим, регулятор, динамическая вольт-амперная характеристика дуги, электромеханический контур.**

Introduction. Arc furnaces are powerful electrotechnological facilities for melting steels and alloys mainly from scrap metal. Considering the considerable installed power and the extremely dynamic asymmetric and non-linear nature of the load, it is not always possible to carry out experimental studies of their modes and parameters of the melting process in the arc furnaces in view of a number of organizational, technical and industrial reasons. Particular difficulties arise when it is necessary to carry out experimental research for various structures of the automatic control system (ACS), for its various parameters, for various circuit changes in the power supply circuit of three-phase arcs, and so on.

Problem definition. One of the approaches to obtaining the indicated information (indicators of dynamics, electrotechnical efficiency and electromagnetic compatibility) is mathematical and computer simulation [1, 2]. However, the existing mathematical and computer models of processes in the arc furnaces in terms of speed, accuracy of reproduction of modes, functional capabilities, the convenience of changing the structure, parameters and setting of model experiments do not meet the modern requirements for a comprehensive study of dynamics, electrotechnical efficiency and electromagnetic compatibility.

Review the recent publications. Existing computer models [3, 4] have a complicated and awkward interface for changing the parameters and structure of the ACS of EM and the power supply of the three-phase arcs, the laws of the control of the electric mode, the operative formation of perturbation characteristics with different stochastic characteristics corresponding to the investigated technological stages melting, statistical processing of simulation results in on-line mode that complicates the computer research of the EM of the arc furnace in search of the best solutions for the structure and parameters of the ACS and the laws governing the EM. Some of the known models are used only for the analysis of the process of coordinate change of the EM in

a power circuit in a power circuit without a closed system of regulating arc lengths in averaged coordinates [5], others have a complicated and awkward interface for changing the structure of the ACS, control laws, indices of parametric and coordinate perturbations, dependencies of dynamic volt-ampere characteristics of arcs, etc. [6-8]. They have peculiar or low accuracy of modes reproduction [5], or limited functional capabilities for setting up and conducting various mathematical experiments [6-8].

Justification of relevance. Therefore, the problem of the creation of new high-precision and high-performance computer models of the power supply system and the ACS of the coordinates of the arc furnaces' EM which takes into account all the main nonlinearities, peculiarities of the changes of parametric and coordinate disturbances in the melting process in which convenient interfaces of the structure change, control laws and parameters of the ACS are implemented, the formulation of mathematical experiments and the statistical processing of the results of research for today is an actual and important scientific and technical task.

The goal of the work is the creation of a three-phase in the instantaneous coordinates structural Simulink model of the system of supply of three-phase arcs and the system of automatic control of the electric mode of the arc furnace and the study of the parameters of the dynamics of electrical regimes and indicators of electromagnetic compatibility with its use.

The scientific task is to create a structured Simulink model of the three-phase arc power supply system and an automatic control system for arc furnace electric regime based on the combination of model elements of the Simulink library and the structural blocks SimPowerSystem of the Matlab code.

Structural Simulink model of the power supply system and the ACS of the coordinates of the EM of the DSP-200 furnace. Fig. 1 shows the developed functional circuit of the power supply system of three-phase arcs without a zero conductor and a one-circuit system of automatic regulation of coordinates of the EM with a differential law for the formation of a control signal on the displacement of electrodes (automatic adjustment of arc lengths).

On the basis of this functional circuit, a Simulink computer model (Fig. 2) was created which is configured for the parameters of the power supply system, power electrical equipment and arc power regulator of ARDMT-12 type (ACS of the coordinates of the EM) of an arc furnace type DSP-200. The testing of the model was carried out by comparing the dynamics indicators of the development of the working out of deterministic and stationary random disturbances by the length (voltage) of the arc obtained on the operating arc furnace DSP-200 and on the developed its Simulink model under differential control law.

For adequate reproduction in the developed computer model of the real dependencies of the dynamic volt-ampere characteristics (DVAC) of arcs occurring at different technological stages of melting, in the modulus of three-phase arcs of the Simulink model the possibility of realization in the current mathematical experiment is envisaged of one of the four models corresponding to the main technological stages of melting – the linear $u_a(t) = R_a(t) \cdot i_a(t)$ and the nonlinear ones – based on the arc tangent function $u_a(t) = 2 \cdot E_{am}(t) \cdot \arctan(k \cdot i_a(t))/\pi$, on the basis of the differential Cassie equation $\theta \frac{dg_a(t)}{dt} = \left(\frac{u_g(t)^2}{E_{am}^2} \right) g_a(t)$ and nonlinear with complex nonlinear functional dependence on the basis of the use of piecewise linear and piecewise nonlinear splines $u_a(t) = \Psi(i_a(t), l_a(t))$ with the possibility of reproduction of the hysteresis properties of the arc, ignition peaks, arc extinguishing, etc., where $g_a(t)$, $R_a(t)$ are the instantaneous arc conductivity and resistance; E_{am} is the maximum value of anti-EMF of the arc; $u_a(t)$, $i_a(t)$, $l_a(t)$) are the instantaneous arc voltage, current and length, Θ_a is the time constant characterizing the thermal inertia of the arc [9].

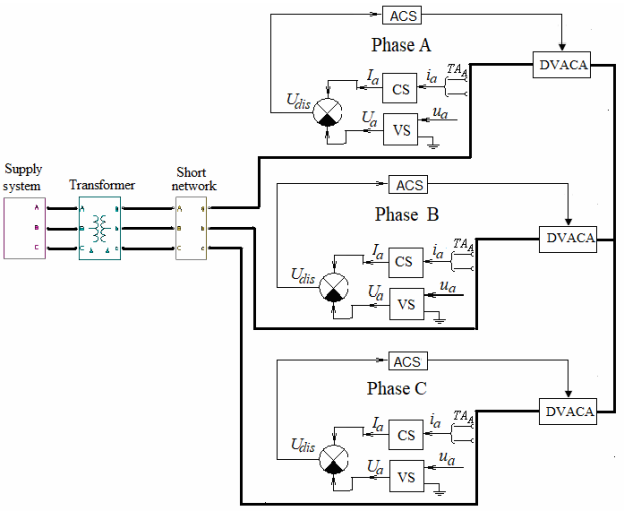

Fig. 1. Functional circuit of the three-phase Simulink model of the power supply system and the ACS of the coordinates of the EM of the DSP-200 furnace

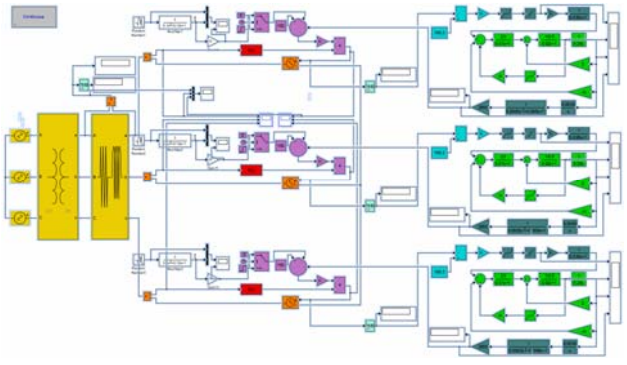

Fig. 2. Structural circuit of the three-phase Simulink model of the power supply system and the ACS of the coordinates of the EM of the DSP-200 arc furnace

The change in the value of the time constant Θ_a in the model can reproduce the conditions of burning arcs at different technological stages of melting, that is, to realize different arcs DVAC (their area characterizes the reactive power of the arc). At the beginning of the melting Θ_a = 0.2÷0.5 ms; Θ_a = 1÷1.5 ms at the interval of formation of the liquid phase of the melt, and in the periods of oxidation and refining – Θ_a =3÷5 ms.

The model of the block of three-phase arcs for making the corresponding structural and parametric changes has the potential to reproduce the above types of arcs DVAC which are inherent in different technological stages of melting.

In Fig. 2 elements of the model of the three-phase symmetric electric network (EN), the furnace transformer unit (FTU) and the secondary conductor – short network (SN) of the furnace which represent a model of the power electric circuits of the supply of the three-phase arcs of the arc furnace with the corresponding DVAC indicated in yellow which are collected on the elements of the SimPowerSystems library (red). On these elements the possibility of reproduction of the four types of dynamic arcs DVAC described above which take place at different technological stages of melting is realized.

Voltage sources reproduce the three-phase sinusoidal voltage of the arc furnace power supply network with a frequency of 50 Hz, amplitude $35\sqrt{2}$ kV and the angle of shift of 120 electrical degrees. Block «furnace transformer» represents a three-phase transformer with a transformation coefficient k_{tr} = 35000/480 = 72.92 and power S = 125 MVA.

The block «total impedance» simulates the total resistance of all active resistances of elements of the power supply system of the arcs (choke, transformer, short network and electrode in each phase) which are united in resistance r_{ss}, and all their inductive resistances are united in resistance x_{ss}.

The red block $I_a(U_a)$ reproduces the static internal characteristic of the arc furnace DSP-200 for the appropriate stage of the power furnace transformer.

The orange block is a controlled voltage source whose input-output characteristic is formed by the block $I_a(U_a)$ and the perturbation setting block.

Violet blocks from the group of elements of the perturbation setting simulate the deterministic and random perturbations along the arc length which arise during the arc furnace operation at arc gaps at different technological stages of melting. The purpose of this group of blocks is the formation of various time realizations of disturbances along the arc length in the phases of a short furnace network, with the same statistical characteristics that correspond to the investigated technological stages of melting.

Blocks of bright blue color reproduce the model of the block of comparison of input signals of the ACS for realization of the corresponding law of formation of the signal of the EM mismatch. Its output signal is the U_{dis} mismatch signal, and its «input-output» dependence $U_{dis}=F(U_a, I_a)$ varies according to the investigated law of electric mode control.

Elements of the Simulink model of dark green color simulate the static dependence «input-output» of the block of the formation of a control signal on displacement of the electrode of a particular phase of the furnace. It implements the «zone of insensitivity» (δ = 2...10 %), the gain factor for lifting and lowering the electrodes, limiting the maximum speed $U_t^{\max}$ for lifting and $U_d^{\max}$ for lowering of the electrodes, reproduces the inertia of the low frequency filter which is connected in each phase at the output of the rectifiers of the current sensor CS and the voltage sensor VS. Fig. 3 shows the static characteristic of the control signal formation block $U_c = f(U_{dis})$.

The block «Reducer» serves to convert the angular velocity of the motor reduced to the angular velocity of the gear, into the linear displacement of the electrode and is represented in the Simulink model by a non-linear link of the type «backlash» and the integrating link that simulate the mechanical gear type «gear-rail». The «oscillating link» block reproduces a limited rigidity of the individual elements of the kinematic circuit of the mechanism of moving the electrodes, in particular the vertical column, the horizontal arm of the electrode holder and the electrode itself.

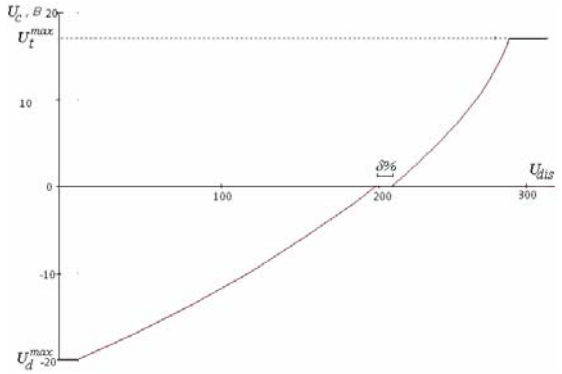

Fig. 3. Dependence «input-output» of the block of formation of the control signal

The group of green elements simulates the electric drive of the mechanism of displacement of the electrode of the ARDM-T-12 type arc power regulator which is assembled according to the circuit «reverse thyristor converter – DC motor» with a nonlinear negative feedback on the current of the armature and a motor negative on speed and with summation of these signals on the input amplifier.

In RMS blocks, the current values of current and arc voltage are continuously calculated in the simulation process by the formula $RMS(f(t)) = \sqrt{\frac{1}{T}\int_{t-T}^{t} f(t)^2}$.

In Table 1 experimental results for the DSP-200 furnace which describe the static external characteristics of this furnace $I_a(U_a)$ and the dependence of the arcs power $P_a(U_a)$ which are reproduced by functional blocks in the model in the power circuit model of the DSP-200 furnace are shown.

In Fig. 4, 5 the model dependences of these two main characteristics of the DSP-200 arc furnace are constructed on the basis of these experimental data.

In Fig. 5 dashed lines show the coordinates of the point of maximum arcs power and arcs power points which corresponds to the steady mode of the furnace at the first stage of the furnace transformer voltage. The coordinates of the point of the steady state (voltage and current of the arc) correspond to the settings of the ARDM-T-12 type arc power regulator on the U_{set} voltage and the I_{set} arc current, respectively.

Table 1

Experimental data for characteristics $I_a(U_a)$ and $P_a(U_a)$ of the arc furnace DSP-200

I_a, A	U_a, V	P_a, W
70962	3.96E-06	0.28101
68808	39.39	2710347
65339	77.98	5095135
60614	115.13	6978490
54723	149.99	8207903
47894	183.34	8780886
43970	198.2	8714854
40800	208.5	8506800
33590	227.9	7655161
27593	241.85	6673367
19392	256.72	4978314
14749	263.25	3882674
7673	271.11	2080227
2877	275.2	791750.4
1428	276.25	394485
142.7	277.08	39539.32
14.27	277.14	3954.788
1.4273	277.16	395.5905

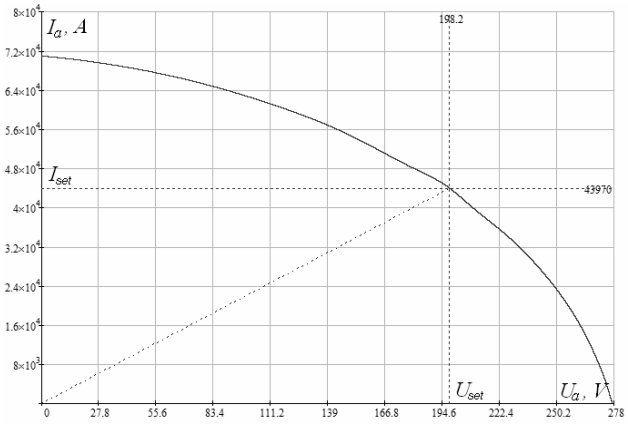

Fig. 4. External characteristic $I_a(U_a)$ of the furnace DSP-200

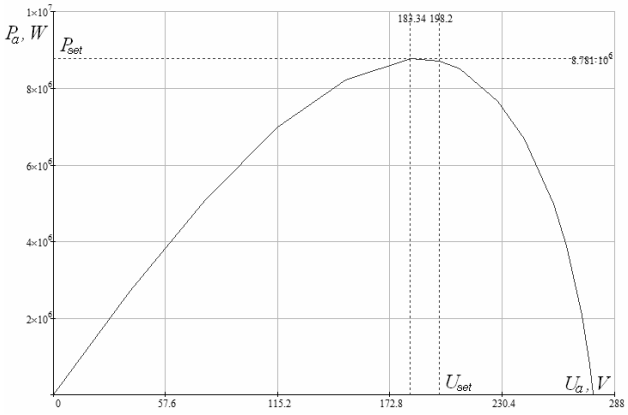

Fig. 5. Power dependences $P_a(U_a)$ of the arcs of DSP-200

The Simulink model structural circuit includes a module of the generator of the deterministic (in particular, the extreme ones which cause symmetric or asymmetric by the phases operational short circuits or breakdowns of the arc) and stationary random disturbances along the length of arcs which, according to the stochastic characteristics, correspond to the perturbations acting in the arc gaps in the investigated technological stages. The created Simulink model also includes a module for calculating the integral characteristics of temporal processes of changing the coordinates of the EM and the indicators of electromagnetic compatibility which in a complex manner characterize the efficiency of the control of the modes and the dynamics of coordinates adjustment of the EM of the furnace DSP-200 with the adjusted structure of the ACS for a certain technological stage, the perturbation characteristics and the chosen control laws for the EM.

The study of the accuracy of the created Simulink model was performed on the basis of a comparison of mathematical expectations and dispersion of the processes of the change in the mean-square values of arcs currents $I_a(t)$ obtained on the operating arc furnace DSPA-200 and its Simulink model at various technological melting stages. Comparison of their meanings was performed on the basis of the M-criterion of Bartlett [10]. The criterion estimates for the mathematical expectation t_M and for the dispersions t_D of arcs currents were obtained by formulas (1) and (2) respectively:

$$t_M = \frac{N-k}{k-1} \cdot \frac{\sum_{i=1}^{k} n_i \cdot (\bar{x}_i - \bar{x})^2}{\sum_{i=1}^{k}\sum_{j=1}^{n_i} (x_{ij} - \bar{x}_i)^2}; \quad (1)$$

$$t_D = \frac{\ln 10}{c}\left[(N-k)\cdot \lg s^2 - \sum_{i=1}^{k} (n_i - 1)\cdot \lg s_i^2 \right];$$

$$c = 1 + \frac{1}{3\cdot(k-1)} \cdot \left(\sum_{i=1}^{k} \frac{1}{n_i - 1} - \frac{1}{N-k} \right); \quad (2)$$

$$s^2 = \frac{1}{N-k} \cdot \sum_{i=1}^{k} (n_i - 1)\cdot s_i^2 ,$$

where $N = \sum_{i=1}^{k} n_i$ is the total data number; k is the number of samples; n_i , i = 1,2,...,k is the size of the i-th sample; $\bar{x}_i = \frac{1}{n_i} \cdot \sum_{j=1}^{n_i} x_{ij}$, $i = 1,2,...,k$ – is the average value of the i-th sample; $\bar{x} = \frac{1}{N} \sum_{i=1}^{k} \sum_{j=1}^{n_i} x_{ij}$ is the total average value of the aggregate of data; $s_i^2 = \frac{1}{n_i - 1} \cdot \sum_{j=1}^{n_i} (x_{ij} - \bar{x}_i)^2$ is the dispersion of the i-th sample.

The obtained values of these criteria did not exceed the acceptable (tabular) value of the criterion – 3.84 which was taken for the 5 % level of significance α. On the basis of comparison of these estimates, we have obtained confirmation of the achievement of sufficient accuracy of reproduction of the real processes of changing the arcs currents $I_a(t)$ in the Simulink model of the arc furnace DSP-200.

Investigation of the dynamics and efficiency of different structures of the ACS of the EM of the DSP-200 furnace. In the first stage of the research, the

simulation of the processes in the electric drive of the mechanism of the displacement of the electrodes (electromechanical system «thyristor converter – motor» (TC-M)) of the ARDM-T-12 type arcs power regulator and the mechanism of electrode displacement (MED) was performed. Their dynamic and static properties significantly affect the parameters of quality of control of arcs lengths (the working out of perturbations along the arcs lengths). Fig. 6 shows a fragment of the general Simulink model of DSP-200 which reproduces the processes of changing the coordinates of the electric drive and the MED in one phase, and Fig. 7 shows obtained on this model dynamical processes of changing the current of the armature $I_m(t)$ and the angular velocity $\omega_m(t)$ of the MED motor in the deterministic changes of the control signal $U_c(t)$ on the input of the thyristor converter.

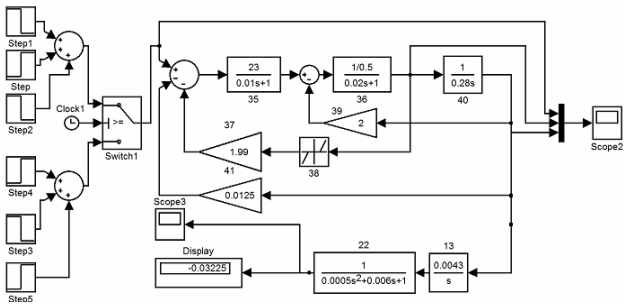

Fig. 6. Simulink-model of the electric drive according to the TC-M circuit of the mechanism of displacement of the electrode of the arcs power regulator ARDM-T-12

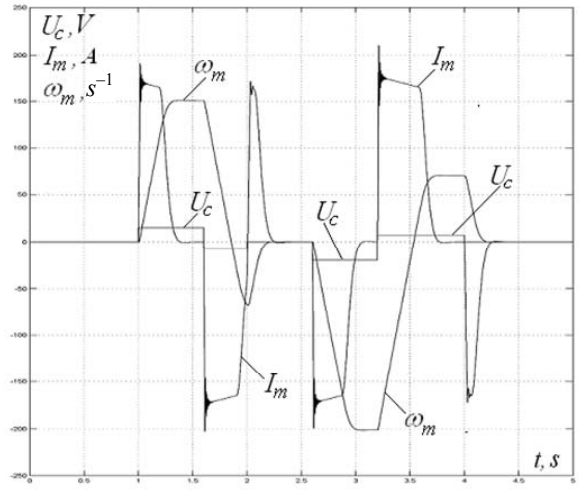

Fig. 7. Dynamics of current $I_m(t)$ and motor speed $\omega_m(t)$ of MED with a deterministic change in control signal $U_c(t)$ of the electric drive of the MED

Fig. 8 shows obtained on the developed Simulink model the temporal dependences of changes of the instantaneous values of the voltage of the secondary winding of the FT $u_{2pf}(t)$ and the current $i_a(t)$ and the voltage $u_a(t)$ of the arc in the phase A in the quasi-stationary mode of working out of random perturbations in the nonlinear arc DVAC which is described by the function of the arctangent. The given temporal dependences illustrate the effect of the trapezoidal shape of the voltage on the arcs which is observed at the end of the melting of the solid charge on the distortion of the sinusoidal shape of the arc current and the phase voltage of the secondary winding of the furnace transformer unit.

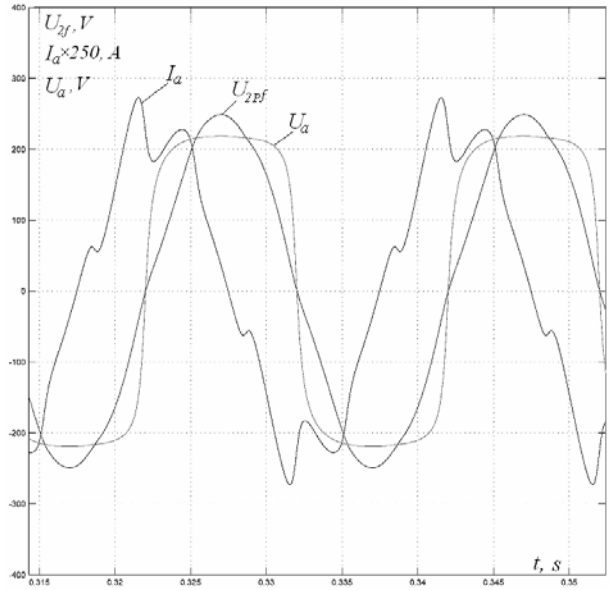

Fig. 8. Temporal dependences of the quasi-stationary process of the change of voltage $u_a(t)$, current $i_a(t)$ of the arc and voltage $u_{2pf}(t)$ of the FTU

On computer models, we also investigated the modes of working out the asymmetrically in the phases deterministic perturbations along the lengths of arcs – modes of one- and two-phase short circuits and breakdowns of the arc and determined their respective indicators of the quality of the dynamics.

So, Fig. 9 shows the obtained processes of changing the current values of voltage $U_a(t)$, current $I_a(t)$, arc and current $I_m(t)$, and the speed $\omega_m(t)$ of the motor of the electric drive of the mechanism of displacement the electrode in all three phases at working out the short circuit in the phase A for a differential control law of the lengths of arcs.

Fig. 10 shows obtained on the developed Simulink model the temporal dependences of the same EM coordinates in each of the phases of the power circuit of the DSP-200 furnace and the motor of the electric drive of the MED of the arc power regulator ARDM-T-12 in the mode of working out of the extreme (symmetrical in phases) of perturbation which leads to a three-phase breakdown of arcs. Analysis of the temporal dependences shown in Fig. 9, 10 shows the oscillating nature of the processes of working out the specified deterministic extreme disturbances with the regulation time of 1.2 s and 1.4 s, respectively.

In addition to the differential law, other laws of the formation of a control signal on the displacement of electrodes were also investigated. Fig. 11 shows obtained on the model the temporal dependences of the change in the coordinates of the EM (voltage $U_a(t)$, current $I_a(t)$, arc) of the arc furnace DSP-200 and the coordinate of the motor of the mechanism of the displacement of the electrode (current $I_m(t)$, speed $\omega_m(t)$ for each of the phases) at working out of the breakdown of the arc in the phase A and regulation by the law of deviation of the arc voltage from the given $U_{dis}=k(U_{a.set}-U_a)$.

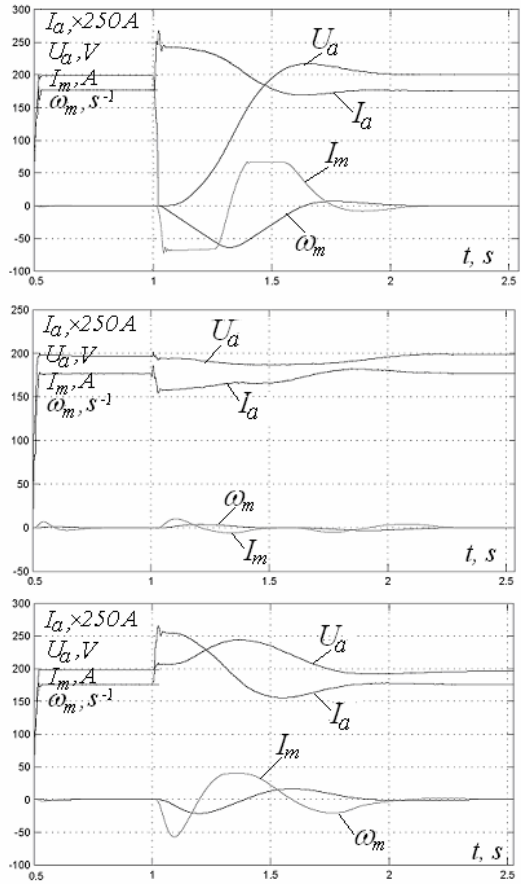

Fig. 9. Temporal dependences of the coordinates of the EM of the furnace DSP-200 and the motor of the MED in each phase at working out the short circuit in the phase A

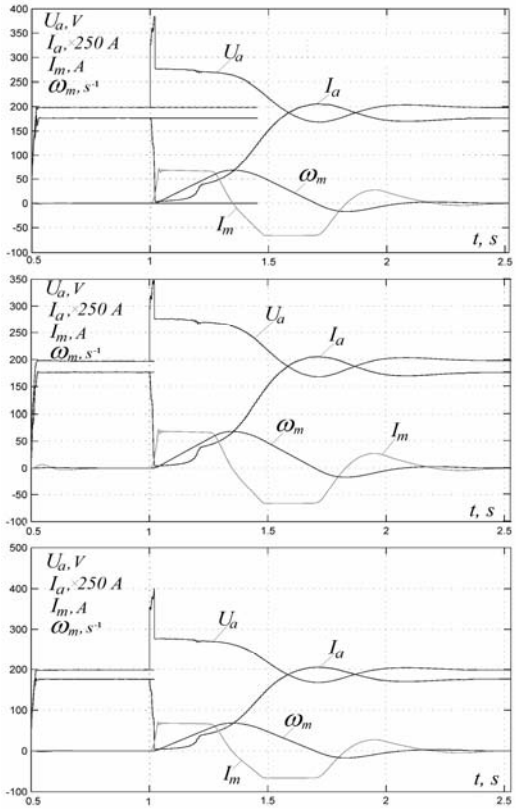

Fig. 10. Temporal dependences of voltage $U_a(t)$, current $I_a(t)$ of the arc of the furnace DSP-200 and current $I_m(t)$ and the speed of the motor $\omega_m(t)$ of the MED of each phase at working out of the three-phase breakdowns of the arc

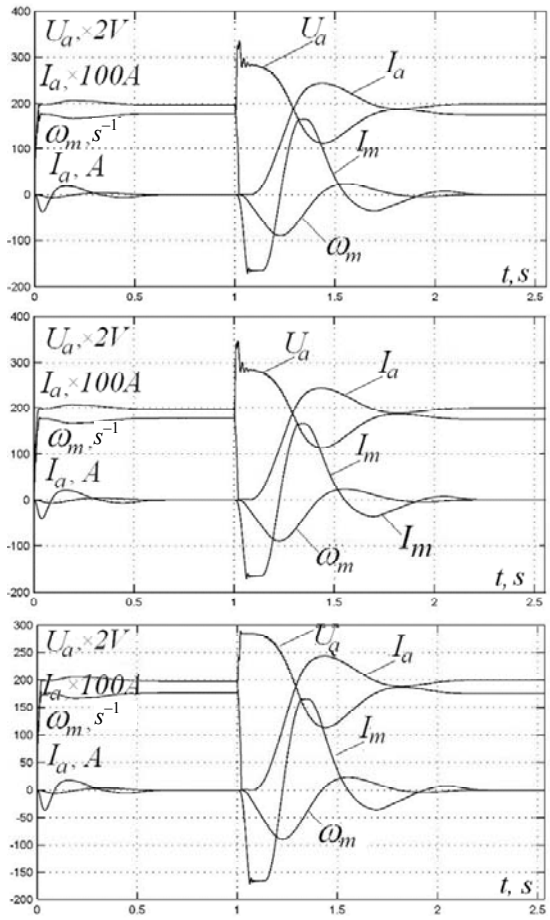

Fig. 11. Changing of the coordinates of the EM $U_a(t)$, $I_a(t)$ of the furnace DSP-200 and the motor of the MED $I_m(t)$ $\omega_m(t)$ of the regulator ARDM-T-12 at working out of the breakdowns of the arc in the phase A by the law of the arc voltage deviation

The main perturbations in the process of melting of charge in an arc furnace are stationary random perturbations along the arc length stochastic characteristics of which vary during melting. With the occasional nature the voltage on the power supply buses of the arc furnace also fluctuates, and also the parameters of the elements of the power circuit (elements of the furnace's short network) also accidentally change, and so on.

To reproduce in the compiled Simulink model the random processes of coordinate and parametric disturbances mentioned above, a module for the generation of three independent implementations of random processes with identical stochastic characteristics and the possibility of changing their parameters in correspondence with the characteristics of these perturbations operating in the studied technological melting stages in the operating arc furnace DSP-200 is developed and included to the model.

In the initial stages, the indicated perturbations have the maximum amplitudes in the range of low frequencies (0.2-1.5 Hz), then the amplitudes decrease, and their frequencies increase, and in the stage of oxidation and refining (in particular the stage of boiling of the slag), the amplitudes are minimal, and their frequencies lie in the band of 5-8 Hz. In the developed module of the generation of random perturbations, the possibility of such a change in their parameters in accordance with the

values of the parameters of stochastic characteristics of real disturbances in the investigated technological stages of melting is realized. A fragment of such random perturbations for the technological stage of fusing wells in the arc furnace DSP-200 is shown in Fig. 12.

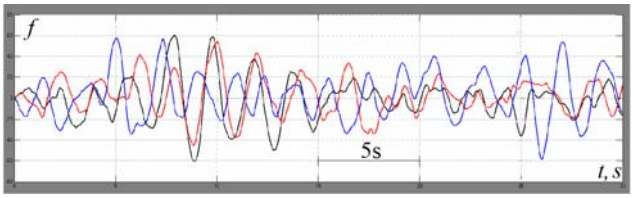

Fig. 12. A fragment of random perturbations along the lengths of arcs $f(t)$ in three phases at the stage of wells fusing

As an example, Fig. 13 shows the obtained on the developed structural Simulink model at the action of stationary random perturbations along the arc lengths the processes of changing the arcs currents at the working out by the power regulator of the type ARDM-T-12 of stochastic perturbations in each phase during the technological period of boiling of the slag and under the control by the differential law.

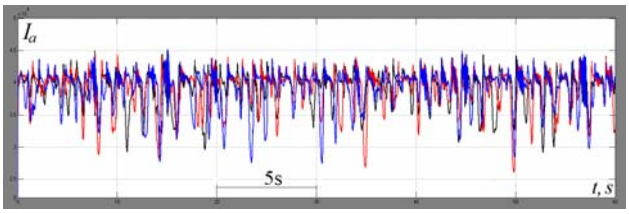

Fig. 13. Temporal dependences of change of currents of arcs $I_a(t)$ of the arc furnace DSP-200 during the technological period of boiling of slag at operation of the regulator ARDM-T-12 (differential law)

On the created Simulink-model, mathematical experiments were conducted to study the dynamical indicators at using each of the above-mentioned control laws in the single-circuit ACS (ARDM-T-12 regulator), as well as at the joint action of the electromechanical circuit (ARDM-T-12 arc power regulator) and only high-speed electric circuit for regulating arcs currents (two-circuit structure of ACS [11]) under the action of both deterministic and stationary random coordinate and parametric perturbations in each phase.

As an example, Fig. 14 shows the results of the performed mathematical experiments on the study of the process of working out of deterministic perturbations which resulted in a symmetrical three-phase short circuit in the DSP-200 furnace only at operation of the electromechanical circuit with a differential control law. (Fig. 14,*a*); only high-speed electric circuit (Fig. 14,*b)* and in the case of joint operation of both circuits (two-circuit ACS, Fig. 14,*c*). As can be seen from the processes shown in Fig. 14, at the use of one-circuit ACS (electro-mechanical circuit – ARDMT-T-12 arcs power regulator), the time of regulating arcs currents is t_{reg} = 1.65 s, at operating the high-speed circuit t_{reg} = 0.05 s, and for the two-circuit ACS t_{reg} = 0.125 s. Some increase in the time of regulation in the two-circuit ACS is due to the asymmetry of the dynamics of the regulation of the electromechanical circuit through the phase-phase asymmetry of the parameters of the power elements of the short network of the arc furnace DSP-200.

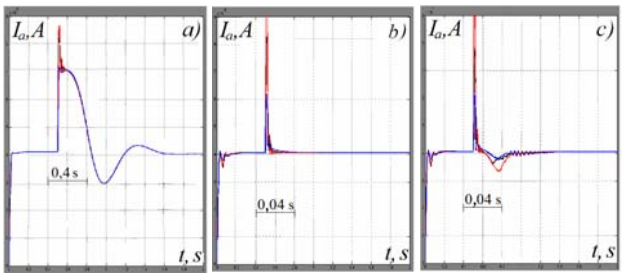

Fig. 14. Arcs currents $I_a(t)$ in three phases at the symmetrical short circuit of the arc DSP-200 and operating ARDM-T-12 (*a*); only high-speed circuit (*b*); and two-circuit ACS (*c*)

Practical interest is the indicators of dynamics of the two-circuit ACS of the electric mode of the DSP-200 in the working out of stationary accidental perturbations along the arc length in different stages of melting, since such disturbances are the main ones on each smelt. That is why on the created Simulink model, a number of mathematical experiments were conducted to study the indicators of the dynamics of the regulation of the EM coordinates, indicators of energy efficiency and electromagnetic compatibility. The purpose of these studies was to obtain integral assessments of the quality of dynamics, in particular the value of the dispersion of currents (voltages, powers) of arcs and indicators of electromagnetic compatibility of arc furnace modes and a network in the operation of a two-circuit ACS, as the most perfect in terms of energy efficiency and, for comparison, the indicators of the other two structures of ACS of the electric modes under the influence of stationary random perturbations in different technological stages of melting.

As an example, Fig. 15, 16 show the temporal dependences of disturbances (Fig. 15,*a* and Fig. 16,*a*) and their corresponding temporal arcs currents dependences (Fig 15,*b* and Fig. 16,*b*) in three phases corresponding to the technological stages of wells collapse and meltdown of a solid charge (Fig. 15 and Fig. 16, respectively), in the operation of the two-circuit system for automatic regulation of arcs currents of the arc furnace DSP-200.

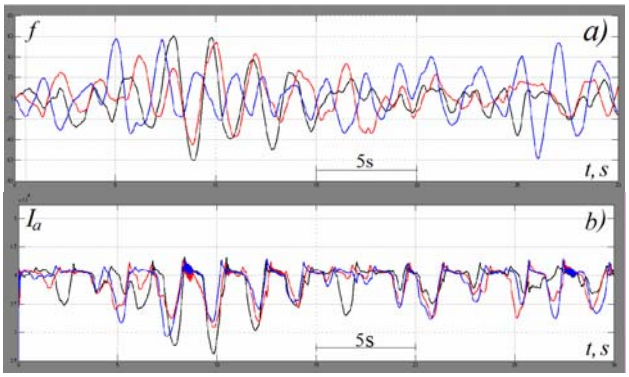

Fig. 15. Perturbations along the lengths of the arcs $f(t)$ in phases (*a*) and the corresponding currents of the arcs $I_a(t)$ (*b*) of the two-circuit ACS at the technological stage of wells collapse

In Table 2 average in phases the values of the dispersions of arcs currents obtained in computer

experiments under the action in arc gaps of the same realizations of three-phase disturbances along the arcs lengths for the same technological stage but at the functioning of different structures of the ACS of the EM of the DSP-200 are presented.

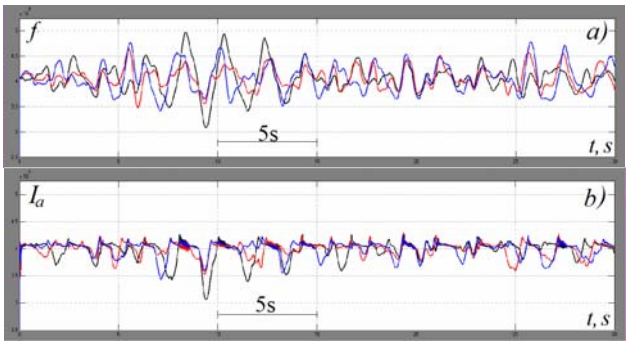

Fig. 16. Perturbations along the lengths of the arcs $f(t)$ in phases (a) and the corresponding currents of the arcs $I_a(t)$ (b) of the two-circuit ACS at the technological stage of meltdown of a solid charge

Table 2

Average over the phases the values of the dispersion of the arcs currents of the DSP-200 furnace for different ACS and different technological stages

ACS structure	Technological stage			
	Start of melting, kA^2	Wells melting, kA^2	Oxidation, kA^2	Refinement, kA^2
One-circuit (ARDM-T-12)	26.0	40	29.0	6.8
High-speed circuit	13.0	16.5	6.9	2.2
Two-circuit	9.5	8.2	6.7	2.0

The analysis of presented in the Table 2 values of dispersions of arcs currents shows that the use in the control system structure of the high-speed electric circuit of regulating arcs currents allows to significantly reduce the dispersion of currents by 2.5-5 times.

Due to the increase of the speed of regulation of arcs currents in the two-circuit structure of the ACS, the phase autonomy (symmetry) of arcs currents regulation, active and reactive powers, as well as the indicators of energy efficiency and electromagnetic compatibility of the arc furnace modes and the network are improved. Table 3 shows the results obtained from model research on the developed Simulink model of integrated estimates of some indicators of electromagnetic compatibility of arc furnace DSP-200 modes and the power supply network.

Table 3

Average in phases indicators of electromagnetic compatibility of the arc furnace DSP-200 during the period of charge melting

Functioning indexes	ACS structures	
	One-circuit ACS	Two-circuit ACS
C_{thd}	0.096	0.081
cosφ	0.82	0.89
δU_{ss}, %	1.42	0.92
F	0.168	0.058

The analysis of the obtained estimates of the parameters of the electromagnetic compatibility of the modes of the DSP-200 furnace and the power supply network at various technological stages of melting showed that the coefficient of distortion of the sinusoidal currents of the power supply network C_{thd} in the operation of the two-circuit ACS compared with the operation of a one-circuit one (power regulator ARDMT-12) decreases by 12-20 %, the coefficient of power cosφ in the operation of the two-circuit ACS increases by 6-10 %, the voltage fluctuations of the power supply network δU_{ss} of the furnace thus decreases by 30-40 %, while the dose of the flicker F-by 48-65 %.

At the same time, due to the significant improvement of the dynamics of arcs currents regulation (reducing the dispersion of arcs currents), in the operation of a two-circuit ACS, the power of electrical losses in a furnace's short network decreases, including for the account of reduced reactive power consumption, respectively the electrical efficiency improves, the dispersion of the arcs power decreases and the uniformity in time and in phases (along the perimeter of the melt) of the input of active power into the furnace improves (thereby melt is more uniformly heating up and, accordingly, the local overheating of the melt and the side walls of the furnace masonry are eliminated). Increasing the speed of regulation of arcs currents positively affects the alignment of the phase loads of the furnace and as a result, the negative effect of the «wild» and «dead» phase is practically eliminated or significantly weakened, as well as the coefficient of phase asymmetry of the electrical supply network voltage is reduced.

Conclusions.

1. Based on the application of the statistic M-criterion of Bartlett it is shown that the created three-phase in instantaneous coordinates Simulink model has sufficient accuracy (adequacy) of the reproduction of the processes of changing arcs currents.

2. Created on the basis of a combination of typical elements of the Simulink application library and SimPowerSystems blocks of the Matlab software, the structured Simulink model of an arc furnace has a convenient setup interface for studying the dynamics indices of the EM and the electromagnetic compatibility indices for different structures and parameters of the ACS and the power circuit of the power supply of three-phase arcs, control laws, dependencies of dynamic volt-ampere characteristics of arcs and parameters of stochastic characteristics of perturbations.

3. Obtained values of quality indicators of dynamics of the investigated structures of the ACS of the EM of the arc furnace DSP-200 have shown that the best indicators of the dynamics inherent in two-circuit control system: compared with one-circuit system (arcs power regulator ARDM-T) the regulation time of arcs currents at working out of extreme disturbances of the electric mode (short-circuit and breakdowns of the arc) using a high-speed circuit in the structure of a two-circuit ACS decreases 20-40 times, and the arcs currents dispersion at working

out the random disturbances at other similar conditions decreases 3-5 times, as well as performance indicators of the electromagnetic compatibility of modes of the arc furnace and power supply network are significantly improved.

REFERENCES

1. Wang Y., Mao Z., Tian H., Li Y., Yuan P. Modeling of electrode system for three-phase electric arc furnace. *Journal of Central South University of Technology*, 2010, vol.17, no.3, pp. 560-565. **doi: 10.1007/s11771-010-0523-3.**

2. Paranchuk Y.S. Modeling and research of electric arc furnace current regulation system modes. *Bulletin of Lviv Polytechnic National University. Series: «Electrical and electromechanical systems»*, 2000, no.403, pp. 126-133. (Ukr).

3. Lozynskyy O.Y., Paranchuk Y.S., Lozynskyy A.O., Maruschak Y.Y. Mathematical model of power supply system and modes control of the EAF-PSN electrotechnology complex. *Scientific Bulletin of the National Mining University*, 2004, no.3, pp. 8-15. (Ukr).

4. Varetsky Y., Lozynsky O., Paranchuk Y. A new design of SVC thyristor controlled reactor. *Proceedings of the International Conference EPQU'03: «Electrical Power Quality and Utilization»*. Krakow, Poland, 2003, pp. 353-360.

5. Balan R., Maties V., Hancu O., Stan S., Lapusan C. Simulation of an electric arc furnace electrode position system. Available at: http://www.freepatentsonline.com/article/Annals-DAAAM-Proceedings/177174488.html (accessed 02 May 2017).

6. Balan R., Maties V., Hancu O., Stan S., Ciprian L. Modeling and control of an electric arc furnace. *2007 Mediterranean Conference on Control & Automation*, Jun. 2007. **doi: 10.1109/med.2007.4433737.**

7. Rahmatollah Hooshmand, Mahdi Banejad, Mahdi Torabian Esfahanj. A new time domain model for electric arc furnace. *Journal of Electrical Engineering*, 2008, vol.59, no.4, pp. 195-202.

8. Mahmood Moghadasian, Emad AlNasser. Modelling and control of electrode system for an electric arc furnace. *2nd International Conference on Research in Science, Engineering and Technology (ICRSET'2014)*, March 21-22, 2014 Dubai (UAE), pp. 129-133. **doi: 10.15242/iie.e0314558.**

9. Paranchuk Y.S. Modeling of the arcs characteristics and processes in arc steelmaking furnace. *Bulletin of Lviv Polytechnic National University. Series: «Electrical and electromechanical systems»*, 2003, no.487, pp. 108-116. (Ukr).

10. Gaydyshev I. *Analiz i obrabotka dannykh: spetsial'nyi spravochnik* [Analysis and processing of data: special reference book]. Saint Petersburg, Piter Publ., 2001. 752 p. (Rus).

11. Paranchuk Y.S. Investigation of the two-level reactive power compensation system in networks with arc steelmaking furnaces. *Technical electrodynamics. Thematic issue «Power electronics & energy efficiency»*, 2004, part 2, pp. 73-78. (Ukr).

Received 20.02.2018

O.Y. Lozynskyi[1]*, Doctor of Technical Sciences, Professor,*
Y.S. Paranchuk[1]*, Doctor of Technical Sciences, Professor,*
R.Y. Paranchuk[1]*, Candidate of Technical Sciences,*
F.D. Matico[1]*, Doctor of Technical Sciences, Associate Professor,*
[1] Lviv Polytechnic National University,
12, S. Bandera Str., Lviv, 79013, Ukraine,
phone +380 2582468,
e-mail: yparanchuk@yahoo.com

How to cite this article:
Lozynskyi O.Y., Paranchuk Y.S., Paranchuk R.Y., Matico F.D. Development of methods and means of computer simulation for studying arc furnace electric modes. *Electrical engineering & electromechanics*, 2018, no.3, pp. 28-36. **doi: 10.20998/2074-272X.2018.3.04.**

UDC 621.3.022: 621.316.9: 537.311.8 **doi: 10.20998/2074-272X.2018.3.05**

M.I. Baranov

POWER DESCRIPTIONS OF A STORM CLOUD OF TROPOSPHERE OF EARTH: FEATURES OF THEIR CALCULATION AND APPLIED UTILIZATION

Purpose. ***Implementation of calculation estimation of such basic power descriptions of the system is a «storm cloud - earth», as total charge of q_Σ, electric potential of φ_r, electric energy of W_0 and amplitude-temporal parameters (ATP) of pulse current $i_L(t)$ in the channel of a long air spark discharge of cloud on earth.*** ***Methodology.*** ***Electrophysics bases of technique of high voltages and large currents, theoretical bases of the electrical engineering, theoretical electrophysics, theory of the electromagnetic field and technique of the strong electric and magnetic fields.*** ***Results.*** ***The results of calculation estimation of basic power descriptions are resulted in the overhigh voltage electrophysics calculation system a «storm cloud - earth». To such descriptions of a storm cloud behave: total electric charge of q_Σ, concentrated in a storm cloud of spherical form of the set volume with the shallow dispersible negatively charged including as particulate dielectric matters the set by an middle closeness; electric potential of φ_r is in the spherical volume of a storm cloud of the set size; electric energy of W_0, accumulated in the spherical volume of a storm cloud of the set radius of R_0; PTP (amplitude of I_{mL} and duration of τ_p at level $0.5I_{mL}$) of aperiodic impulse of current $i_L(t)$ of linear lightning in the plasma channel of a long air spark digit of a storm cloud on earth. The ground of possibility of the use is given in close practical calculations in place of the real storm cloud of the simplified calculation model of a storm cloud, containing the spherical volume of V_0 by the radius of R_0 is shown that at $R_0 \approx 985$ m and accordingly $V_0 \approx 4 \cdot 10^9$ m^3 in the examined model of a storm cloud his indicated power descriptions arrive at the followings numeral values: charge of $q_\Sigma \approx -55.6$ C, potential on the outward surface of cloud of $\varphi_R \approx -506$ MV, electric energy of $W_0 \approx 14.1$ GJ in a cloud and amplitude of aperiodic impulse of current of $I_{mL} \approx -262.1$ кА at duration of his flowing $\tau_p \approx 142.4$ μs in the plasma channel of a long air spark digit of cloud on earth. This calculation information well correlates with the known experimental information, characteristic for the short shots of lightning in surface objects.*** ***The receive results will be instrumental in possibility of prognostication of a sticky storm wicket specialists at presence of only minimum initial information about a storm cloud in earthly troposphere.*** ***Originality.*** ***First at the analysis of a storm situation in troposphere of Earth offered approach, related to bringing the real storm cloud over the volume of V_0 to an equivalent on volume spherical storm cloud by the radius of R_0, for which will apply the physical and mathematical vehicle of analysis of flowings in him electrophysics processes developed an author.*** ***Practical value.*** ***Application of the in practice calculation findings will allow to deepen scientific and technical knowledge in area of nature of atmospheric electricity, will be instrumental in further development of physics of linear lightning and successful decision of global problem of protecting from lightning of surface objects and auxiliary them personnel.*** References 12, figures 2.

Key words: **atmospheric electricity, storm cloud, accumulated charge, electric potential and energy of cloud, current in the channel of discharge of cloud on earth, calculation, experimental information.**

Приведены результаты расчетной оценки основных энергетических характеристик сверхвысоковольтной системы «грозовое облако-земля», содержащей сплошную заряженную сферу облака. В качестве этих характеристик грозового облака рассмотрены: электрический заряд q_Σ, сосредоточенный в сферическом грозовом облаке заданного объема с мелкодисперсными заряженными включениями в виде твердых диэлектрических частиц с усредненной объемной плотностью; электрический потенциал φ_r в сферическом объеме грозового облака заданного радиуса; электрическая энергия W_0, накопленная в сферическом объеме принятого грозового облака; амплитудно-временные параметры тока молнии в плазменном канале длинного воздушного искрового разряда грозового облака на землю. Полученные результаты будут способствовать возможности прогнозирования грозовой обстановки при минимальной исходной метеорологической информации, дальнейшему развитию природы атмосферного электричества, физики линейной молнии и решению глобальной проблемы молниезащиты объектов и обслуживающего их персонала. Библ. 12, рис. 2.

Ключевые слова: **атмосферное электричество, грозовое облако, накопленный заряд, электрический потенциал и энергия облака, ток в канале разряда облака на землю, расчет, экспериментальные данные.**

Introduction. One of the problematic tasks in the field of atmospheric electricity and lightning protection of terrestrial and near-earth air objects still remains one that is connected with the determination, with minimal initial information about the thunderstorm situation in the area of this or that territory of the planet studied by specialists (engineers and meteorologists) energy characteristics of the thundercloud cloud in the Earth's troposphere. Such characteristics of a thundercloud include: firstly, the total electric charge q_Σ accumulated in such a cloud; secondly, the electric potential φ_r in the volume of a thunderstorm cloud; thirdly, the electric energy W_0 accumulated by fine-dispersed inclusions (for example, small drops and water vapor, small granules and ice crystals and small solid dielectric particles [1, 2]) of the atmospheric cloud under consideration in the «storm cloud - earth» electrostatic system; fourth, the probable amplitude-temporal parameters (ATPs) of the pulsed current $i_L(t)$ in the channel of the high-current discharge of a thunderstorm cloud to the ground or to the protected object. Their forecast of a possible thunderstorm threat to land-based objects and aircraft caught up in the area of the atmospheric cloud depend on these data. Knowledge of indicated energy characteristics of a thunderstorm cloud makes it possible to predict a thunderstorm situation in

the investigated area of terrestrial land, and also in a certain way extends knowledge of people in the field of atmospheric electricity and the physics of a long air spark discharge (lightning) and the consequences of its (this high-current discharge) action on the protected objects and their environment. It should be noted that usually under a thundercloud, meteorologists understand a cumulonimbus cloud for which a number of critical conditions are met as indicated in [1]. As for the concept of the Earth's troposphere, it means the lower part of the earth's atmosphere, with a height of up to 11 km in temperate latitudes which contains 4/5 of the entire mass of the atmosphere, almost all water vapor, and various kinds of clouds develop [1, 3]. In this connection, an approximate determination by calculation of the quantities q_Σ, φ_r, W_0 and ATPs of the discharge current $i_L(t)$ in the superhigh-voltage electrostatic system «thundercloud - earth» in which the atmospheric cloud has even a canonical geometric shape and a simplified internal «stuffing» from a number of above-mentioned fine-dispersed inclusions, is an actual applied scientific and technical task of great importance in the world.

The goal of the paper is the calculation estimation of such basic energy characteristics of the «lightning cloud - ground» system as the charge q_Σ, the potential φ_r, the energy W_0 and the amplitude-temporal parameters of the pulsed current $i_L(t)$ in the channel of the long air spark discharge of the cloud to the earth.

1. Problem definition. For convenience in analyzing the distribution of atmospheric electricity in the Earth's troposphere, let us consider one of the special cases when the thundercloud has the shape of a sphere of radius $R_0\approx985$ m (Fig. 1), inside which, with an average volume density $N_0\approx5\cdot10^7$ m^{-3}, solid dielectric particles with a radius $r_0\approx10\cdot10^{-6}$ m are mainly placed[1], each of which at the stage of formation of the cumulonimbus cloud obtained by electrifying in the warm ascending air streams of the Earth's atmosphere a negative electric charge of $q_0\approx -2.78\cdot10^{-16}$ C and at the stage of formation of a thunderstorm cloud was freed from the covered them electrically neutral molecular dipoles of water [2]. The choice of the indicated numerical value of radius R_0 of the cloud was due to the fact that in order to simplify the calculations, as in [2], its initial calculation volume $V_0\approx4\cdot10^9$ m^3 was a rectangular prism with dimensions in a horizontal base of 1000 m × 1000 m and a height of 4000 m, the center of which was located at a height of $H_0\approx3000$ m above the flat surface of the Earth (see Fig. 1). According to [1] it is from such heights that the formation of cloud charges begins in the Earth's troposphere. Proceeding from the fact that in the adopted approximation $V_0=4\pi R_0^3/3=4\cdot10^9$ m^3, and this numerical value of R_0 follows. As for the numerical values of the quantities N_0 and r_0, they were chosen by us on the basis of the experimental data given in [1]. The calculation determination in the cloud of the indicated numerical value of the charge $q_0\approx-2.78\cdot10^{-16}$ C of solid dielectric particles of radius $r_0\approx10\cdot10^{-6}$ m was carried out in [2], taking into account the theory of a double electric layer, the foundations of which are given in [1, 4]. Individual charges q_0 of density N_0 determine in the cloud their averaged volume density $\sigma_V\approx q_0N_0\approx-1.39\cdot10^{-8}$ C/m^3, uniformly distributed over its spherical volume V_0. Let normal atmospheric conditions be satisfied in the air gap of the «lightning cloud - earth» system (the air pressure is about $1.013\cdot10^5$ Pa, and its temperature is 0 °C. [4] It is required, taking into account these assumptions, in approximate form, to determine by calculations the required values of the accumulated by the thunderstorm cloud of the total charge q_Σ, the electric potential φ_r in the spherical volume of the thunderstorm cloud, its electric energy W_0 and the ATPs of the discharge pulsed current $i_L(t)$ in the electrostatic system «thunder cloud - earth».

2. Calculation estimation the electric charge q_Σ of a thunderstorm cloud. Taking into account the above assumptions at the stage of the formation of a thunderstorm cloud accompanied by the «liberation» of its separate numerous charges q_0 from electrically neutral molecular water dipoles [2], the total electric charge q_Σ of the atmospheric cloud under consideration can be determined in the following form:

$$q_\Sigma = q_0N_0V_0\,. \qquad (1)$$

From (1) at accepted initial data when $q_0\approx-2.78\cdot10^{-16}$ C, $N_0\approx5\cdot10^7$ n^{-3} and $V_0\approx4\cdot10^9$ m^3, it is following than in the considered case the value of $q_\Sigma\approx -55.6$ C.

The modulus of the numerical value of the total electric charge $q_\Sigma\approx55.6$ C in the considered lightning cloud obtained in accordance with (1) completely corresponds to the normalized charge $q_L=(50\pm10)$ C for a short lightning strike with a pulsed discharge aperiodic current of a temporal shape 10 μs/350 μs to ground technical facilities that satisfy III-IV lightning protection levels according to the requirements of the International Standard IEC 62305-1:2010 [5, 6].

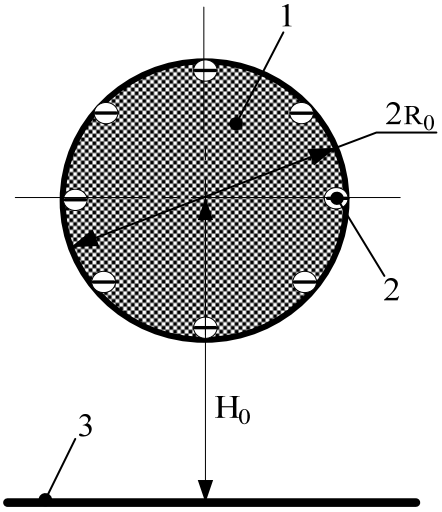

Fig. 1. Schematic view of a simplified calculation model of a negatively charged thunderstorm cloud of spherical shape located above the Earth's flat surface
(1 – cloud, 2 – electron, 3 – flat surface of the Earth)

In addition, we indicate that the used numerical value of the averaged volume charge density of the

lightning cloud under investigation, defined as $\sigma_V \approx q_0 N_0 \approx -1.39 \cdot 10^{-8}$ C/m^3, corresponds to known experimental data for the mean value of the space charge density in a thunderstorm cloud [1 , 2].

3. Calculation estimation of the electric potential φ_r of a thunderstorm cloud. Applying the approach given in [7] to finding in the cloud the values of the electric potential φ_r for the radial distribution of the required potential φ_r in the simplified model of the thundercloud, we obtain:

$$\varphi_r = q_\Sigma (3R_0^2 - r^2)/(8\pi\varepsilon_0 R_0^3) , \qquad (2)$$

where r is the current radius in the spherical volume of the cloud; ε_0=8.854·10^{-12} F/m is the electric constant[4].

From (2) at r=0 for the electric potential φ_r=φ_0 in the center of the assumed thunderstorm cloud, we find:

$$\varphi_0 = 3q_\Sigma /(8\pi\varepsilon_0 R_0) . \qquad (3)$$

At r=R_0 from (2) for the electric potential φ_r=φ_R the following calculation relation follows on the outer surface of the sphere of a thunderstorm cloud:

$$\varphi_R = q_\Sigma /(4\pi\varepsilon_0 R_0) . \qquad (4)$$

Analysis of the above calculation expressions (3), (4) shows that the electric potential φ_0 in the center of the thunderstorm cloud is 1.5 times higher than the electric potential φ_R acquired by the outer spherical surface of the cloud. Hence, the deep mechanism of charge «recharge» of the plasma channel of a long spark discharge of a thundercloud on the ground or a protected technical object becomes physically more understandable in the theory of atmospheric electricity. After all, at such a radial distribution in the thundercloud of the electric potential φ_r in the case of an electric discharge in the «thunder cloud - earth» system (see Fig. 1) of an air gap of length (H_0−R_0) to compensate the decrease of the electric potential φ_R on the outer surface of the cloud to it from inner zones of a cloud with a higher electric potential φ_r, the electric charges (in our case free electrons) will «leak» which replenish the carriers of the electric current $i_L(t)$ in the channel of the discharge itself.

Numerical estimation by (3), (4) of the electrical potentials inside and outside the thunderstorm cloud under consideration at $q_\Sigma \approx -55.6$ C and $R_0 \approx 985$ m indicates that in this case the required values are approximately equal by modulus to $\varphi_0 \approx 759$ MV and $\varphi_R \approx 506$ MV. From the quantitative data known to the author for the electric potential φ_r of a thunderstorm cloud, only its numerical value of about 100 MV, given in [8], can be indicated.

In order to verify the reliability of the obtained electric potential value $\varphi_R \approx 506$ MV of the thunderstorm cloud under consideration, let us use a numerical estimation of the value of the electrostatic field strength E_R near its outer spherical surface ($r \approx R_0$). On the one hand, $E_R \approx \varphi_R/R_0 \approx 513$ kV/m [4]. On the other hand, in order to find E_R in the investigated electrostatic case, we apply a more accurate analytic relation of the form [2, 7]:

$$E_R = q_\Sigma /(4\pi\varepsilon_0 R_0^2) . \qquad (5)$$

From (5) at $q_\Sigma \approx 55.6$ C and $R_0 \approx 985$ m we find that $E_R \approx 515$ kV/m. It is evident that both numerical values given for E_R practically coincide. In this connection, we can speak of the efficiency of the calculated ratios (1), (4) that determine the total charge q_Σ in the adopted thunderstorm cloud model and the electric potential φ_R of the outer spherical surface of the cloud under investigation. By the way, the value of E_R by (5) is the largest in the radial distribution of the electrostatic field strength in the spherical volume V_0 of the cloud. As is well known, for this high E-field according to a relation of the form [2, 7]:

$$E_r = q_\Sigma r /(4\pi\varepsilon_0 R_0^3) , \qquad (6)$$

at r = 0 the strength E_r will be equal to zero (at $r = R_0$ (6) becomes (5) and determines the level of the E-field on the outer surface of this cloud).

The data presented for the radial distribution of the electrostatic field strength E_r in the «storm cloud - earth» system unequivocally indicate that in the case of a homogeneous (in the composition [3]) character of the change in the carriers of electricity in the spherical volume V_0 of the assumed thunderstorm cloud, the development of electron avalanches [1, 8] which are the forerunner of the appearance in our system of lightning (spark breakdown in the troposphere of the Earth of a long air gap) will always start from the outer surface of the cloud. Note that the indicated numerical value of $E_R \approx 515$ kV/m at the accepted atmospheric conditions approaches the critical E-field value corresponding to the pre-breakdown stage of processes in the long air gap our system of the length (H_0−R_0) of our system [1, 8].

4. Calculation estimation of the electrical energy W_0 of a thunderstorm cloud. Preliminary calculation estimations of the numerical values of the electric energy W_0 accumulated in the storm cloud under investigation revealed the presence of a number of features in its determination. Thus, it turned out that the direct application of the principles and formulas from [9] for its electric capacitance to the calculation system «thunder cloud - earth» (see Fig. 1) leads to erroneous results in calculating the values of the W_0 energy of a thunderstorm cloud. In order to demonstrate the results obtained with respect to the energy W_0 with such a calculated approach, we first start from the fact that at the electric potential φ_R of the cloud found above (in Section 3) and the a priori zero earth electrical potential (φ_E=0) for calculating of the electrical energy W_0 for the «storm cloud - earth» calculation system that is used, it remains to determine only the value of its electrical capacitance. The «direct» definition in the case under consideration ($H_0/R_0 \approx 3.04$) of its electrical capacitance C_0, according to the recommended [9] for the inequality H_0/R_0>1.5 an approximate formula of the form:

$$C_0 = 2\pi\varepsilon_0 / \ln(2H_0 / R_0) , \qquad (7)$$

leads to significantly lowered values of the electrical capacitance in the calculation system «thunder cloud -

earth». For example, assuming the initial data H_0≈3000 m and R_0≈985 m, according to (7), the value of C_0 is approximately C_0≈30.8·10^{-12} F. Therefore, the value W_0≈$C_0U_0^2$/2 [4], where U_0=(φ_R − φ_E) is the difference between the electrical potentials of a thunderstorm cloud and a flat ground surface, assumes a numerical value of only 3.94 MJ for U_0≈506 MV and the huge volume V_0≈4·10^9 m^3 of a thunderstorm cloud used by us. The reason for this is that (7) takes into account only the distribution of electric charge along the outer surface of the calculated sphere of radius R_0. It does not take into account the effect of the electric charge distributed with volume density σ_V≈q_0N_0 in volume V_0=4πR_0^3/3 of this sphere. In this regard, the value of the electric energy W_0 of a thunderstorm cloud is recommended to be determined by the following approximate relationship:

$$W_0 \approx 0{,}5C_EU_0^2, \qquad (8)$$

where C_E≈q_Σ/U_0 is the equivalent capacitance of the superhigh-voltage system «thunder cloud - earth».

It should be noted that when using (8) a some error is introduced into the approximate calculation of C_E and W_0 values, due to the previously described the corresponding radial distribution of the electric potential φ_r over the spherical volume of the received thunderstorm cloud. However, this error is incommensurable small in comparison with the error introduced by (7) into the calculation of the electric capacitance and electric energy W_0 in our system «thunder cloud - earth».

From (8) at q_Σ≈−55.6 C и U_0≈−506 MV, we find that with the recommended author's approach for the system «thunder cloud - earth» under consideration, the value of its equivalent electric capacitance C_E will assume a numerical value of about 1.1·10^{-7} F, and the value of electric energy accumulated in it is W_0≈14.1·10^9 J (as we see, it is almost 3578 times larger than with the use of formula (7) in calculating C_0 and W_0). The author currently does not have quantitative data for W_0 by other researchers of atmospheric electricity in the world. It can only be assumed that if the values of the total charge q_Σ by (1) and the electric potential φ_R by (4) are found correctly (we have given the above fairly convincing electrophysical justifications of these calculations), then the approximate determination by (8) of the value of the electric energy W_0 of the thunderstorm cloud is also correct.

5. Calculation estimation of the ATP of current $i_L(t)$ in the thunderstorm discharge channel on the earth. For this estimation, with reference to the discharge circuit of the capacitance C_E of the thunderstorm cloud through the plasma channel in the air to the earth, we use the classical electrical engineering approach characteristic for electromagnetic processes in the *RLC* circuit [10]. First, we estimate the numerical value of the inductance L_k of a cylindrical plasma channel with the radius r_k of a high-current spark discharge of a thunderstorm cloud in the air gap of length l_k≈(H_0–R_0) to the earth according to the following formula [11]:

$$L_k = (2\pi)^{-1}\mu_0 l_k\left[\ln(2l_k / r_k) - 1\right], \qquad (9)$$

where μ_0=4π·10^{-7} H/m is the magnetic constant [4].

From (9), at l_k≈(H_0–R_0)≈2015 m and r_k≈11·10^{-3} m [12] it follows that in our case the concentrated inductance L_k of the thunderstorm cloud discharge channel on the earth will take a value numerically equal to about 4.76 mH. When evaluating the numerical value of the active resistance R_k of a cylindrical lightning air discharge channel, we proceed from the fact that the line active resistance R_{k0} of the investigated high-current channel, according to the calculation-experimental data from [12] for the repetitive pulsed *D*- component of the artificial lightning current of the amplitude I_{mD}≈–92.3 kA (Fig. 2, where t t_{mD}≈15 μs is the time corresponding to the first amplitude I_{mD} of the current) is numerically about 0.92 Ω/m. As a result, for the active resistance R_k of the thunderstorm plasma channel of the investigated cloud to the earth (see Fig. 1) we find that R_k ≈R_{k0}·l_k ≈ 0.92 Ω·m^{-1} × × 2015 m ≈ ≈ 1.85 kΩ. It is seen that in the case under consideration the inequality R_k>2(L_k/C_E)$^{1/2}$ is satisfied for the electrical parameters R_k, L_k and C_E of the discharge circuit under consideration. This means that an aperiodic current pulse $i_L(t)$ will flow in the lightning current channel [10, 12].

For the ATP of the discharge current $i_L(t)$ at an aperiodic law of its variation with time t, the following calculation relation can be used [10, 12]:

$$i_L(t) = U_0\left[(\alpha_2 - \alpha_1)L_k\right]^{-1}\left[\exp(-\alpha_1 t) - \exp(-\alpha_2 t)\right], \qquad (10)$$

where α_1, α_2 are the pulsed current shape coefficients equal to α_1=δ–(δ^2–ω_0^2)$^{1/2}$ and α_2=δ+(δ^2–ω_0^2)$^{1/2}$; δ=R_k/(2L_k) is the attenuation coefficient of discharge current; ω_0=(L_kC_E)$^{-1/2}$ is the own circular frequency of the discharge current of a cloud.

The time t_{mL} corresponding to the amplitude I_{mL} of the lightning current of the discharge in accordance with (10) will be equal to the analytical relation known in electrical engineering [10]:

$$t_{mL} = \ln(\alpha_2 / \alpha_1)/(\alpha_2 - \alpha_1). \qquad (11)$$

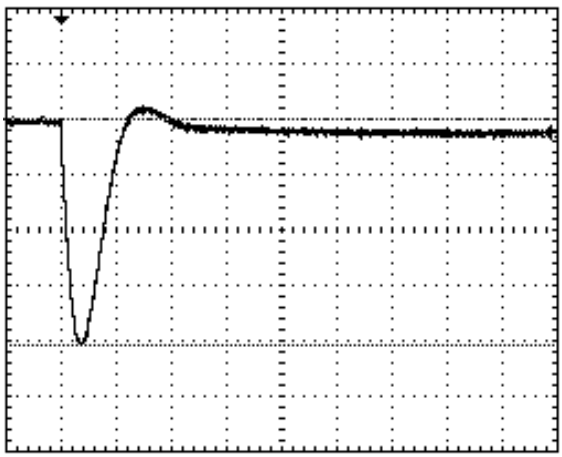

Fig. 2. Typical oscillogram of the *D*- component of the current Of artificial lightning (I_{mD}≈–92.3 kA; t_{mD}≈15 μs, vertical scale – 22.52 kA/cell, horizontal scale – 50 μs/cell) obtained in the high-current discharge circuit of the high-voltage lightning current generator УИТОМ-1 [12]

For the obtained initial data R_k≈1.85 kΩ, L_k ≈ 4.76 mH and C_E≈110 nF, we see that in the case under consideration: $\delta \approx 1.94 \cdot 10^5$ s^{-1}; $\omega_0 \approx 43.7 \cdot 10^3$ s^{-1}; $\alpha_1 \approx 5 \cdot 10^3$ s^{-1}; $\alpha_2 \approx 3.83 \cdot 10^5$ s^{-1}; $t_{mL} \approx 11.47$ μs (see Fig. 2, where the experimental time for the pulse amplitude of the artificial lightning current was about 15 μs). At $U_0 \approx -506$ MV and $t_{mL} \approx 11.47$ μs, the calculated value of the amplitude of the lightning current for the investigated case according to (10) will be approximately $I_{mL} \approx -262.1$ kA. The obtained quantitative values for t_{mL} and the amplitude I_{mL} of the current in the discharge channel of the assumed thunderstorm cloud to earth are well correlated with the ATPs of the pulse current characteristic for short strokes of the linear lightning to ground objects satisfying the I level of their lightning protection according to the stringent requirements of the International Standard IEC 62305-1:2010 [5, 6]. As for the duration τ_p of the aperiodic lightning current pulse at the level 0.5 I_{mL}, for our case it is approximately equal to $\tau_p \approx 0{,}7 R_k C_E \approx 142.4$ μs. Thus, with minimal information on the electromagnetic situation in the zone of formation and development of a thunderstorm cloud (only in terms of its approximate dimensions and height of placement above the Earth's surface), experts can reasonably predict a thunderstorm «picture» for the superhigh-voltage electrophysical system «thunder cloud - earth» under consideration.

Conclusions.

1. It is shown that by engineers and meteorologists a spherical cloud model with an outer radius R_0 and a volume $V_0 = 4\pi R_0^3/3$ can be adopted as a simplified calculation model of a thundercloud cloud containing distributed over its spherical volume with an average density of $N_0 \approx 5 \cdot 10^7$ m^{-3} negatively electrified in the warm ascending air flows of the Earth's troposphere, small solid dielectric particles with a radius of $r_0 \approx 10 \cdot 10^{-6}$ m and a charge of $q_0 \approx -2{,}78 \cdot 10^{-16}$ C. Varying the numerical values of the radius R_0 and, correspondingly, the volume V_0 of such a thundercloud cloud, one can also change its basic energy characteristics within a wide range corresponding to the normative and technical documents in force in the world.

2. An example of a thunderstorm cloud of the Earth's troposphere of radius $R_0 \approx 985$ m and volume $V_0 \approx 4 \cdot 10^9$ m^3 at $H_0 \approx 3000$ m demonstrates the possibilities of the proposed approach in the field of atmospheric electricity investigations for the approximate determination by specialists of the modules of such its energy characteristics as the total electric charge $q_\Sigma \approx 55.6$ C, electric potential at the center $\varphi_0 \approx 759$ MV and on the outer surface $\varphi_R \approx 506$ MV of the cloud, accumulated by fine-dispersed inclusions of the cloud electric energy $W_0 \approx 14.1$ GJ and ATPs of the aperiodic impulse current $i_L(t)$ in the plasma channel of the long air spark discharge of the cloud to earth ($I_{mL} \approx 262.1$ kA; $t_{mL} \approx 11.5$ μs; $\tau_p \approx 142.4$ μs). The obtained quantitative data for q_Σ, φ_R, W_0 and ATPs of lightning impulse current on the earth's surface satisfy a number of requirements of the International Standard IEC 62305-1:2010 for short strokes of linear lightning to ground objects.

3. The results obtained will contribute to the possible fulfillment by engineers and meteorologists of the prediction of the electromagnetic situation in the area of formation and development in the Earth's troposphere of a real thunderstorm cloud, previously reduced by the volume of V_0 occupied by it to an equivalent storm cloud of spherical shape with radius R_0. This approach, thanks to the developed physical and mathematical apparatus, makes it possible in an approximate form to find the indicated basic energy characteristics (q_Σ, φ_R, W_0 and ATPs of the channel current) of an equivalent thundercloud cloud and opens up certain new possibilities in the world practice of solving the actual problems of lightning protection of ground objects and in-flight aircraft that have found themselves in a hazardous zone of high electromagnetic influence on their electrical equipment (first of all, on their low-current electronics) of a thunderstorm cloud with its huge in terms of numerical indicators energy characteristics.

REFERENCES

1. Bortnik I.M., Beloglovskiy A.A., Vereshchagin I.P., Vershinin Yu.N., Kalinin A.V., Kuchinskiy G.S., Larionov V.P., Monastyrskiy A.E., Orlov A.V., Temnikov A.G., Pintal' Yu.S., Sergeev Yu.G., Sokolova M.V. *Elekrophizicheskie osnovy techniki vysokih naprjazhenij* [Electrophysics bases of technique of high voltage]. Moscow, Publishing house of MEI, 2010. 704 p. (Rus).

2. Baranov M.I. New hypothesis and electrophysics nature of additional mechanisms of origin, accumulation and division of electric charges in the atmospheric clouds of Earth. *Electrical engineering & electromechanics*, 2018, no.1, pp. 46-53. **doi: 10.20998/2074-272X.2018.1.07.**

3. *Bol'shoj illjustrirovannyj slovar' inostrannyh slov* [Large illustrated dictionary of foreign words]. Moscow, Russkie slovari Publ., 2004. 957 p. (Rus).

4. Kuz'michev V.E. *Zakony i formuly fiziki* [Laws and formulas of physics]. Kiev, Naukova Dumka Publ., 1989. 864 p. (Rus).

5. IEC 62305-1: 2010 «Protection against lightning. Part 1: General principles». Geneva, IEC Publ., 2010.

6. Baranov M.I., Koliushko G.M., Kravchenko V.I., Rudakov S.V. A generator of aperiodic current pulses of artificial lightning with a rationed temporal form of 10 μs/350 μs with an amplitude of ±(100–200) kA. *Instruments and Experimental Techniques*, 2015, vol.58, no.6, pp. 745-750. **doi: 10.1134/s0020441215060032.**

7. Javorskij B.M., Detlaf A.A. *Spravochnik po fizike* [Handbook of physics]. Moscow, Nauka Publ., 1990. 624 p. (Rus).

8. Brzhezitskiy V.A., Bilyy I.V., Boyko N.I., Gul′ V.I., Gurin A.G., Il′enko O.S., Isakova A.V., Kondra B.M., Kopshin V.A., Kravchenko V.I., Naboka B.G., Protsenko O.R., Rudakov V.V., Khimenko L.T., Khominich V.I., Shostak V.A., Yanishevskiy V.I. *Tehnika i elektrophizika vysokih naprjazhenij* [Technics and Electrophysics of High Voltages]. Kharkiv, Tornado Publ., 2005. 930 p. (Ukr).

9. Iossel' Yu.Ya., Kochanov E.S., Strunskiy M.G. *Raschet elektricheskoj emkosti* [Calculation of electric capacity]. Leningrad, Energoizdat Publ., 1981. 288 p. (Rus).

10. Neyman L.R., Demirchyan K.S. *Teoreticheskie osnovy elektrotekhniki. V 2-kh t. T. 1* [Theoretical bases of electrical engineering. In 2 vols. Vol. 1]. Leningrad, Energoizdat Publ., 1981, p. 536. (Rus).
11. Knopfel' G. *Sverkhsil'nye impul'snye magnitnye polia* [Ultra strong pulsed magnetic fields]. Moscow, Mir Publ., 1972. 391 p. (Rus).
12. Baranov M.I. *Izbrannye voprosy elektrofiziki. Tom 3: Teorija i praktika elektrofizicheskih zadach* [Selected topics of Electrophysics. Vol. 3: Theory and practice of electrophysics tasks]. Kharkiv, Tochka Publ., 2014. 400 p. (Rus).

Received 19.02.2018

M.I. Baranov, Doctor of Technical Science, Chief Researcher,
Scientific-&-Research Planning-&-Design Institute «Molniya»
National Technical University «Kharkiv Polytechnic Institute»,
47, Shevchenko Str., Kharkiv, 61013, Ukraine,
phone +380 57 7076841,
e-mail: baranovmi@kpi.kharkov.ua

How to cite this article:
Baranov M.I. Power descriptions of a storm cloud of troposphere of Earth: features of their calculation and applied utilization. *Electrical engineering & electromechanics*, 2018, no.3, pp. 37-42. **doi: 10.20998/2074-272X.2018.3.05.**

UDC 621.318:537.852 **doi: 10.20998/2074-272X.2018.3.06**

Yu.V. Batygin, E.A. Chaplygin, S.A. Shinderuk, V.A. Strelnikova

THE MAIN INVENTIONS FOR TECHNOLOGIES OF THE MAGNETIC-PULSED ATTRACTION OF THE SHEET METALS. A BRIEF REVIEW

Purpose. ***The description of the Equipment for the Magnetic-Pulsed Attraction (or EMF-attraction) of the sheet metals which allows non-contact deforming of ferromagnetics (the low carbon steels, for example), the non-magnetic billets from aluminium alloys and the practical realization of the new advanced technologies in the modern processing manufacture.*** ***Methodology.*** ***Comparative analysis of characteristics and operating conditions of the systems under consideration.*** ***Results.*** ***Physically, all magnetic-pulsed methods of attraction are based on the Lorentz repelling forces decreasing and on increasing the attracting forces when the sheet billets being deformed are transparent for the low working frequency acting electromagnetic fields. The ferromagnetic samples attraction is caused by their magnetic properties. For the non-magnetic metals attraction an accessory conducting screen is being introduced in construction of the inductor system which is the method tool. In this case the attraction effect is caused by the force interaction of the unidirectional currents induced in the screen and in sheet billet. The different constructions of the attracting tools attended for fulfilling the different production operations (for example, it can be stamping, flattening etc.) with metals owning by different electrophysical properties are represented.*** ***Originality.*** ***The novelties in the magnetic pulsed installations used as the power sources in the complex equipment for the automobile bodies repair are given.*** ***Practical value.*** ***The practical application of the elaborated systems for the dents removing in the sheet metals are suggested and successfully approbated. In the whole these works can be considered as new scientific direction and used for different manufacturing aims though the main attention is paid to the practical application in the field of the automobile bodies repair. The most part of the described inventions is defended by the Ukrainian Patents (23 from total quantity – 33 References) and little known to the west specialists in the area of the magnetic pulsed technologies. From the authors view point this is a main particularity and usefulness of the present paper.*** References 33, figures 11.

Key words: **magnetic-pulse metal working, electromagnetic forming, electromagnetic attractive forces, ferromagnetic materials, non-magnetic metals, low frequency discharges.**

В статье описано оборудование, предназначенное для магнитно-импульсного притяжения листовых металлов, которое позволяет бесконтактное деформирование, как ферромагнетиков, так и немагнитных заготовок из алюминиевых сплавов и практического применения новых передовых технологий в современной индустрии. Притяжение ферромагнитных образцов обусловлено их магнитными свойствами. Для притяжения немагнитных металлов в конструкцию индукторной системы, являющейся инструментом метода, вводится вспомогательный проводящий экран. Представлены различные конструкции инструментов притяжения для выполнения различных производственных операций по обработке металлов, обладающих различными электрофизическими свойствами. Описана новизна магнитно-импульсных установок, используемых в качестве источников энергии в комплексах оборудовании для ремонта автомобильных кузовов. Библ. 33, рис. 11.

Ключевые слова: **магнитно-импульсная обработка металлов, электромагнитная формовка, электромагнитные силы притяжения, ферромагнитные металлы, немагнитные металлы, низкочастотные разряды.**

Introduction. The Magnetic-Pulse Metal Working (the abbreviation – MPMW, the other known title is Electromagnetic Forming, the abbreviation – EMF) is a field of the Mechanical Engineering using an impulse or high speed forming technologies united by general principle of action the essence of which consists in the force action of the pulsed electromagnetic fields on the conducting work-pieces. In the recent very detailed review [1] provided a development historical perspective of the MPMW traditional technologies and highlighted the state of the art on modeling, coil design, sheet metal forming, tube forming, crimping, welding, cutting, spring-back calibration and hybrid processes including the Magnetic-Pulsed Methods. Besides it was marked that good electrical conductivity of the work-pieces metal is the major requirement for the traditional MPMW to be efficient. Practically, the last remark means using rather high frequencies of the acting electromagnetic fields. All applications discussed by [1] are based on repelling so named Lorentz forces between the EMF-tool and conductive blank. In such configuration, the tool and other accessories (forming die, mandrel to which the blank is welded or crimped, shearing edge which is cutting the blank) are positioned from opposite sides of the blank. But there is another configuration of the EMF processes where the blank is attracted to the tool working surface. This is the new both scientific and practical development direction the modern Magnetic-Pulse Metal Working.

The goal of the paper is the description of the main inventions and the according technology operations in the field of the Magnetic Pulsed Attraction of the sheet metals which can be realized for different manufacturing aims though the main attention is paid to the practical application in the field of the automobile bodies repair. Concretely this is an external non-contact removal of the dents on their surfaces. A main particularity of this paper consists in a wide illumination of the author's inventions in Ukraine created on a base of the great practical experience and little known to the west specialists in this area of the magnetic pulsed technologies. These inventions defended by the national patents are evidence not only of advancement in the marked new direction of the modern MPMW. They open the real possible ways for creation of the progressive industrial technologies in the present and probably in a future.

The attraction under superposition of the high and low frequency electromagnetic processes. Chronologically, this review should be started from the first fundamental suggestion by the metals electromagnetic attraction which was formulated in the middle of the last century yet. In 1965 H.P. Furth patented the EMF process with the multiturn coil and an additional single turn with open ends [2]. The electric discharge employed for this process was rather slow and, therefore, allowed diffusion of electromagnetic field through the blank. After the induced voltage

achieves of some determined value the additional single turn with initially opened ends will be short circuited by the electrical discharge spark what will conduct to electromagnetic field eliminating from the side of the blank facing the coil. As result, the electromagnetic pressure from the side of the blank facing the coil was absent, while the pressure from the diffused electromagnetic field to the opposite side of the blank attracted it to the coil. In fact, issuing from the modern physical conceptions the described process consists in generating two frequencies of discharge: slow and fast. The fast discharge eliminates the slow field from the side of the blank facing the coil while the slow field diffused through the thickness of the sheet metal deforms the blank. This physical principle was incorporated in a number of the next electromagnetic tool designs and configurations. So, Hansen and Hendrickson [3] suggested a method and apparatus for electromagnetically removing dents from conductive materials by introducing a slow discharge through a multiturn coil and a rapid pulse of countercurrent. In [4] introduced a system of two coils and portable pulse generator generating both repelling and pulling forces to correct both concave and convex areas of the dent. In [5] introduced a crow bar system capable of shaping the pulse comprised of the fast and slow frequencies in most favorable way for the dent removal process. The final modern construction of the electromagnetic attraction systems with two working frequencies was elaborated by engineers of American firms «Electroimpact» and «Fluxtronic» [6, 7]. Given devices (Fig. 1) are intended for the dents removing on the damaged airplanes bodies panels. Their distinguished particularity is a work in regime of many-times repeating the force actions. As inventors verify this regime is obligatory for the dent removing. Deforming the damaged panel metal is impossible under the single pulse of the force action. The practical possibilities of «Electromagnetic Dent Removers (EDR)» of «Electroimpact» and «Fluxtronic» allow successful straightening the aluminum sheets by thickness about ~ 2 mm. Proceeding from obvious physical evaluations the represented EDR will not be able to work with ferromagnetics. Influence of their magnetic properties will mean the fields penetration intensity decreasing and as consequence the attraction forces falling down.

Another purely theoretical concept of sheet metal attraction by the coil was introduced in 1981 by Shneerson based on sudden interruption of a single frequency discharge [8]. In this case, the diffused electromagnetic field still produces the attraction forces. Should be noted this approach is similar to the before described two-frequency methods. Shneerson's suggestion looks simpler. However, its efficiency is dependent upon how fast the discharge can be interrupted. But it is very complicated technical problem. Generalizing above conducted consideration leads to conclusion: the main disadvantages of all two-frequency suggestions consist in their very complicated technical realizing, the power electronics usage, the different temporal processes synchronization etc. As result the high price of the produced equipment has a place.

The tools of the ferromagnetics attraction by the low frequency electromagnetic fields. The concept of a sheet metal single frequency attraction was introduced in [9, 10] for ferromagnetic materials.

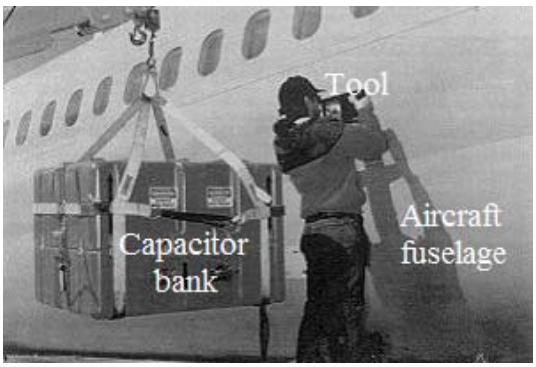

a

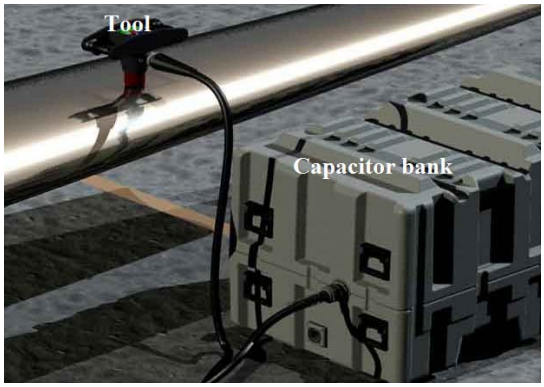

b

c

Fig. 1. The equipment and realization of the technological processes: *a*) the technology of «Electroimpact»; *b*) the equipment of «Fluxtronic»; *c*) the technology of «Fluxtronic»

This concept was discovered during EMF experiments with thin steel sheet plates deformed by electric discharges with different frequencies. The suggested concept quickly found its practical application in dent removal devices in automotive bodies where majority of exterior panels are fabricated from low carbon steel. The discovered phenomenon was laid in a base of [11]. The identical Patent Application was given in [12]. They have represented the specific coil designs as well as practical aspects of dent removal in automotive panels. Here should be added that Concern «Betaginnovation» by the representatives of which are the mentioned above applicants of patents have represented the technical complex titled as «Magnetic Dent Remover (MDR)» [13]. The single frequency experiments initially discussed in [14] indicated that the direction of the electromagnetic pressure for ferromagnetic steel sheet metal blanks is a function of the frequency of the discharge. At some limit, the applied electromagnetic force was changing its direction.

For high frequencies repelling took place, but for low frequencies attraction was watched at. Formally, the acceptable low frequencies diapason had been fixed in [9] and in [10] to the ferromagnetics attraction:

$$\omega << \frac{1}{\mu \cdot \gamma \cdot d^2}, \qquad (1)$$

where $\omega = 2\pi \cdot f$ – the working frequency, μ – the permeability of metal, γ – electrical conductivity of sheet metal, and d – sheet metal thickness.

It should explain that formula (1) provides only the upper limit of the frequency where attraction can be expected. The actual boundary frequency between attraction and repelling can be order of magnitude lower. Physically, formula (1) can be further interpreted in the following way: it compares the sheet metal thickness with the skin-layer value for the given frequency. After not complicated transforming the inequality (1) can be represented in a view:

$$\frac{d}{\Delta} << \frac{1}{\sqrt{2}}, \qquad (2)$$

where $\Delta = \sqrt{\frac{2}{\omega \cdot \mu \cdot \gamma}}$ – the skin-layer value or by other definition Δ – this is the so named effective depth of the electromagnetic field penetration with the frequency – ω in environment with the permeability – μ and the electrical conductivity – γ.

From a physical view point the formulas (1) and (2) give an approximate notion, what part of the magnetic field's energy remaining in the work-piece goes on excitation of the eddy currents and the Lorentz forces but without taking into account any influence of the magnetic attraction forces. Actually, the formulas (1) and (2) illustrate the approximate conditions when the Lorentz forces integral action is negligible small and the attraction is possible. Often, their fulfilling is quite enough for the necessary engineer evaluations. On principle, workability of the for first time suggested way of the ferromagnetic sheet billets attraction showed in [10] is based on three fundamental statements. The first of them consists in suppressing the natural Lorenz repelling forces. The second one this is excitation of the attraction forces caused by the sheet billets magnetic properties influence. The final third statement consists in the conditions creation when the attraction magnetic forces are prevailing over the repelling Lorenz forces. In the total, three above formulated statements provide the ferromagnetic sheets attraction by the low frequency electromagnetic fields. For effectiveness increasing the patented inductor system as the tool for the ferromagnetic sheet attraction consists of two main components as a rule. This is the single turn inductor (separately it is shown on Fig. 2,*d*) and the matching transformer [14, 15]. By the physical essence the last one this is the usual impulse air transformer. It can have two different constructions. The first of them has a multi turn primary winding on an external surface of an inner hollow lengthy metallic cylinder (with longitudinal cut) playing a role of the secondary winding. The external primary winding is connected to the power source. The inner secondary winding is loaded by the single turn inductor. Such construction type got name «the cylindrical matching transformer» (it is shown on Fig. 2,*a* and Fig. 2,*c* on the left side) [14]. The other type of the matching transformer has a multi turn flat spiral winding placing through isolating insert on a flat surface of the single turn inductor. Such construction type got a name «the matching disk transformer» (it is shown on Fig. 2,*b* and Fig. 2,*c* on the right side) [15]. The appointment of the matching transformer consists in the inductor current increasing under preserving the electromagnetic energy from the power source.

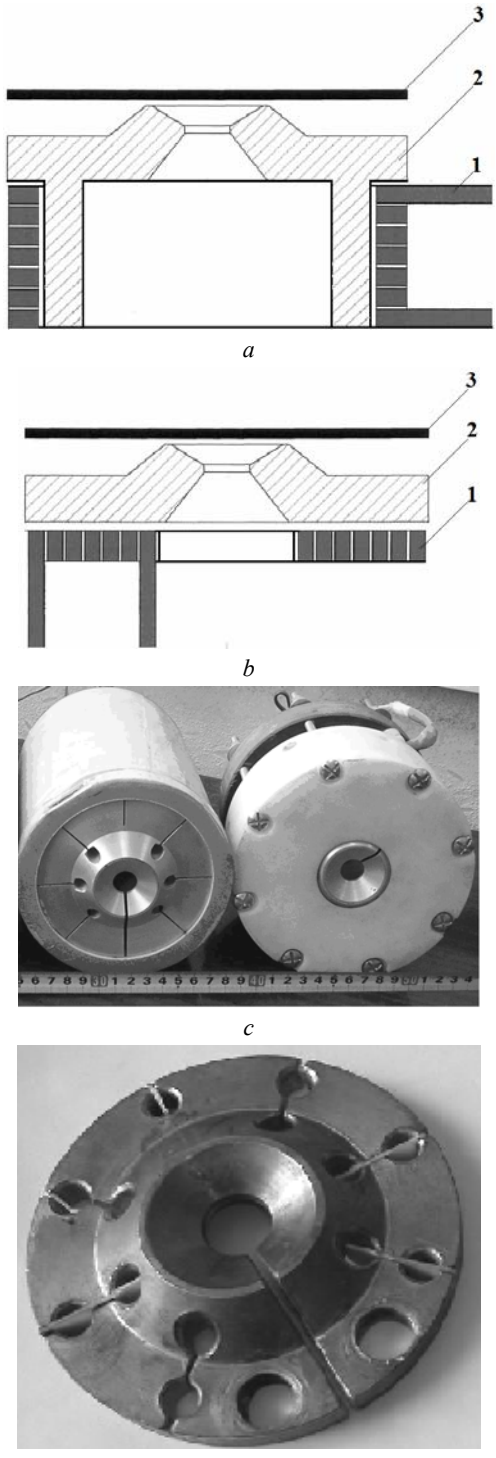

Fig. 2. The matching transformers of different constructive fulfilling, *a*) a principle scheme of the «the matching cylindrical transformer», *b*) a principle scheme of the «the matching disk transformer», 1 – the primary winding, 2 – the single turn inductor, 3 – the sheet billet; *c*) the cylindrical and disk constructions photos; *d*) a single turn inductor with the conical inner bore

Concerning the matching disk transformers the last useful remark. The primary winding is being experienced the great electrodynamical efforts repelling it from the massive single turn of the secondary winding. Their action weakens electromagnetic connection between windings, decrease current in the single turn inductor and as consequence decrease the attraction efforts. Eventually, the repelling forces destroy the primary winding coil. In order to avoid these negative effects some damping device can be installed. Two according solutions were suggested and patented [16]. The first one this is application of a damping elastic insert between the primary winding external surface and upper cover of the disk transformer body. The second solution supposes installation of the additional massive conducting screen on the primary winding external surface. In this case the excited repelling forces will act as from the side of the single turn inductor as from the side of the additional screen. Choosing its parameters the result as a sum of two oppositely directed forces will allow unloading the disc transformer primary winding. The elaborated tools for the ferromagnetics attraction were tested in a special experiment with the different sheet steel specimens. A first part of the conducted experiment consisted in creating two convexities on the smooth surface of plates with thickness ~ 0.008 m by the magnetic-pulsed attraction. One of them will be object for further removing but already as a dent and second will stay for comparison. Both convexities had the half-spherical shape with diameter approximately about ~ 0.015 m and depth about ~ 0.002 m. In the experiment next part the plates were being turned over. The plates were placed on the flat insulated surface of inductor so that one of the dents turned out opposite the inductor inner hole. The dent removing was made by the magnetic-pulsed attraction. After the five times force action this dent was disappeared practically.

The surface of the sheet, where it was, had been becoming quite smooth. It should be noted the quite interesting circumstance here. The subsequent magnetic-pulsed attraction could lead to appearance of a new dent with opposite curvature in relation to the initial one. So this experiment demonstrated a possibility of the controlled deforming demanded part of the sheet metal. One of the experimental specimens with initial and removed dents is shown below on Fig. 3.

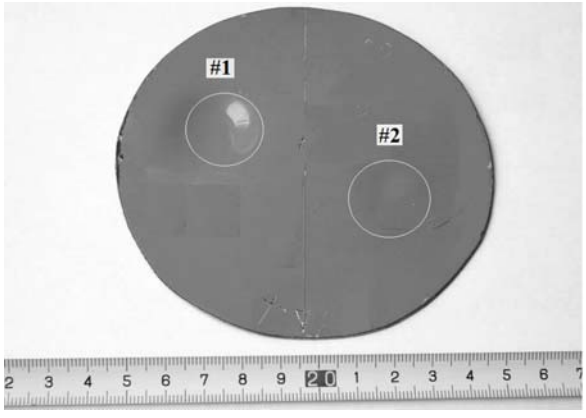

Fig. 3. The experimental specimen from the sheet steel of the body car «Mitsubishi»: #1 – the dent got by the magnetic-pulsed attraction on the sheet assigned part, #2 – the sheet surface part with the removed dent

The low frequency electromagnetic tools of the non-magnetic metals attraction. For a better understanding it should start from the main statements providing operability of the patented way for the non-magnetic metals magnetic-pulsed attraction [17] in comparison of the previous consideration for ferromagnetics [10]. As before the first statement consists in suppressing the natural Lorenz's repelling forces. As before this problem can be solved by work in the low frequency temporal regime (formulas (1) – (2)). The second statement about workability consists in the attracting forces excitation. In the previous consideration these were the forces conditioned by the magnetic properties of the ferromagnetic which is being deformed. The suggested way for non-magnetic metals believes application of the known Ampere's Law according to which the unidirectional currents experience the mutual electrodynamical attraction. For practical realization of this suggestion it is necessary introducing an auxiliary screen into the inductor system construction. This additional constructive element has to be placed parallel to surface of the sheet which is being deformed. The currents induced in metal of the screen and of the sheet billet will experience the mutual attraction. The electrodynamical attraction tool of the described action principle was named as «Inductor System with Attracting Screen (ISAS)». The constructive particularity of the ISAS first variant consisted in what the single-turn inductor was located between the sheet metal blank and the accessory attracting screen [17]. The photograph of this construction intended for the model experiments is shown on Fig. 4. The visual notion about physical picture of the occurring processes can be got from the scheme on Fig. 4.

As it is seen from Fig. 4 in the inner space between the screen and the billet the intensities of magnetic fields ($H_{\tau 1,2}$) which are being excited by the unidirectional induced currents ($J_{1,2}$) are directed oppositely. They are being subtracted from each other. The resultant magnetic intensity will be decreasing and in an idealized case it will be tending to zero. Outside of the system the excited magnetic field intensities have the same directions. They are being summed. The resultant intensity of the external magnetic fields will grow and tend to doubled value of the field intensity excited separately by each from the induced currents (an idealized case). Thus, the inner magnetic field is falling down but the external field is growing. As consequence the magnetic pressure from outside will be a reason of the sheet billet attraction to the fixed screen. Quite conventionally, the corresponding stressed state of the inductor system conditioned by Ampere's attraction forces can be defined as its «compression». But besides of the attraction forces corresponding to Ampere's Law the Lorentz repelling forces are being excited as well. Their action is conditioned by summing the magnetic fields intensities of the induced currents and the inductor current in the inner space and subtracting these intensities in outside the inductor system. So, the Lorentz's forces acting on the screen and sheet billet from inside will exceed the forces acting in outside. Quite conventionally, the corresponding stressed state of the inductor system conditioned by Lorentz's repelling forces can be defined as its «expansion». In integral, if «compression» prevails over «expansion» the represented ISAS will work as the attraction tool of the sheet blanks from metals of any electrophysical nature (as from ferromagnetics as from non-ferromagnetics). In whole all

further cited Patents ISAS are dedicated to their effectiveness increasing. As a rule with this goal some constructive components are being introduced and modified. But presence of the base elements such as low working frequencies (inequalities (1) – (2)), the additional auxiliary screen and the inductor with the exciting current is staying invariable. The review of the patented tools for the non-magnetic metals magnetic pulsed attraction is divided on two main blocks: ISAS of the cylindrical geometry and ISAS of the rectangular geometry. A physical difference between the marked out constructions shapes consists in the following: in the cylindrical ISAS the induced currents have the circular flowing ways but in the rectangular ISAS they are flowing along the rectilinear trajectories. Taking into account these factors the induced currents densities distribution and the excited fields' concentration in the tools working zones can be varied.

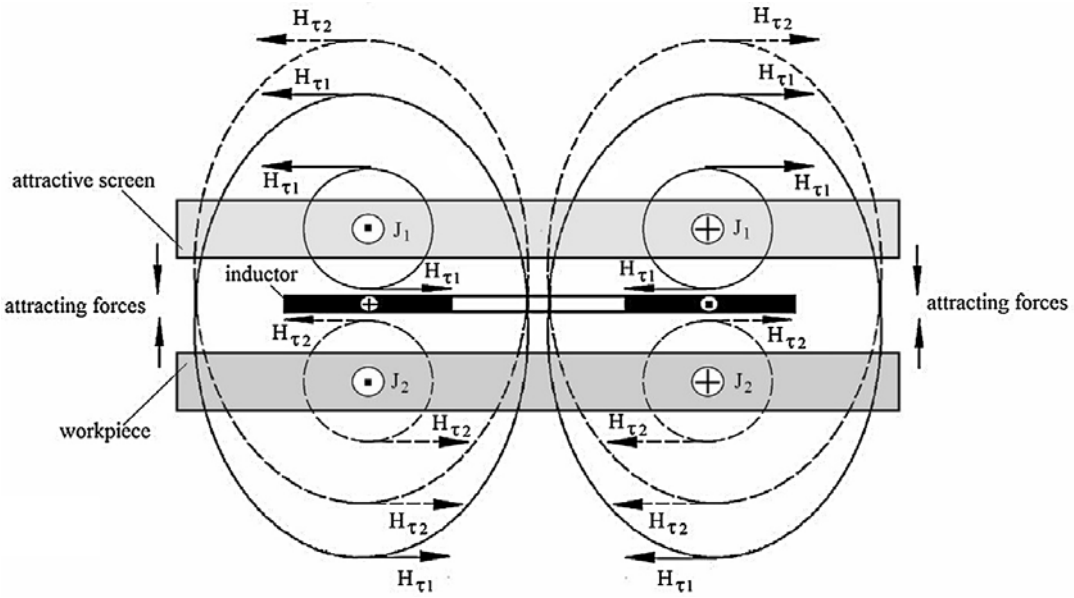

Fig. 4. Schematic illustration of the physical processes in ISAS, $J_{1,2}$ – the unidirectional currents induced in the screen and in the blank, $H_{\tau 1,2}$ – the tangential components of the magnetic field intensity being excited by the currents $J_{1,2}$

«Inductor Systems with Attracting Screens» cylindrical constructions. Placing the single-turn inductor in the slot of the screen with finite thickness from side of the billet which is being processed is suggested in [18]. The present construction modification demands the working frequency limitation by the least value from:

$$f << \frac{1}{\pi \cdot D^2 \cdot \mu_0 \cdot \gamma_s} \text{ or } f << \frac{1}{\pi \cdot d^2 \cdot \mu_0 \cdot \gamma_b}, \quad (3)$$

where D, d – the thicknesses of the screen and billet accordingly, γ_s, γ_b – the specific conductivity of the screen and billet accordingly.

The aim of [19] consists in increasing the acting field amplitudes. The authors suggested the circular inductor which has to be made of two separate concentric rings with two opposite slits along the diameter axis. The rings have to be connected in such a way as to provide unidirectional currents in the inner turns of ring at connection of the inductor to a power source. A novelty of [20] consists in a possible choice of the screen geometry. Its thickness remains the same along the cross section and can be defined from inequality: $d_s << \Delta$, where Δ – a skin layer value. A method of pulsed magnetic attraction of metal objects by a double-coil circular inductor system and with a thin screen is represented in [21 – 23]. The difference of the cited Patents is the difference of the coils constructive fulfilling. The essential novelty being suggested consists in what inductor is designed as two flat coils. One of them is placed under the screen from the billet side. The second is situated above the screen. Current in the coils flows in one direction. The excited fields are summed. As in the previous patent the thickness of the auxiliary screen is chosen the same along all cross section. Unlike to the previous suggestions, in [24, 25] the inductor represented by the single-turn [24] or multi-turn flat coil [25] is placed on the external surface of the auxiliary screen. This solution permits weakening the repelling Lorentz forces between the current induced in the billet metal and the current in inductor. It occurs because of screening them each of other by the conducting auxiliary screen. Besides of that the external placing the inductor coil allows constructively to increase the strength of the attraction tool in whole. The last what can be added as advantage this is a possibility to place all construction including the inductor winding and auxiliary screen in a closed body. The scheme of the most successful ISAS construction [25] given on Fig. 5.

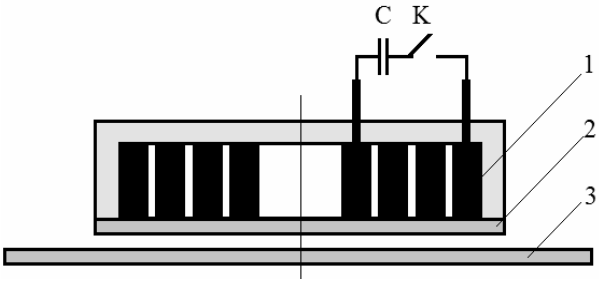

Fig. 5. Schematic representation of ISAS with the external flat multi-turn winding of inductor, 1 – the winding; 2 – the screen; 3 – the sheet billet

Speaking about applications it should be noted the present attraction tool can be very comfortable for exter-

nal non-contact straightening a body of car or aircraft (without disassembly) and as well in machine building where processing a blank can be done only from one side.

«Inductor Systems with Attracting Screens» rectangular constructions. The main difference of the below represented inventions from before suggested cylindrical constructions consists in the rectangular form of the inductors used as the magnetic field generators. The demanded frequencies from [18] are the same to [26], but the inductor placed between the screen and billet is already made in the shape of two coplanar loops of rectangular form electrically connected in series to each other. Their current-conductors limiting the working area are parallel. A single-turn rectangular inductor placed between the screen and billet which has two cuts along the axis of symmetry and which divide it into two separate branches, in series or parallel connection of which to each other is patented [27]. This construction allows adjusting inductance of the inductor and amplitude of exciting fields in dependence on the above mentioned separate branches connection view. The suggestion in [28] is identical to the patented suggestion in [21 – 23]. The main difference and essential novelty consists in what inductor is designed as two single-turn flat rectangular coils. But the same as in [21 – 23] one of them is placed under the screen from the billet side. The second is situated above the screen. Current in the coils flows in one direction. The excited fields are summed. The last variation of the inductor geometrical form (in comparison with solution in [24]) is patented by authors [28]. Unlike previous claims with rectangular inductors this suggestion consists in placing the rectangular single-turn inductor not between the screen and sheet billet but fully above the auxiliary screen. For visual imagine the above described constructions of the inductor systems for the sheet billets attraction are given below on Fig. 6.

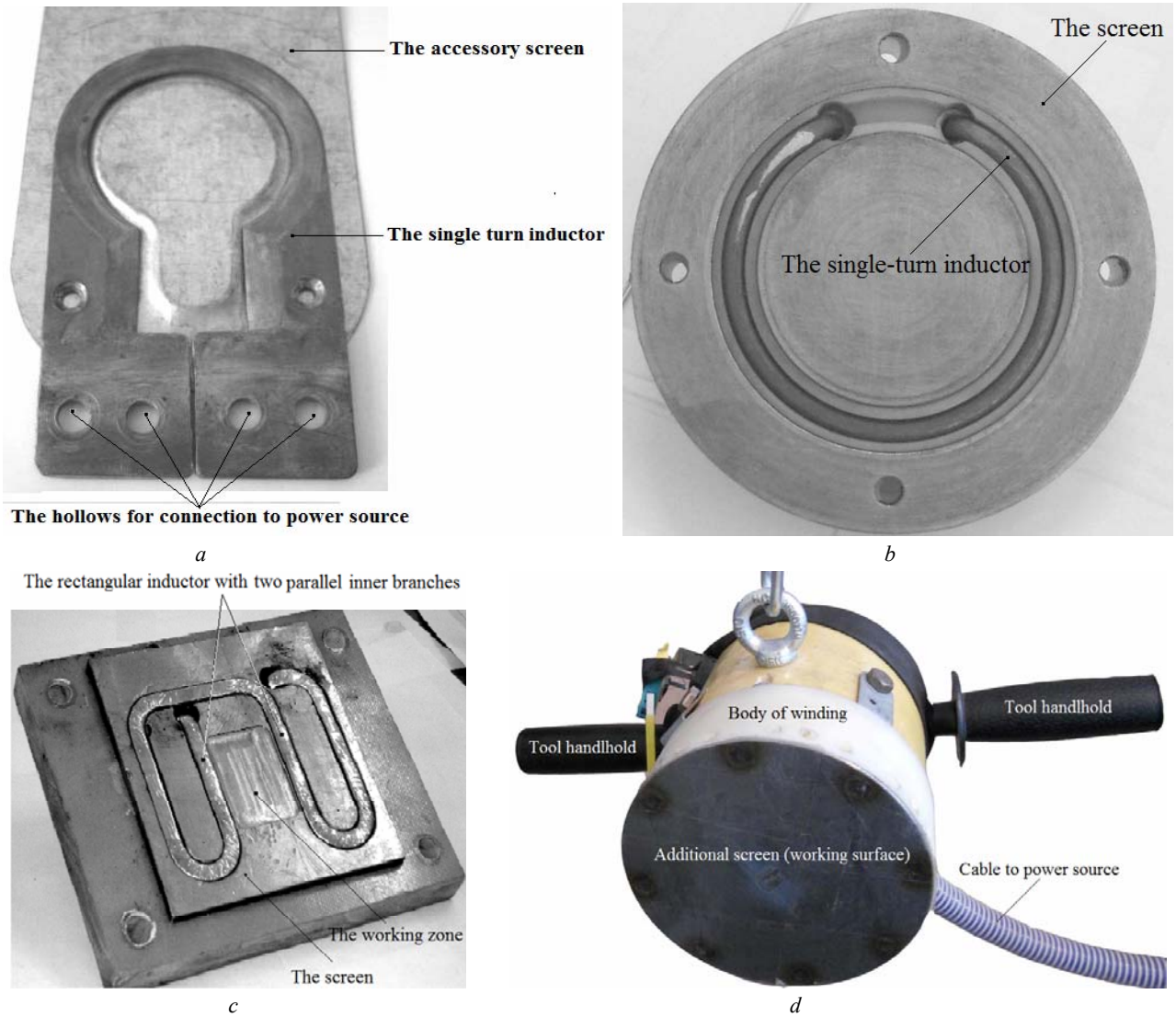

Fig. 6. Experimental models of «Inductor Systems with Attracting Screen», *a*) the first construction for experiments; *b*) the circular single-turn inductor in depression on a screen surface; *c*) the rectangular inductor with two inner parallel branches; *d*) the construction with the external flat multi-turn winding in assembly

Generalizing of the represented inventions of the «Inductor Systems with Attracting Screens» as the tools for work with the thin-walled metals it should be added that all described constructions were tested in experiments which affirmed their workability. Some results of the ISAS experimental testing are represented on Fig. 7.

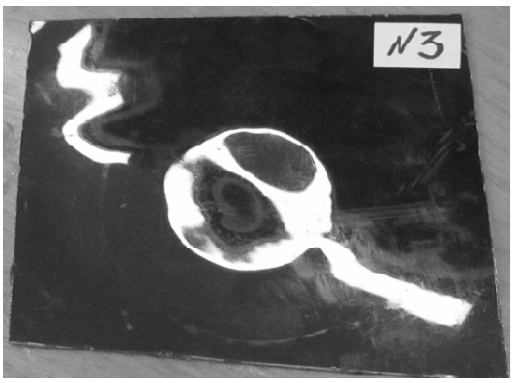

a

b

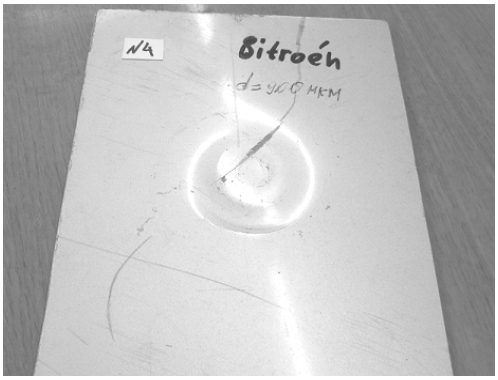

c

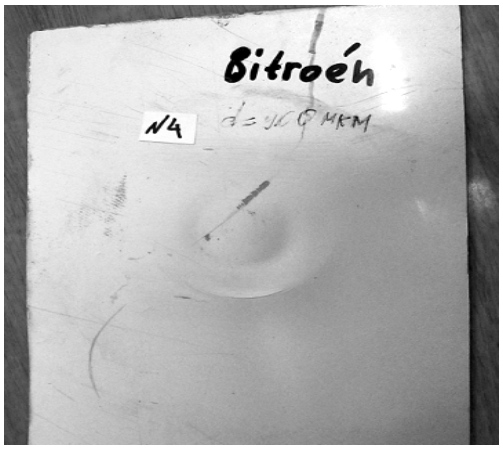

d

Fig. 7. The experimental samples from different automotive steels, «Subaru»: *a* – before the power action, *b* – after attraction; «Citroen»: *c* – before the power action, *d* – after attraction

The magnetic-pulsed installation as the power source in the equipment for the metal sheets attraction. The experimental investigations were conducted on the magnetic-pulsed installation – MPIS-2 created in Laboratory of Electromagnetic Technology of the Kharkov National Automobile & Highway University (Fig. 8) and used as the power source with stored energy ~ 2 kJ under maximal voltage ~ 2200 V and own frequency ~ 7.5 kHz.

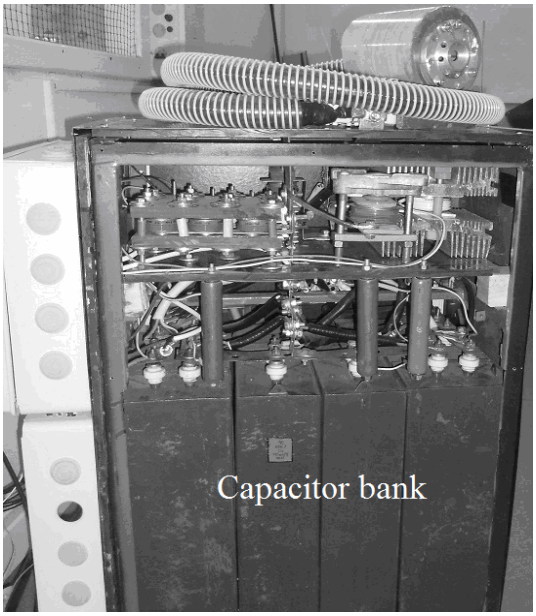

a

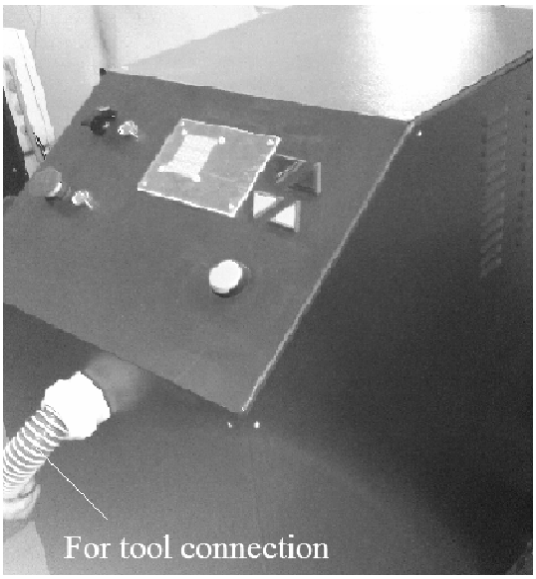

b

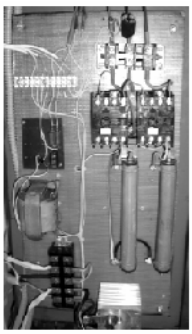

c

d

Fig. 8. The main components of MPIS – 2, *a*) the inner arrangement; *b*) the external view; *c*) the control block; *d*) the remote control panel

Not stopping on the known components of the power source in equipment for the MPMW let us point out the main feature of the represented magnetic-pulsed installation is a work in regime automatically repeating force action pulses with repetition preset frequency (till ~ 10 Hz). The present regime is provided by introduction of the thyristor synchronizing device in the installation electrical scheme [29]. It should be noted the further increasing the repetition frequency of the force action pulses is limited by possibilities of the industrial network. In [30] the patented suggestion consists in usage of the capacitive energy storage special type that is named as «ionistor». Usage of ionistor instead of the traditional capacitive energy storage allows essential decreasing the working voltages without decreasing the working currents what leads to decreasing the power source cost eventually in whole. As it is known the natural discharge of capacitor in an electrical circuit with inductance and resistor has to have the harmonic temporal form for minimum energy losses. But the current and voltage oscillations are decreasing a life cycle the capacitive energy storage. Besides, as it turned out from practice the thyristor commutators in the installation control scheme cannot work in this temporal regime. By this reasons the aperiodic or unipolar temporal form of discharge is more preferential. The problem forming unipolar pulses with minimum energy losses in the discharging circuit is solved by authors [31]. Very interesting scheme of the charging block is patented in [32]. The suggestion essence is based on so named «step-by-step charge» of the capacitive energy storage bank by the serial pulses of the equal energy. This scheme permits excepting the step-up transformer from the charging block and decreasing a cost of the installation in the whole.

The magnetic-pulsed attraction of sheet metals for dents removing on the body car surfaces. The patents [25] and [33] are dedicated to the practical applications of the magnetic pulsed attraction of thin-walled metals. In the [25] the most effective magnetic-pulsed tool of attraction is described (it was represented before as ISAS). Should remind this inductor-tool to remove dents on the surface of the object being processed is fulfilled as a complicated system consisting of the multiturn coil which plays the role of matching transformer and auxiliary attracting screen. The coil is placed on the external surface of the screen. Its opposite inner surface is the tool working surface from side of which the dent in sheet metal is being located. Undoubted advantage of this tool construction is essential decreasing the repelling Lorentz forces at expense of remoting the coil current from the current induced in the sheet metal being processed. In [33] the full complex (Fig. 9) of the external non-contact magnetic-pulsed flattening is represented which includes and the tool and the electromagnetic power source.

In main the equipment for the external magnetic pulsed straightening unites previously described and patented components. A detailed description of such complexes is showed in «The complex of the external magnetic pulsed straightening» [25]. The complex contents a remote portable tool allowing processing any demanded parts of the sheets with dents. The magnetic-pulsed installations are being connected to the inductor-tool by flexible cable. If the tool for ferromagnetics attraction is being used then this connection fulfils through the matching transformer. The charging and discharging circuits are connected through the thyristor-electronic device which synchronizes the work of these circuits. Their interconnection determines the resistor value for limitation of the charging current which provides the installation functionality in the whole:

$$R_{ch} >> 2\delta_0 \cdot \sqrt{\frac{L_{disch}}{C}}\,, \qquad (4)$$

where R_{ch} – the resistor in the charging circuit, δ_0 and L_{disch} – the relative damping decrement and the integral inductance of the discharging circuit.

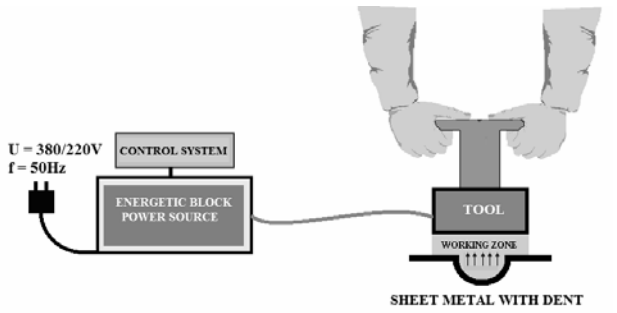

Fig. 9. Schematic illustration of magnetic-pulsed removing the dents in the sheet metal

The discharging circuit of the magnetic-pulsed installation can be represented by several parallel branches which consist of the same capacitors and synchronized thyristor commutators with a common exit to the inductor-tool. Their quantity has to provide the normal work conditions of all power electronics devices. The «ionistor» can be used as the energy storage in the magnetic pulsed installation. But its including in the working scheme demands reforming of the charging and discharging circuits accordingly to the nomenclatorial characteristics of the concrete «ionistor». The discharging circuit has to contain the system for transformation the natural harmonic temporal form of the discharging current pulses to the aperiodic one. This can be the bridge circuit or the well known from the Electrical Engineering «a crowbar circuit». The own frequency of the magnetic pulsed installation is being determined by its parameters and is fixed value. That is why the integral characteristics of the power action tools (with the matching transformer or without this component in the charging circuit) have to be chosen by such way in order to provide the needed working frequency of the fields being excited. The constructions of the inductor-tools, its parameters (independently on the principle action) and its location place on the sheet metal being processed have to be chosen so in order to the high effectiveness providing the dents removing operation according to all previous recommends. Should add that place location of any inductor system has to provide the best electrodynamical tie between the sheet metal being processed and the dent removing tool. In conclusion of the present consideration some documental illustration of the practical magnetic pulsed removing the dents by the flattening complex are represented. The first photographs (Fig. 10) illuminate the repair technology of the automobile «Audi» door by the tool «Inductor System with Attracting Screen».

The next photos (Fig. 11) illustrate a technological route as algorithm of the dent removing on the automobile «Subaru» door.

a *b* *c*

Fig. 10. The external EMF flattening in the real repair process, *a*) the door before flattening; *b*) the tool ISAS in action; *c*) the door after flattening

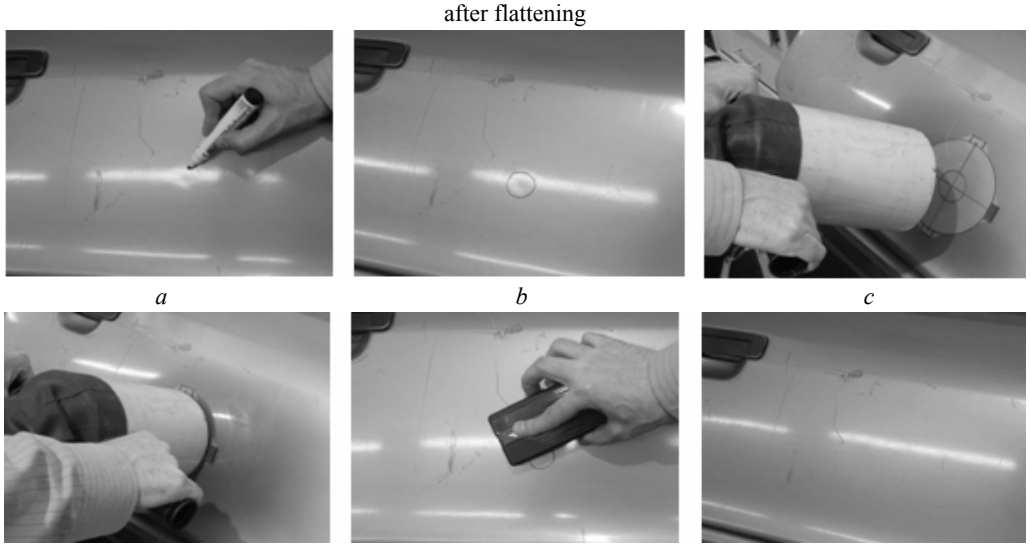

a *b* *c*

d *e* *f*

Fig. 11. Photo-illustrations of the technological route, *a*) determination of the dent; *b*) marking the boundary dimensions; *c*) fixing the tool over the dent; *d*) the magnetic pulsed action; *e*) the marker removing; *f*) the car door panel after the flattening

Technological process. It should be noted that during the experiments of the magnetic-pulsed removing the dents there were approbated many samples steel coverings of the bodies European and Japanese cars. Visual car body parts surface inspection in order to determine a dent to be removed (Fig. 11,*a*). The geometrical dimensions and nature of this dent determine the level and intensity of the required force action. A special dielectric insert is placed on the car panel element over the dent. Its purpose consists in fixation of the tool working area toward to the external boundaries of the dent to be removed (Fig. 11,*c*). The necessary energy level and the pulses quantity are set by the operator on the control panel (Fig. 11,*d*). The operator places the tool working surface above the dent area (Fig. 11,*d*). The operator turns the system on and implements an external non-contact flattening (Fig. 11,*e*). The excited forces attract metal of the dent to the surface needed level. After flattening the tool and the insert are taken away and the surface is cleaned up (Fig. 11,*f*). If it is necessary, technological process is repeated few times, till the complete damage removing. In the case, when the dent has big enough size another approach may be used. It consists in its gradual removing. The process should be begun from the edges of the dent and move to its centre.

Conclusions. The fundamental inventions in the field of the Magnetic Pulsed Attraction of the sheet metals using low frequency discharges are illuminated. The most part of them is defended by the Ukrainian Patents and little known to the west specialists in the area of the magnetic pulsed technologies.

The different types of the attracting tools based on different physical principles and attended for work with metals owning by different electrophysical properties are represented. They can deform the ferromagnetics such as low carbon steels and the non-magnetic metals such as alloys of aluminum for example.

The novelties in the magnetic pulsed installations used as the power sources in the complex equipment for the automobile bodies repair are given. The practical application of the elaborated systems for the dents removing in the sheet metals are suggested and successfully approbated.

In the whole these works can be considered as new scientific direction and used for different manufacturing aims though the main attention is paid to the practical application in the field of the automobile bodies repair.

REFERENCES

1. Psyk V., Risch D., Kinsey B.L., Tekkaya A.E., Kleiner M. Electromagnetic forming – A review. *Journal of Materials Processing Technology*, 2011, vol.211, no.5, pp.787-829. **doi: 10.1016/j.jmatprotec.2010.12.012.**

2. Furth H. et al. Devices for metal-forming by magnetic tension. US Patent, no.3,196,649, 1965.

3. Karl A. Hansen, Iver Glen Hendrickson. Electromagnetic dent puller. US Patent, no.3,998,081, 1976.

4. I. Glen Hendrickson, Karl A. Hansen. Electromagnetic dent remover with tapped work coil. US Patent, no.4,986,102, 1991.

5. Peter B. Zieve. Power supply for electromagnetic proof load tester and dent remover. US Patent, no.5,046,345, 1991.

6. Available at: http://www.electroimpact.com (accessed 15 January 2018).

7. Available at: http://www.fluxtronic.com (accessed 15 January 2018).

8. Shneerson G.A. *Polya i perehodnye processy v apparature sverhsilnyh tokov* [Fields and transients in equipment superstrong currents]. Leningrad, Energoizdat Publ., 1981. 200 p. (Rus).

9. Batygin Yu.V., Lavinsky V.I., Khimenko L.T. Direction Change of the Force Action upon Conductor under Frequency Variation of the Acting magnetic Field. *Proceedings of the 1st International Conference on High Speed Metal Forming*. March 31/April 1, 2004. Dortmund, Germany, pp. 157-160.
10. Batygin Yu.V., Lavinskiy V.I. Khavin V.L., Khimenko L.T. *Sposib magnitno-impul'snoi' obrobky tonkostinnyh metalevyh zagotovok* [Method of magnetic-pulse working of thin-walled metallic billets]. Patent UA, no.75676, 2006.
11. Meichtry R., Kouba I. International Patent Application, no.2006119661, 2006.
12. Meichtry R., Basler B., Kouba I. International Patent Application, no.20160044748, 2016.
13. Available at: http://www.betaginnovation.com (accessed 15 January 2018).
14. Argun Sh.V., Batygin Yu.V., Gnatov A.V., Smirnov D.O., Trunova I.S., Chaplygin Ye.A., Shchigoleva S.A. *Sposib magnitno-impul'snoi' obrobky tonkostinnyh metalevyh zagotivok z vykorystannjam uzgodzhuval'nogo prystroju* [The method of magnetic pulsed processing of thin-walled metal billets with using a matching device]. Patent UA, no.69467, 2013.
15. Argun Sh.V., Batygin Yu.V., Gnatov A.V., Trunova I.S., Chaplygin Ye.A. *Sposib magnitno-impul'snoi' obrobky tonkostinnyh metalevyh zagotovok* [The method of magnetic pulsed processing of thin-walled metal billets]. Patent UA, no.68745, 2011.
16. Argun Sh.V., Batygin Yu.V., Gnatov A.V., Trunova I.S., Chaplygin Ye.A., Shchigoleva S.A. *Sposib magnitno-impul'snogo prytjagannja metalevyh ob'jektiv sumishhenym dyskovym pogodzhuval'nym prystrojem z dempfernoju konstrukcijeju* [The method of magnetic pulsed processing of the metal objects by integrated matching disk device with a damping construction]. Patent UA, no.75790, 2012.
17. Batygin Yu.V., Lavins'kij V.I., Khavin V.L. *Sposib magnitno-impul'snoyi obrobki tonkostinnih metalevih zagotovok* [Method of the magnetic-pulse processing thin metal work pieces]. Patent UA, no.74909, 2006.
18. Chaplygin Ye.A., Batygin Yu.V., Bondarenko A.Yu. *Sposib magnitno-impul'snoi' obrobky metalevyh zagotivok metodom prytjagannja do induktora* [Method of magnetic-pulse working of metallic billets by attraction to inductor]. Patent UA, no.31751, 2008.
19. Batygin Yu.V., Gnatov A.V., Chaplygin Ye.A., Smirnov D.O. *Sposib magnitno-impul'snogo prytjagannja metalevyh ob'jektiv odnovytkovym cylindrychnym induktorom, rozdilenym na dvi gilky* [Method of magnetic pulse attraction of metal objects by two-wind cylindrical inductor divided into two branches]. Patent UA, no.54753, 2010.
20. Batygin Yu.V., Gnatov A.V., Argun Sch.V., Chaplygin Ye.A., Gopko A.V., Drobinin A.M. *Sposib magnitno-impul'snogo prytjagannja metalevyh ob'jektiv odnovytkovoju induktornoju systemoju z tonkym ekranom* [Method of pulsed magnetic attraction of metal objects by single-turn inductor system with thin screen]. Patent UA, no.70055, 2012.
21. Batygin Yu.V., Gnatov A.V., Shigoleva S.A., Chaplygin Ye.A., Gopko A.V., Drobinin A.M. *Sposib magnitno-impul'snogo prytjagannja metalevyh ob'jektiv dvovytkovoju krugovoju induktornoju systemoju z tonkym ekranom* [The method of magnetic-pulse attraction of metal objects by double-turn circular inductor system with a thin screen]. Patent UA, no.70734, 2012.
22. Batygin Yu.V., Gnatov A.V., Chaplygin Ye.A., Shinderuk S.A., Sabokar O.S. *Sposib magnitno-impul'snogo prytjagannja tonkostinnyh lystovyh metaliv bagatovytkovoju krugovoju indukcijnoju induktornoju systemoju* [The method of pulsed magnetic attraction of thin sheet metals by induction multiturn rotary inductor system]. Patent UA, no.92037, 2014.
23. Batygin Yu.V., Gnatov A.V., Chaplygin Ye.A, Shinderuk S.A., Sabokar O.S. *Bagatovytkova krugova indukcijna induktorna systema dlja magnitno-impul'snogo prytjagannja tonkostinnyh lystovyh metaliv* [The multiturn rotary induction coil system for pulsed magnetic attraction of thin sheet metals]. Patent UA, no.92436, 2014.
24. Batygin Yu.V., Gnatov A.V., Chaplygin Ye.A., Trunova I.S., Gopko A.V., Sabokar O.S. *Sposib magnitno-impul'snogo prityagannya metalevih zagotivok odnovitkovim krugovim induktorom, roztashovanim nad dopomizhnim ekranom* [Method of the magnetic-pulse attraction metal workpeaces single-turn circular inductor located on the auxiliary screen]. Patent UA, no.77579, 2013.
25. Batygin Yu.V., Gnatov A.V., Chaplygin Ye.A, Sabokar O.S. *Sposib magnitno-impul'snoi' obrobky poverhon' kuzovnyh elementiv* [The method of magnetic pulsed processing surface body elements]. Patent UA, no.104509, 2015.
26. Batygin Yu.V., Bondarenko A.Yu., Serikov G.S. *Sposib magnitno-impul'snoi' obrobky metalevyh zagotivok* [Method of magnetic-pulse working of metallic billets]. Patent UA, no.31752, 2008.
27. Batygin Yu.V., Gnatov A.V., Serikov G.S., Drachenko S.A. *Sposib magnitno-impul'snogo prytjagannja metalevyh ob'jektiv prjamokutnym induktorom, z dvoma rozrizamy* [Method of magnetic pulse attraction of metal objects by rectangular inductor with two slots]. Patent UA, no.53968, 2010.
28. Batygin Yu.V., Gnatov A.V., Chaplygin Ye.A., Shinderuk S.A., Shchigoleva S.A., Sabokar O.S. *Sposib magnitno-impul'snogo prytjagannja metalevyh zagotivok induktornoju systemoju z dvoma prjamokutnymy vytkamy ta tonkym ekranom* [The method of the magnetic pulsed attraction of the metallic billets by the inductor system with two rectangular turns and by the thin screen]. Patent UA, no.78243, 2013.
29. Batygin Yu.V., Bondarenko A.Yu., Gnatov A.V., Serikov G.S., Chaplygin Ye.A. *Generator bagatorazovyh impul'siv strumu dlja magnitno-impul'snoi' obrobky metaliv* [Generator of repeated current pulses for magnetic pulse working metals]. Patent UA, no.44933, 2009.
30. Batygin Yu.V., Gnatov A.V., Chaplygin Ye.A., Gnatova Sh.V., Trunova I.S. *Generator bagatokratnyh impul'siv strumu dlja obrobky metaliv tyskom impul'snogo magnitnogo polja* [Generator of multiple pulses of current for metal forming by pulsed magnetic field pressure]. Patent UA, no.61417, 2011.
31. Batygin Yu.V., Gnatov A.V., Chaplygin Ye.A., Dzubenko A.A., Argun Sh.V., Drobinin A.M. *Generator bagatorazovyh unipoljarnyh impul'siv strumu dlja magnitno-impul'snoi' obrobky metaliv* [The generator of multiple unipolar current pulses for magnetic-pulse metal working]. Patent UA, no.73733, 2012.
32. Batygin Yu.V., Chaplygin Ye.A., Sabokar O.S. *Peretvorjuvach energii' zarjadnogo konturu magnitno-impul'snoi' ustanovky* [The energy transducer for the magnetic pulsed installation charging circuit]. Patent UA, no.110809, 2016.
33. Batygin Yu.V., Gnatov A.V., Chaplygin Ye.A., Argun Sh.V., Shinderuk S.A., Sabokar O.S. *Kompleks zovnishn'ogo magnitno-impul'snogo ryhtuvannja* [The complex of the external magnetic pulsed straightening]. Patent UA, no.101413, 2015.

Received 06.02.2018

Yu.V. Batygin[1], *Doctor of Technical Sciences, Professor,*
E.A. Chaplygin[1], *Candidate of Technical Sciences, Associate Professor,*
S.A. Shinderuk[1], *Candidate of Technical Sciences, Associate Professor,*
V.A. Strelnikova[1], *Postgraduate Student,*
[1] Kharkiv National Automobile and Highway University,
25, Yaroslava Mudrogo Str., Kharkov, 61002, Ukraine,
e-mail: yu.v.batygin@gmail.com; chaplygin.e.a@gmail.com;
s.shinderuk.2016102@ukr.net; v.strelnikova91@gmail.com

How to cite this article:
Batygin Yu.V., Chaplygin E.A., Shinderuk S.A., Strelnikova V.A. The main inventions for technologies of the magnetic-pulsed attraction of the sheet metals. A brief review. *Electrical engineering & electromechanics*, 2018, no.3, pp. 43-52. **doi: 10.20998/2074-272X.2018.3.06.**

UDC 621.373; 577.2; 577.3 **doi: 10.20998/2074-272X.2018.3.07**

M.I. Boyko, A.V. Makogon, A.I. Marynin

ENERGY EFFICIENCY OF THE DISINFECTION TREATMENT OF LIQUID FOODSTUFFS BY HIGH-VOLTAGE PULSE EFFECTS

Purpose. ***Experimentally determine the rational modes and energy efficiency of decontamination treatment of flowing food products using high-voltage impulse actions in comparison with traditional pasteurization.*** ***Methodology.*** ***We used pulse generation method with the help of a step-up transformer, high-voltage pulse capacitors and spark gaps with a system of peaking of pulse front to obtain high-voltage pulses in working chambers - the generator load. The pulses on the load were measured by a low-resistance resistive voltage divider, were transmitted over a broadband coaxial cable and recorded using an analog C8-12 oscilloscope or a Rigol DS1102E digital oscilloscope with a bandwidth of 100 MHz for each. The working chambers were filled with water, milk or milk whey and consisted of an annular hull made of PTFE and metal electrodes forming the bottom and the chamber cover having flat linings of food grade stainless steel for contact with the food product inside the chamber.*** ***Results.*** ***We obtained high-voltage pulses on the generator load with a base duration of 300 to 1200 ns at pulse repetition rates up to 500 pulses per second. We obtained experimentally the amplitude of the voltage pulses on the generator load up to 75 kV, and the electric field strength up to 35 kV/cm in working chambers with a gap of 22 mm and up to 50 kV/cm in working chambers with a gap of 15 mm. These characteristics of the pulses allowed complete and irreversible inactivation of microorganisms in food liquids in working chambers.*** ***Originality.*** ***We showed that there are modes of treatment food products with the help of high-voltage pulse actions, which allow better to preserve the biological and nutritional value of the products in comparison with heat treatment with their complete disinfection and at a significantly lower specific energy consumption.*** ***Practical value.*** ***The experimental regimes for treating milk, whey and water with reduced specific energy consumption open the prospect of industrial application of a complex of high-voltage pulse actions for the disinfecting treatment of water-containing food products.*** References 7, tables 3, figures 10.

Key words: **generator of high-voltage pulses, transformer, capacitor, multi-gap discharger, multichannel switch, working chamber, disinfecting food treatment.**

Цель. ***Экспериментально определить рациональные режимы и энергоэффективность обеззараживающей обработки текучих пищевых продуктов при помощи высоковольтных импульсных воздействий в сравнении с традиционной пастеризацией.*** ***Методика.*** ***Для получения высоковольтных импульсов на рабочих камерах – нагрузке генератора применена методика генерирования импульсов при помощи повышающего трансформатора, высоковольтных импульсных конденсаторов и разрядников с системой обострения фронта импульсов. Импульсы на нагрузке измерялись при помощи низкоомного резистивного делителя напряжения, передавались по широкополосному коаксиальному кабелю и регистрировались при помощи аналогового осциллографа С8-12 или цифрового осциллографа Rigol DS1102E с полосой пропускания 100 МГц у каждого. Рабочие камеры заполнялись водой, молоком или молочной сывороткой и состояли из кольцеобразного корпуса, выполненного из фторопласта, и металлических электродов, образующих дно и крышку камеры, имеющих плоские накладки из пищевой нержавеющей стали для контакта с пищевым продуктом внутри камеры.*** ***Результаты.*** ***Получены высоковольтные импульсы на нагрузке генератора с длительностью по основанию 300-1200 нс при частотах следования импульсов до 500 имп/с. Экспериментально полученные амплитуды импульсов напряжения на нагрузке генератора – до 75 кВ, а напряженности электрического поля – до 35 кВ/см в рабочих камерах с зазором 22 мм и до 50 кВ/см в рабочих камерах с зазором 15 мм. Указанные характеристики импульсов позволили осуществить полную и необратимую инактивацию микроорганизмов в пищевых жидкостях в рабочих камерах.*** ***Научная новизна.*** ***Показано, что существуют режимы обработки пищевых продуктов при помощи высоковольтных импульсных воздействий, позволяющие лучше сохранить биологическую и пищевую ценность продуктов по сравнению с тепловой обработкой при их полном обеззараживании и при существенно меньших удельных энергозатратах.*** ***Практическая значимость.*** ***Полученные экспериментально режимы обработки молока, молочной сыворотки и воды с уменьшенными удельными энергозатратами открывают перспективу промышленного применения комплекса высоковольтных импульсных воздействий для обеззараживающей обработки водосодержащих пищевых продуктов.*** Библ. 7, табл. 3, рис. 10.

Ключевые слова: **генератор высоковольтных импульсов, трансформатор, конденсатор, многозазорный разрядник, многоканальный разрядник, рабочая камера, обеззараживающая обработка пищевых продуктов.**

Introduction. Traditional thermal methods of disinfecting treatment (pasteurization and thermal sterilization) of liquid food products, wine materials, beverages are energy-consuming and do not allow to preserve their initial biological and nutritional value to a sufficient extent [1, 2]. One of the most promising ways of non-thermal disinfection treatment of products is the way of processing by means of a complex of high-voltage impulse actions (CHVIA). The English-language scientific literature uses the term PEF-treatment (PEF – pulsed electric field, treatment with a pulsed electric field). Most liquid food products are water-containing. Therefore, the important question is also about rational modes of decontaminating water treatment by using CHVIA.

The goal of the work is to experimentally determine the rational modes and energy efficiency of decontaminating treatment of liquid food products by means of high-voltage impulse actions in comparison with traditional pasteurization.

Experimental installation. To carry out experimental studies, we used a facility, which was first

described in [3]. The electrical circuit of the installation with the control system is shown in Fig. 1.

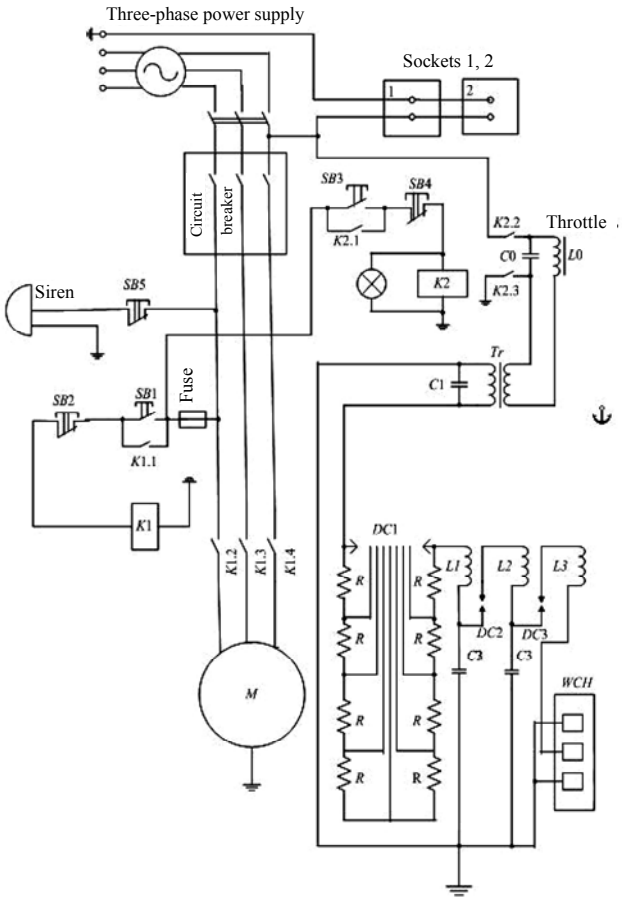

Fig. 1. Electrical circuit of the CHVIA installation with a control system

The installation consists of low-voltage and high-voltage parts. The high-voltage part consists of a generator of high-voltage pulses and a load – a working chamber *WCH*. The generator contains a start cascade (*C*1, *DC*1) and two cascades of sharpening (*C*2, *DC*2 and *C*3, *DC*3). Each cascade contains a capacitor and an discharger. The discharger *DC*1 of the start cascade is multi-gap. All arresters are multi-channel. In the simplest mode of operation, only the first cascade is used. The disadvantage of this mode is the insufficient steepness of the pulse front on the load – the *WCH* working chamber. Therefore, the main amount of the experiments was carried out using all three cascades.

After connecting to a three-phase power supply, during flow processing, pressing the button *SB1* starts the pump electric motor *M* which pumps the processed product through the *WCH* working chamber. Pressing the button *SB3* energizes the relay *K2*, its contacts *K*2.1, *K*2.2, *K*2.3 are closed, and the phase voltage of the power network through the filter *L*0 - *C*0 is fed to the primary (low-voltage) winding of the transformer *Tr* starting the installation. As a result, on the load – the *WCH* working chamber, pulses are formed of high voltage (up to 120 kV) and current of both polarities with repetition frequency up to 500 pulses. The button *SB*4 switches off the supply of voltage to the filter *L*0 - *C*0 and to the primary winding of the transformer *Tr*. By pressing the button *SB*2, the pump electric motor *M* is switched off.

Working chambers. The working chambers (WCH) which are the load for the CHVIA installation are divided into stationary and flowing. In stationary chambers, portions of the product are replaced manually, and in flow chambers through the flow through the chamber which provides the pump and a pumping system. The latter contains containers for feeding and receiving the treated liquid product and hoses. It is in the WCH that energy is released which is initially stored in the main high-voltage capacitor of the installation.

Typical stationary and flow chambers are shown in Fig. 2 and Fig. 3, respectively.

Fig. 2. Variant of stationary WCH with cover – electrode located near

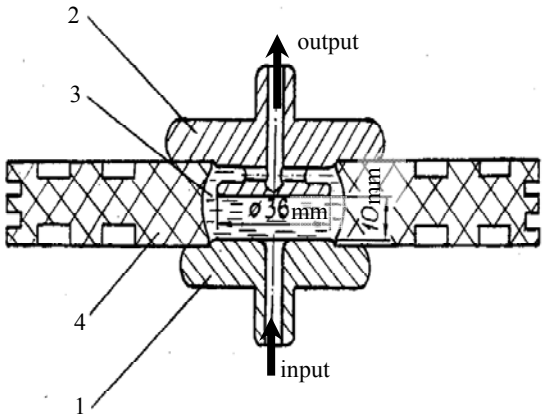

a

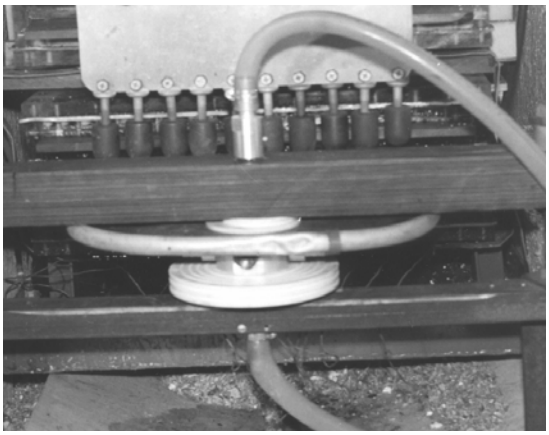

b

Fig. 3. *a* - variant of the design of the flowing technological WCH: 1, 2 – electrodes, 3 – internal volume of the chamber, 4 – dielectric housing; *b* – WCH

Experimental studies of CHVIA methods for the treatment (PEF-treatment) of food products and water treatment. We experimentally investigated the effect of CHVIA treatment on microbiological contamination, sanitary and hygienic properties and organoleptic parameters of milk, milk whey and water. The investigations were carried out in different treatment modes in stationary and flowing WCHs at the CHVIA installation described above.

A photo of an operating CHVIA installation during the experiments is shown in Fig. 4. The product to be processed was poured into a WCH which was previously sterilized with an alcohol burner, and the chamber was closed with a sterilized lid. Two types of cameras were used: with an interelectrode gap (the distance between the disk cover of the chamber and its bottom) of 15 mm and with an interelectrode gap of 22 mm. We varied the treatment time from 10 s to 30 s. Fig. 5 shows a WCH with an interelectrode gap of 22 mm.

Fig. 4. Photo of operating CHVIA installation

To measure the characteristics of pulses on the load of the CHVIA installation - the working chamber, a resistive low-resistance voltage divider with a division coefficient k_d=1000 was used. As the recording device an analog storage oscilloscope C8-12 with a bandwidth of 100 MHz and a digital oscilloscope RIGOL DS1102E with a bandwidth of 100 MHz were used.

To protect against electromagnetic interference, the oscilloscope was located in a shielding cabin with a door screened circuit along the contour. The signal from the low-voltage arm of the voltage divider to the oscilloscope in the measuring cabinet was fed using a coaxial cable with a double braid. The door in the measuring cabinet can be opened and closed tightly both from the outside and from the inside.

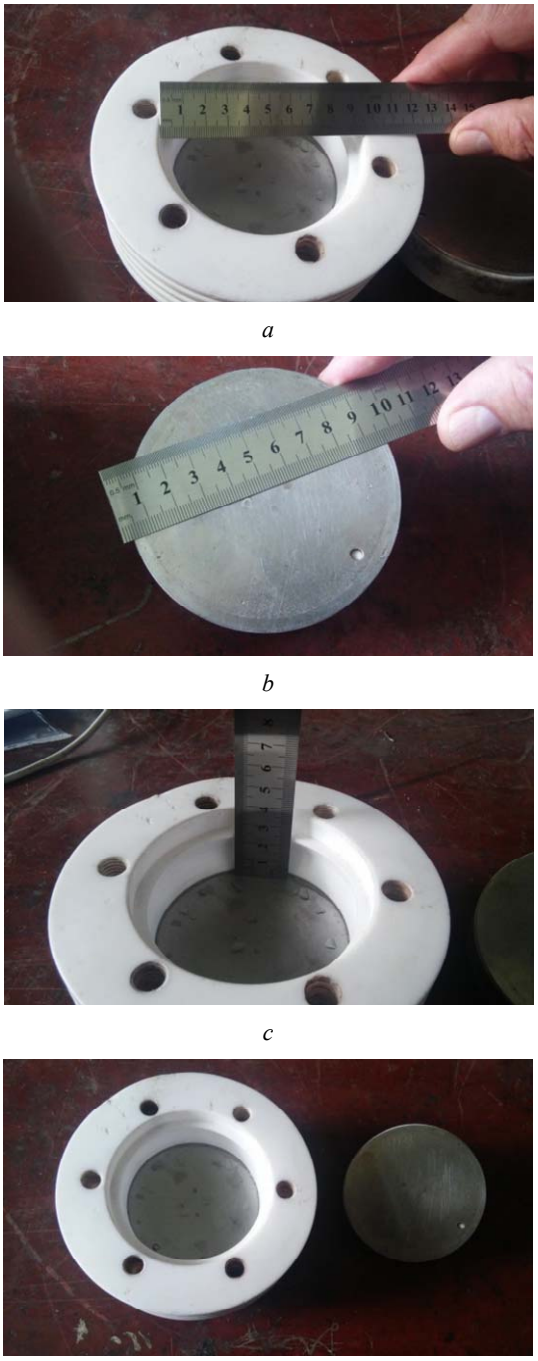

a

b

c

d

Fig. 5. Working chamber with an interelectrode gap of 22 mm: *a* – body made of fluoroplastic, *b* – cover, *c* – interelectrode gap of 22 mm, *d* – cover near the chamber

The inactivating effect of CHVIA on various milk products (milk, whey, yogurt), as well as water, was investigated. To do this, our colleagues, co-executors from the National University of Food Technologies (NUFT), the city of Kiev, prepared water for experiments. They took water «Sofia Kiev» and infested it with bacteria of the *E-coli* group. At each treatment mode of all the fluids studied, three repetitions were performed.

The values of the interelectrode gap in the spark dischargers had the following values: for a multi-gap discharger (MGD), the value of an individual gap is approximately 5 mm, for the first sharpening discharger approximately 20 mm, for a second sharpening discharger approximately 20 mm. At the same time, the number of gaps involved in the MGD was from 4 to 7 inclusive.

The treatment of samples of liquid products and water in the WCH in all modes was carried out by pulses of both polarities. During the period of 20 ms of the AC network voltage during the half-period of the positive voltage of 10 ms, approximately 4 pulses of the same polarity were applied to the WCH, and about 4 pulses of a different polarity were applied to the WCH during the half-period of the negative voltage of 10 ms.

Results of experimental studies of the methods of CHVIA treatment (PEF-treatment). Fig. 6 shows an oscillogram of pulses on the WCH with milk at 7 ruptured gaps of 8 in a multi-gap discharger – MGD without the influence of electromagnetic interference and with a clearly visible pulse front.

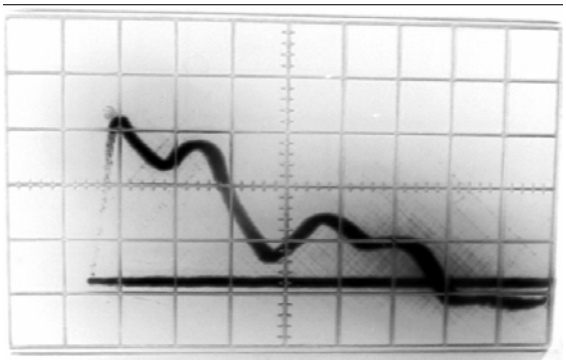

Fig. 6. Typical oscillogram of the voltage pulse on the WCH with raw milk. The scale division along the time axis is 50 ns/div; along the axis of the process is 20 kV/div. In multi-gap discharger 7 gaps of 8 are ruptured. The gap in the WCH is d = 22 mm

It follows from the oscillogram that the pulse front duration in milk is about 20 ns and the pulse duration along the base before passing through zero is about 300 ns. Amplitude of the voltage pulse is not less than 60 kV. From this it follows that the amplitude of the electric field strength in milk is 60/2.2≈27.3 kV/cm. It is also important that in milk which has a resistivity less than tap water or table water, the pulse shape is slightly oscillatory.

Fig. 7 shows a typical oscillogram of the pulse voltage on the WCH with water, contaminated with *E-coli*. The oscillogram was obtained using a digital oscilloscope Rigol 1102 E.

From the oscillogram in Fig. 7 it follows that the amplitude of the voltage on the WCH with water in this mode is not less than 72 kV, the pulse duration on the base is approximately 1200 ns, and the pulse shape is aperiodic, unipolar, does not pass through the zero line. The zero line is shown in Fig. 7 and further by the arrow located to the left of the oscillogram.

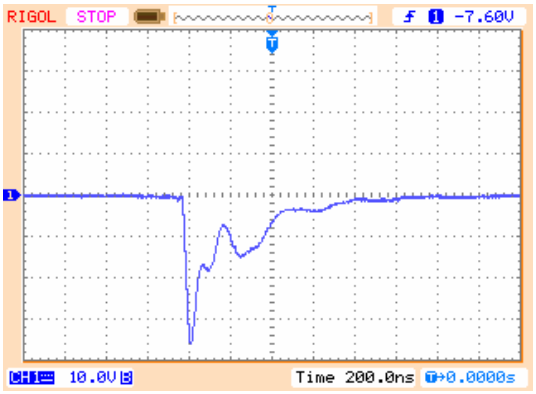

Fig. 7. Typical oscillogram of the voltage pulse on a working chamber with water «Sofia Kiev» seeded by *E-coli*. The scale division along the time axis is 200 ns/div; along the axis of the process is 20 kV/div. In the multi-gap discharger 6 gaps of 8 are ruptured. The gap in the WCH is d=22 mm. A low-resistance resistive voltage divider with division coefficient k_d ≈2000 is used

Two additional bursts at the fall of the pulse on this oscillogram, as well as on other oscillograms, are due to the presence of three high-voltage capacitive storage devices: the main one and two sharpening ones. The front part of the pulse is due to the last (second) sharpening cascade with the second sharpening capacitive storage, the first additional burst at the pulse decay is due to the presence of the first cascade of sharpening with the first sharpening capacitive storage, and the second additional surge at the pulse decay is due to the presence of the main high-voltage capacitive storage device.

The results of microbiological analyzes of water are given in Table 1.

Table 1

Detection of the bacteria of the family *E.coli* in water

The name of the indicator (units of measure CFU/cm^3)	Results of investigations, CFU/cm^3	Approximated treatment mode, (E, kV/cm)	Calculated treatment mode, (E, kV/cm)	Treatment duration (t, s)
Water sterile. Dilution E.coli 10^6	210	30	20.09	10
Water sterile. Dilution E.coli 10^6	0	30	31.8	20
Water sterile. Dilution E.coli 10^8	60	30	19.0	10
Water sterile. Dilution E.coli 10^8	0	30	1.8	20

*Note: CFU – colony forming units.

Fig. 8 shows a typical oscillogram of pulse voltage on the WCH with milk whey.

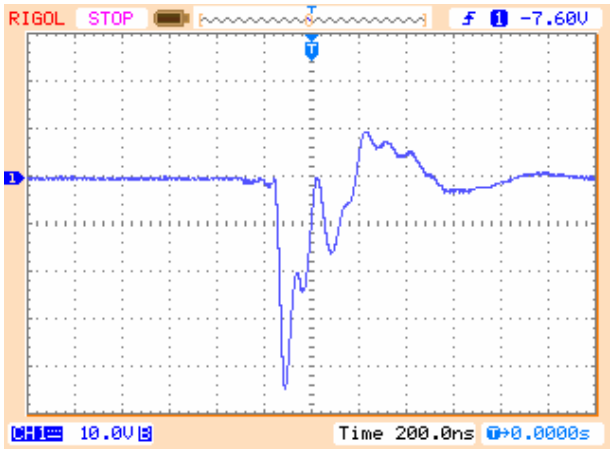

Fig. 8. Typical oscillogram of the voltage pulse on a working chamber with milk whey. The scale division along the time axis is 200 ns/div; along the axis of the process is 10 kV/div. In the multi-gap discharger 6 gaps of 8 are ruptured. The gap in the WCH is d=22 mm. A low-resistance resistive voltage divider with division coefficient k_d ≈1000 is used

The pulse duration along the base on the oscillogram (Fig. 8) is approximately 350 ns. The pulse shape is oscillatory with a large decrement of oscillations. The amplitude of the voltage pulse on this oscillogram is approximately 45 kV, and the amplitude of the voltage is approximately 20.45 kV/cm.

In Fig. 9 shows a typical oscillogram of the pulse voltage on the WCH with raw milk.

The results of microbiological analyzes of milk whey treated with CHVIA pulses, a sample oscillogram of which is presented in Fig. 8, are given in Table 2-5.

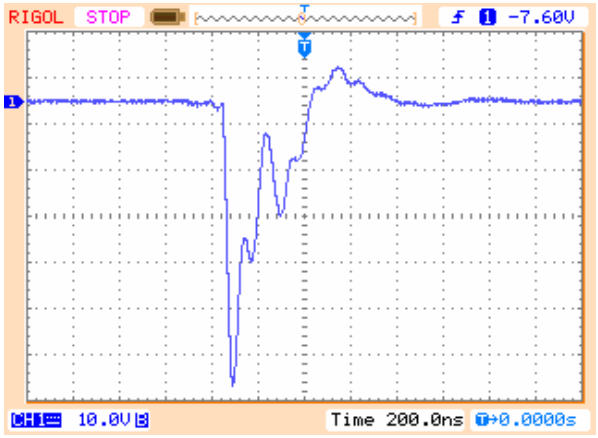

Fig. 9. Typical oscillogram of the voltage pulse on a working chamber with raw milk. The scale division along the time axis is 200ns/div; along the axis of the process is 10 kV/div. In the multi-gap discharger 6 gaps of 8 are ruptured. The gap in the WCH is d=22 mm. A low-resistance resistive voltage divider with division coefficient k_d≈1000 is used

Table 2

The results of the analyzes on the detection of *E.coli* family bacteria in milk whey after CHVIA treatment

The name of the indicator, units of measure CFU/cm^3 *E.coli*	Result, CFU/cm^3
at E≈30 kV/cm, total treatment duration t=10 s and dilution 10^6	30
at E≈30 kV/cm, total treatment duration t=20 s and dilution 10^6	0
at E≈30 kV/cm, total treatment duration t=10 s and dilution 10^8	20
at E≈30 kV/cm, total treatment duration t=20 s and dilution 10^8	0

Table 3

Physicochemical parameters of initially raw milk after CHVIA treatment

The name of the indicator, units of measure	ND for testing techniques	Investigation result	Indicator value in accordance with ND	Compliance with ND
1	2	3	4	5
Determination of the mass portion of vitamin C by titrimetric method in food products				
mass part of vitamin C, ppm	GOST 30627.2-98	5.0	not regulated	corresponds to ND
Determination of peroxidase by the method of qualitative analysis in food products				
peroxidase for baked, ultra-pasteurized, sterilized milk	DSTU 7380:2013	detected	absent	does not correspond
Determination of phosphatase of milk and milk products by method of qualitative analysis				
phosphatase for pasteurized milk	DSTU 7380:2013	not detected	absent	corresponds

From Table 2 it follows that after complete treatment of milk whey in the WCH during 20 s by high-voltage pulses (see Fig. 8) complete inactivation of *E.coli* bacteria is guaranteed. When treated during 10 s from 20 to 30 colony forming units remain not inactivated. Thus, the existence of a mode of complete guaranteed inactivation at CHVIA treatment of products was confirmed experimentally. In control (not treated by CHVIA) samples of milk whey, a continuous growth of *E.coli* bacteria (>>1000 CFU/cm^3) was observed.

The pulse duration along the base on the oscillogram in Fig. 9 is approximately 350 ns. The pulse shape is oscillatory with a large decrement of oscillations (weakly vibrational). The amplitude of the voltage pulse on this oscillogram is approximately 60 kV, and the amplitude of the electric field strength is approximately 60/2.2≈27.3 kV/cm.

The results of laboratory studies of the physicochemical parameters of milk after CHVIA treatment (see Fig. 9) are given in Table 3.

From the results given in Table 6 it follows that in CHVIA treated milk there is a peroxidase enzyme, the absence of which is characteristic of baked, ultra-pasteurized, sterilized milk, that is, milk that was amenable to processing at high temperatures (greater than 100 °C). However, in CHVIA treated milk, no enzyme phosphatase was detected, the absence of which is characteristic of pasteurized milk. In addition, from the data of Table 6 it follows that the amount of vitamin C which is very sensitive to different treatments, after CHVIA treatment has remained at the level meeting the requirements of normative documentation (ND), that is, CHVIA treatment is soft processing. All analyzes (microbiological and sanitary-hygienic) of treated and control samples of water-containing foods and water were conducted by specialists of the public utility «Sanepidservice» (public unity «SES», the Kharkiv city). This enterprise is accredited by the National Agency of Ukraine for Accreditation (Accreditation Certificate No. 2H1207 of 25.02.2015).

Energy efficiency of high-voltage prototype of CHVIA installation. Energy efficiency is determined by two components: high degree of microbiological (microbial) disinfection of the processed product at a given specific energy input and reduced specific energy consumption in comparison with known methods (for example, thermal sterilization and pasteurization). The first component can be estimated by conducting CHVIA processing and making the corresponding microbiological analyzes of the processed product (water, milk, milk whey). The second component of energy efficiency can be estimated on the basis of what part of the energy consumed from the power supply network by the CHVIA installation was delivered to the WCH and there it was dissipated leading to the required degree of inactivation of microorganisms in the water. Since in all elements of the CHVIA installation, including in high-voltage capacitors, a transformer and dischargers, not more than 0.1 total energy consumed from the network dissipates in total, efficiency of the installation can be estimated as 0.9, or 90% [4-6]. It is more difficult to estimate how much energy is dissipated in the WCH. We do this with the help of oscillograms of voltage pulses on the WCH with the treated product. A typical oscillogram of the voltage pulse on a chamber with water being treated is shown in Fig. 10.

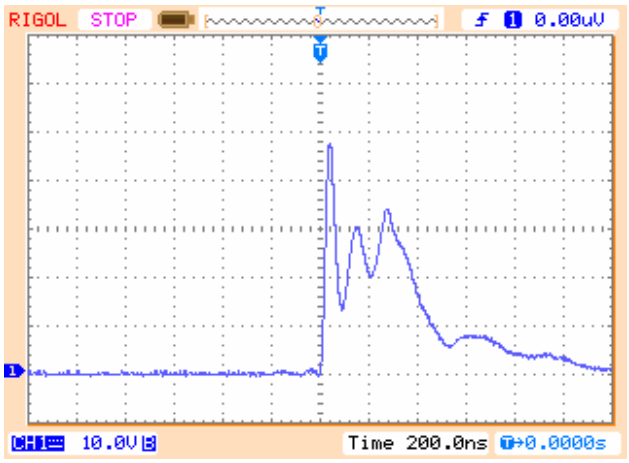

Fig. 10. Typical voltage pulse oscillogram on a working chamber with treated water

The three peaks (maximums), as mentioned above, on the oscillogram correspond to the processes of discharge of three capacitors ($C1$, $C2$, $C3$) on the load – the working chamber, in this case filled with water (see Fig. 1). The first (largest) peak after the pulse front is the maximum voltage on the WCH due to the energy input to the chamber from the most low-inductive discharge circuit with the capacitive storage $C3$. The second peak corresponds to the process of connecting and discharging capacitor $C2$ on the WCH. The third peak corresponds to the process of connecting to the discharge on the WCH of capacitance $C1$, more remote from the WCH and having the greatest inductance.

Energy which is released in the WCH during processing can be estimated by the formula

$$E = nT\int iudt = nTi_{av}u_{av}t, \qquad (1)$$

where i is the current as a temporal function, u is the voltage as a temporal function, i_{av} is the averaged current, u_{av} is the averaged voltage, t is the duration of one pulse at half-height – the length of time during which the energy of the pulse is released in the WCH, n is the pulse repetition rate, T is the treatment duration.

We suppose that water in the WCH is a purely resistive load. The pulse duration is determined from the oscillograms.

According to the voltage oscillogram, it is possible to find the active resistance R_{wch} of water in the chamber, knowing the value of the high-voltage capacitance C_{hv} in which energy is accumulated before after transformation in the transformer ИОМ 100/100 [7]

$$(t/0.7) = R_{wch}\cdot C_{hv}, \qquad (2)$$

where t is the pulse duration at half-height, and $t/0.7$ is the pulse duration before the measured value decreases from the amplitude value in $e \approx 2.71828$ time.

For our installation $C_{hv} \approx 10^{-8}$ F, $t \approx 380$ ns (see oscillogram in Fig. 10). Thus

$$R_{wch} = (t/0.7)/C_{hv} = (3.8\cdot10^{-7}/0.7)/10^{-8} \approx 54.3\ \Omega.$$

Taking into account that $u_{av} \approx 40$ kV, $i_{av} = u_{av}/R_{wch} = 40000$ V/54.3 Ω ≈ 736.65 A. From here it follows that at $n = 400$ pulses/s, $T = 10$ s, $t = 3.8\cdot10^{-7}$ s, the energy E_{wch} dissipated in the chamber is $E_{wch}=nTi_{av}u_{av}t = 400$ pulses/s × × 10 s × 736.65 A ×40000 V × 3.8×10^{-7} s = 16 × 736.65 × × 3.8 ≈ 44.8 kJ.

Here, the averaged power P consumed in the WCH with water approximately equals $P = E_{wch}/T = 44.8$ kJ/10 s ≈ ≈ 4.5 kW.

The energy E_{1C1} initially stored in the high-voltage discharge circuit in the capacitor $C1$ before each discharge can be estimated by the formula

$$E_{1C1} = C1\cdot u_{C1}^2/2 \approx 10^{-8}\cdot(50\cdot10^3)^2/2 = 12.5\ \text{J}.$$

We estimate the total energy E_{C1} accumulated in $C1$ during time T

$$E_{C1} = nTE_{1C1} = 400\ \text{pulses/s} \times 10\ \text{s} \times 12.5\ \text{J} = 50000\ \text{J} = 50\ \text{kJ}.$$

$$E/E_{C1} \approx 44.8/50 = 0.896.$$

The resistivity of the water in WCH can be estimated by the formula

$$\rho = R_{WCH}\times S/l, \qquad (3)$$

where S is the cross-sectional area of WCH with the liquid to be treated relative to the current flow direction, l is the length of the interelectrode gap in the WCH i.e. its (working chamber's) height.

At $S = 3.14 \cdot 4.75^2 \cdot 10^{-4} = 7.1 \cdot 10^{-3}$ m^2, $l = 1.5 \cdot 10^{-2}$ m:

$\rho = 54.3\ \Omega \times 7.1 \times 10^{-3}$ m^2/$1.5 \cdot 10^{-2}$ m = 25.7 Ω·m.

We estimate the heating Δt of water in a non-current (stationary) WCH for $T = 10$ s with energy $E \approx 44.8$ kJ dissipated in the chamber. If we assume that half of this energy was used to heating the water, and the other half to heating the metal electrodes - the covers of the WCH and its insulating (fluoroplastic) housing, then

$$E = 2 \cdot c \cdot V \cdot \gamma \cdot \Delta t, \text{ i.e. } \Delta t = 0.5 \cdot E/(c \cdot V \cdot \gamma), \qquad (4)$$

where $c = 4200$ J/(kg·K) is the specific heat of water, V is the water volume in the WCH, $\gamma = 10^3$ kg/m^3 is the density of water.

$$V = S \cdot l = 7.1 \cdot 10^{-3}\ \text{m}^2 \cdot 1.5 \cdot 10^{-2}\ \text{m} \approx 10^{-4}\ \text{m}^3.$$

So:

$$\Delta t = 0.5 \cdot 44.8 \cdot 10^3 \text{J}/(4200\ \text{J/(kg·K)} \times \times 10^{-4}\ \text{m}^3 \cdot 10^3\ \text{kg/m}^3) = 53.3\ \text{K}.$$

The obtained calculated result is in good agreement with the experimental result on heating water in a given WCH under CHVIA treatment. The measurements were carried out with a M890G tester using a thermocouple. The measured temperature drop from the initial (start) t_{start} to the final t_{final} was $\Delta t_{exp} = t_{final} - t_{start} \approx 74 - 20 = 54$ K. Hence the conclusion follows that practically all the electromagnetic energy reaching the WCH is released in it in the form of heat. This is of fundamental importance, since both electromagnetic factors (electric and magnetic field strength, voltage and current in the WCH) and thermal energy are synergistically directed (unidirectional) factors. This unidirectional effect leads to an increase in the degree of inactivation of microorganisms in the flowable liquid products processed in the WCH. At the same time, all energy supplied to the WCH is used for its intended purpose – microbiological disinfection of the product processed in the chamber. If we now assume that all the heat released in the chamber is transferred through a heat exchanger to an unprocessed product that has not yet passed through the WCH, then the efficiency η_e for the given technological process $\eta_e \approx$ 85-99.5%.

An important indicator is also the specific energy consumption of E_{sp}, that is, the amount of energy expended for processing a unit (for example, units of volume or mass) of the product. At CHVIA processing in industrial flowing option, when rational heat exchange is involved, this is the amount of electromagnetic energy E_{flow} introduced into the WCH which in the chamber passes into thermal energy. Here, the product heating Δt_{flow} is guaranteed in the flow mode, while it flows through the WCH, by several K (for example, by 5 K) and the transition from the subcritical temperature to the supercritical temperature of the product which ensures irreversible inactivation of microorganisms under the action of high external pulsed electric field.

Estimation of E_{flow} and E_{sp}

$$E_{flow} \approx c \cdot V \cdot \gamma \cdot \Delta t_{flow} = 4200\ \text{J/(kg·K)} \times 10^{-4}\ \text{m}^3 \times 10^3\ \text{kg/m}^3 \times \times 5\ \text{K} = 2100\ \text{J};$$

$$E_{sp} = E_{flow}/V = c \cdot \gamma \cdot \Delta t_{flow} = 2100\ \text{J}/10^{-4}\ \text{m}^3 = 2.1 \cdot 10^7\ \text{J/m}^3 = = 2.1 \cdot 10^4\ \text{kJ/m}^3 = (21000/3600)\ \text{kW·h/m}^3 = = 5.83\ \text{kW·h/m}^3.$$

Thus, the estimated value of the specific energy consumption in the flowing mode at CHVIA treatment of products is $E_{sp} = 5.83$ kWh/m^3. AT the traditional scheme of microbiological milk disinfection (with the help of heat treatment – pasteurization), the specific energy consumption is more, at least 4 times [1, 2].

Conclusions.

1. Rational modes of operation of CHVIA installation for the tested working chambers take place at amplitudes of pulsed electric field strength $E \approx 30$ kV/cm in the liquid in the working chamber and at the treatment duration of 20 s with high-voltage pulses of duration 300-1200 ns at pulse repetition rate $n \approx 400$ pulses/s.

2. At rational modes in the treated water, milk whey and milk, the demonstrative *E.coli* bacteria are completely and irreversibly inactivated. In this case, the enzyme peroxidase in milk is preserved. Consequently, the tested rational mode of disinfecting milk treatment is milder than the mode of thermal sterilization, and approximately corresponds to pasteurization.

3. The amount of vitamin C, highly sensitive to various treatments, after treating milk in rational modes is maintained at a level that meets the requirements of regulatory documentation, that is, CHVIA treatment is a soft treatment that preserves the biological and nutritional value of the products.

4. Estimated value of specific energy consumption in flowing mode AT CHVIA treatment of products is $E_{sp} \approx 6$ kWh/m^3, which is about 4 times less than at traditional heat treatment. At the same time, the energy efficiency of the proposed complex of high-voltage pulse actions is 4 times higher compared with pasteurization.

5. The results of the performed investigations open the prospect of the industrial application of a complex of high-voltage pulse actions for the disinfecting treatment of water-containing food products.

REFERENCES

1. Minuhin L.A., Gaffner V.V., Menshenin G.A. Study the possibility of reducing energy consumption during the pasteurization of milk on small enterprises. *Agrarnoe obrazovanie i nauka*, 2016, no.3. (Rus).

2. Solovyov S.V. *Povyshenie effektivnosti protsessa teplovoy obrabotki moloka putem obosnovaniya konstruktivnykh i tekhnologicheskikh parametrov nagrevatelya. Diss. cand. techn. nauk* [Improving the efficiency of the process of milk thermal processing by justifying the design and technological parameters of the heater. Cand. tech. sci. diss.]. Velikie Luki, Russia, 2016. 155 p. (Rus).

3. Boyko N.I., Tur A.N., Evdoshenko L.S., Zarochentsev A.I. High-voltage pulse generator with an average power of up to 50 kW for treatment of food products. *Instruments and experimental technique*, 1998, no.2, pp. 120-126. (Rus).

4. Kuchinskiy G.S. *Vysokovoltnye impulsnye kondensatory.* [High-voltage pulse capacitors]. Leningrad, Energiya Publ., 1973. 176 p. (Rus).

5. *Losses and efficiency in transformers*. Available at: www.ets.ifmo.ru/usolzev/SEITEN/u2/tr/1_9.htm (accessed 15 May 2017). (Rus).
6. Mesiats G.A. *Impul'snaia energetika i elektronika* [Pulsed power and electronics]. Moscow, Nauka Publ., 2004. 704 p. (Rus).
7. Bogatenkov I.M., Imanov G.M., Kizevetter V.E. *Tekhnika vysokikh napriazhenii: Uchebnoe posobie dlya vuzov* [High voltage techniques]. Saint Petersburg, PEIPK Publ., 1998. 700 p. (Rus).

M.I. Boyko[1], *Doctor of Technical Sciences, Professor,*
A.V. Makogon[1],
A.I. Marynin[2], *Candidate of Technical Sciences, Associate Professor,*
[1] National Technical University «Kharkiv Polytechnic Institute»,
2, Kyrpychova Str., Kharkiv, 61002, Ukraine,
phone +380 57 7076245,
e-mail: qnaboyg@gmail.com
[2] National University of Food Technologies,
68, Volodymyrska Str., Kyiv, 01601, Ukraine,
e-mail: andrii_marynin@ukr.net

Received 13.03.2018

How to cite this article:
Boyko M.I., Makogon A.V., Marynin A.I. Energy efficiency of the disinfection treatment of liquid foodstuffs by high-voltage pulse effects. *Electrical engineering & electromechanics*, 2018, no.3, pp. 53-60. **doi: 10.20998/2074-272X.2018.3.07.**

UDC 621.31 **doi: 10.20998/2074-272X.2018.3.08**

H. Glaoui, A. Harrouz

SLIDING MODE CONTROL OF THE DFIG USED IN WIND ENERGY SYSTEM

This paper, presents the application of the direct vector control using the sliding mode control (SMC) on the doubly fed induction generators (DFIG). The synthesis of the control laws is based on the model obtained by the orientation of the stator flux. The active and reactive powers that are generated by the doubly fed induction generators will be decoupled by the orientation of the stator flux and controlled by sliding mode controllers that have been developed. In order to rule on the validity as well as the performance of this type of adjustment, we will check its robustness by varying some parameters of the machine doubly fed induction. References 34, figures 9.
Key words: **doubly fed induction generators (DFIG), vector control, sliding mode control.**

Цель. В статье представлено применение прямого векторного управления с использованием управления режимом скольжения (SMC) на индукционных генераторах двойного питания (DFIG). Синтез законов управления основан на модели, полученной с помощью ориентации потока статора. Активные и реактивные мощности, генерируемые индукционными генераторами двойного питания, разделены ориентацией потока статора и управляются разработанными контроллерами режима скольжения. Чтобы определить достоверность и эффективность данного типа регулирования, проверяется его надежность путем варьирования ряда параметров машины двойного питания. Библ. 34, рис. 9.
Ключевые слова: **индукционные генераторы двойного питания (DFIG), векторное управление, управление режимом скольжения.**

Introduction. The technique of sliding mode control (SMC) was first developed for a linear system of the second order, and since then, the spectrum of its use has been extended to a larger case of linear, nonlinear, discrete and multi-variable systems [1, 2]. Variable structure control has gained some popularity because of its simplicity and efficiency. In such a system, the command by switching makes it possible to bring the figurative point of the evolution of the system on the super sliding surface. When this hyper-surface is reached, the sliding regime occurs [3-5].

Many strategies have been developed over the past decade to optimize the power extracted from the wind energy conversion system. Several authors have tackled the control problem of electrical machines operating in the field-weakening region. For example, Taraft and all [6], Saleh Mobayen, Fairouz Tchier [7], Ansarifar, and all [8], Bartolini and al. [9], Benbouzid and al. [10], Seibel and al. [11] which used the sliding mode approach to achieve active and reactive power control. Hongchang Sun and all [12] explored the maximum wind power tracking of doubly fed wind turbine system based on adaptive gain second-order sliding mode. Kassem and all [13], Belmokhtar and all [14] proposed a dynamic modeling and robust power control of doubly fed induction generators (DFIG) driven by wind turbine at infinite grid. Weng and al. [15] a sliding mode regulator for maximum power tracking and copper loss minimisation of a doubly fed induction generator. Abdeddaim and all [16] Optimal tracking and robust power control of the DFIG wind turbine.

With the planned strategy, the generated wind energy can reach twice its nominal value thanks to a fast and reliable electric control completely robust. Indeed, by employing an appropriate control technique where the power produced in DFIG mode is derived from both the stator and the rotor. In addition, the power supplied by the rotor increases in this case by 100 % with respect to the nominal power of the stator. However, this solution makes it possible to maintain the operation of the wind energy conversion system in its stable zone.

The system considered consists of a dual-feed induction generator whose stator is directly connected to the gate and its rotor is powered by a matrix converter. In this paper, the sliding-mode approach to performing active and reactive power control is used.

This last enjoys interesting strong properties such as the insensitivity to the variations of the parameters of the controlled part as well as to the disturbances, which can act on this last one. Its behavior does not depend any more than the parameters that define the hyperactive surface of the slip. Despite having various advantages, this control technique also has a disadvantage that limited its use initially. Indeed, in practice, imperfections such as switching delays and hysteresis generate oscillations around the sliding surface. Several techniques have been proposed to overcome this disadvantage [11, 17]. Some consist in approximating the discontinuous function by a continuous function in the vicinity of the switching surface, the reduction of chattering taking place at the cost of a loss of precision. Due to the many advantages of variable structure control, such as robustness, speed, and simplicity of implementation, this type of control seems to us quite suitable for dual feed generators for which performance can be required. Moreover, as some parameters of the generator prove to vary during the operation and that the load is often unknown; the control will have to take into account these parametric disturbances and variations to avoid a degradation of performances [18]. The main objective of this paper is to advance the understanding of the controlled SMC in the wind system, by studying its behavior with wind energy system. Taking into account many unresolved issues associated with wind energy, the results of the analysis and evaluation of discretization behaviors in the SMC systems are essential for their applications in the control of renewable energies [19].

However, the analysis and evaluation of discretization behaviors in SMC systems has proved to be a difficult task due to the lack of work done on this topic. There is apparently a gap between the expected ideal dynamic performance based on continuous-time system models and the actual dynamic performance when the

control system is discretized. Delay in delivery of control signals due to discretization is the key factor affecting control performance. This is especially true when the control is of a discontinuous nature, such as SMC. «Disruptive» switching may cause incorrect actions due to the timely delivery of control signals. These behaviors can cause serious damage to industrial control devices such as actuators [19]. In addition, the deteriorated invariance property can worsen the reliability of SMC systems, making controlled industrial processes vulnerable to unexpected environmental changes.

Issues of interest in studying discretization behaviors in SCM systems include:

- conditions to ensure stability;
- steady state boundary conditions;
- system trajectory models (periodicity);
- sensitivity of trajectories to initial conditions;
- relationship between trajectory models and their symbolic sequences;
- dynamic behavior change with respect to the sampling period.

To our knowledge, this research is the first to systematically study the discretization behaviors of SMC systems, and to develop methods for controlling the wind system based on the DFIG generator. The significance of this work lies in the fact that it promotes the understanding of discretization behaviors in SMC systems, thus providing useful measures to prevent potential behavior from occurring. It also results in new methods useful not only for the analysis of the discretization of the SMC systems, but also for the synthesis of the laws of the controls as a function of the model obtained by the orientation of the stator flux.

The characteristic feature of a continuous time SMC systems is that a sliding mode occurs on a prescribed manifold, or switching surface, where a switching control is employed to maintain the state on that surface [20-23]. Since the theory has been originally developed from a continuous time perspective, implementation of sliding mode for sampled data systems encounters several incompatibilities due to limited sampling rate, sample/hold effect, and discretization errors. As a result, a direct translation of continuous-time SMC design for discrete implementation leads to the chattering phenomenon in the vicinity of the switching surface.

In this paper, basic results obtained in the study of continuous-time and discrete-time SMC systems theory during its over twenty years history are reviewed. The discretization issue of SMC systems is introduced.

Machine model. Flux-Oriented Vector Control presents an attractive solution for achieving better performance in variable speed applications for the doubly fed induction machine in both generator and motor operation. With this in mind, we have proposed a control law for the DFIM (doubly fed induction machine) based on the orientation of the stator flux, used to make it work as a generator. The latter highlights the relationships between the stator and rotor quantities [24-26]. These relationships will allow to act on the rotor signals to control the active power exchange and reactivate between the stator of the machine and the power system.

The wind turbine rotates at a speed that depends on the wind speed (Fig. 1). This speed is matched to that of the electric generator through a gearbox [27, 28].

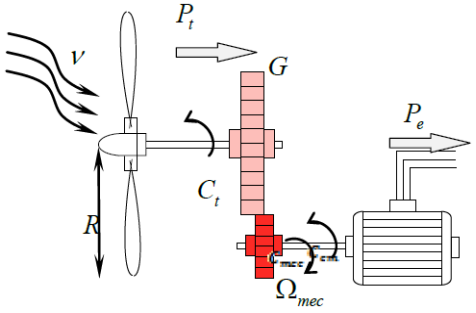

Fig. 1. Wind turbine model

The output power of wind turbine is given as

$$p_m = \frac{\rho A}{2} C_p(\lambda, \beta) v_{wind}^3 , \quad (1)$$

where, p_m is mechanical output power of the turbine (W); ρ is air destiny (kg/m^3); A is turbine swept area (m^2); β is blade pitch angle (deg); λ is tip speed ratio of the rotor blade tip speed to wind speed; C_p is performance coefficient of wind turbine, which is the function of β and λ; v_{wind} is wind speed (m/s).

The tip speed ratio λ is calculated as

$$\lambda = \frac{R\omega_T}{v_{wind}} . \quad (2)$$

From an engineering point of view, there are many different representing methods of performance coefficient C_p.

But they all represent C_p as a nonlinear function of β and λ. In this paper, C_p is denoted as

$$C_p(\lambda, \beta)) = C_1((\frac{C_2}{\lambda_i} - C_3(\beta + 2.5) - C_4)e^{\frac{-C_5}{\lambda_i}} + C_6\lambda_i , \quad (3)$$

where $C_1 = 0.645$, $C_2 = 116$, $C_3 = 0.4$, $C_4 = 5$, $C_5 = 21$, $C_6 = 0.00912$.

Variable λ_i can be calculated as

$$\frac{1}{\lambda_i} = \frac{1}{\lambda + 0.08(\beta + 2.5)} - \frac{0.035}{(\beta + 2.5)^3 + 1} . \quad (4)$$

Wind turbine dynamics simulations have been run for wind step changes. The characteristic feature of the dependence of the wind turbine power upon the wind speed has been illustrated in Fig. 2 (the nominal power being 2 MW) [29].

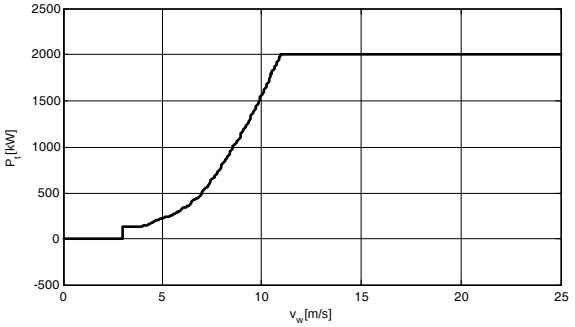

Fig. 2. Static characteristic of wind turbine mechanical power as a function of mean wind speed

For a given wind speed v_m the wind turbine power p_t and the moment $m_t = p_t / w_t$.

Model of generator «DFIG». In order to implement the decoupling control of active and reactive power, it is essential to transform the voltage and current of induction generator stator and rotor from 3-phase form to *dq* form under synchronous rotation coordinates. In addition, the voltage and flux equations of induction generator are seen as (5) and (6) respectively

$$\begin{aligned} V_{ds} &= R_s I_{ds} + \frac{d}{dt}\psi_{ds} - \dot{\theta}_s \psi_{qs}; \\ V_{qs} &= R_s I_{qs} + \frac{d}{dt}\psi_{qs} - \dot{\theta}_s \psi_{ds}; \\ V_{dr} &= R_r I_{dr} + \frac{d}{dt}\psi_{dr} - \dot{\theta}_r \psi_{qr}; \\ V_{qr} &= R_r I_{qr} + \frac{d}{dt}\psi_{qr} - \dot{\theta}_r \psi_{dr}; \end{aligned} \quad (5)$$

$$\begin{aligned} \psi_{ds} &= L_r I_{ds} + M I_{dr}; \\ \psi_{qs} &= L_s I_{qs} + M I_{qr}; \\ \psi_{dr} &= L_r I_{dr} + M I_{ds}; \\ \psi_{qr} &= L_r I_{qr} + M I_{qs}, \end{aligned} \quad (6)$$

where V_{ds}, V_{qs}, V_{dr} and V_{qr} are respectively the *dq* coordinates components of stator and rotor voltage; I_{ds}, I_{qs}, I_{dr} and I_{qr} are respectively the *dq* coordinates components of stator and rotor current; ψ_{ds}, ψ_{qs}, ψ_{dr} and ψ_{qr} are respectively the *dq* coordinates components of stator and rotor flux; L_r, L_s and $M = L_m$.

The electromagnetic torque is expressed as:

$$C_{em} = 3/2(\psi_{ds} I_{qs} - \psi_{qs} I_{ds}); \quad (7)$$

$$P = V_{ds} I_{ds} - V_{qs} I_{qs}; \quad (8)$$

$$Q = V_{qs} I_{ds} - V_{ds} I_{qs}.$$

This strategy consists to turn the rotor flux towards d axis, and the stator flux towards q axis. After orientation the stator and rotor fluxes are presented in Fig. 3

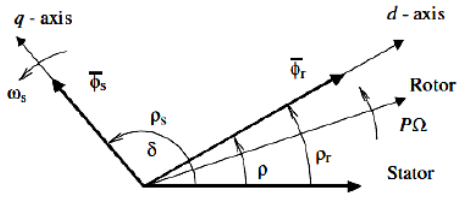

Fig. 3. DFIG vector after orientation

Consequently, the two fluxes become orthogonal and we can write:

$$\psi_{qs} = \psi_s; \quad \psi_{dr} = \psi_r; \quad \psi_{qr} = \psi_{ds} = 0. \quad (9)$$

If resistance R_s is neglected we have:

$$V_{qs} = \frac{d}{dt}\psi_{qs} = 0; \quad V_{ds} = V_s.$$

The developed active power and reactive power can be rewritten as follows:

$$P = V_s I_{ds}; \quad Q = -V_s I_{qs},$$

where

$$I_{ds} = -\frac{M}{L_s} I_{dr}; \quad I_{qs} = -\frac{L_r}{M} I_{qr},$$

where

$$P = -V_s \frac{M}{L_s} I_{dr}; \quad Q = V_s \frac{L_r}{M} I_{qr}.$$

Sliding Mode Control. The term *«variable structure systems»* appears because of the particular structure of the system or regulator used, where this structural change in a discontinuous manner between two or more structures.

In the formulation of any practical control problem, there will always be a discrepancy between the actual plant and its mathematical model used for the controller design. These discrepancies (or mismatches) arise from unknown external disturbances, plant parameters, and parasitic/modeled dynamics [30, 31]. Designing control laws that provide the desired performance to the closed-loop system in the presence of these disturbances/uncertainties is a very challenging task for a control engineer. This has led to intense interest in the development of the so-called robust control methods, which are supposed to solve this problem. One particular approach to robust controller design is the so-called sliding mode control technique.

The behavior of nonlinear systems with discontinuities can be formally described by the generalized state equation:

$$\dot{X}(t) = F(X, t, U), \quad (10)$$

where $X \in \Re^n$ is the state vector, t time and is the function describing the evolution of the system over time. This class of system has a term which represents, at the same time, the discontinuity and the control: U.

Historically, the first regulators built on this model have been simple relays. Easy to implement. They have led the automation engineers to develop a theory that can describe such an operation. The bases of such a theory have been laid: it suffices to say that the behavior of the system is described by two distinct differential equations, depending on whether the equation of evolution of the system is greater or less than a surface called hyper-surface (increased surface) switching where:

$$S(X) = (S_1(X), S_2(X), ..., S_m(X)).$$

So we have

$$U(X) = \begin{cases} U^+(X,t), & \text{if} \quad S(X,t) > 0; \\ U^-(X,t), & \text{if} \quad S(X,t) < 0. \end{cases} \quad (11)$$

We consider a nonlinear system defined as

$$x^{(n)}(t) = f(x,t) + b(x,t)u(x,t), \quad (12)$$

where x is the state vector and are nonlinear functions and is the control input $f(x, t)$, $b(x, t)u$.

To design a sliding mode control law, we must firstly, choose the switching surface (Fig. 4).

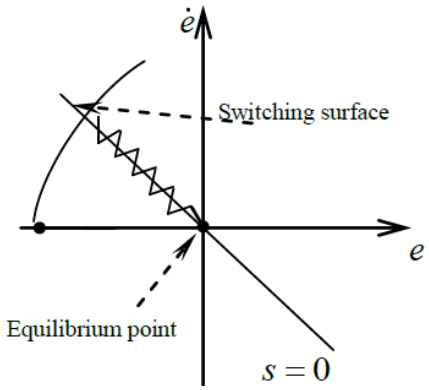

Fig. 4. Sliding mode in a phase plane

We take the general form proposed by Slotine [24]:

$$S = \left(\frac{d}{dt} + \lambda\right)^{(n-1)} e, \qquad (13)$$

where $e = x - x_d$ is the tracking error; is x_d the desired state, is n the system order and λ is a positive coefficient.

After choosing the sliding surface, we must choose the control law where the reaching condition defined by Lyapunov equation satisfied

$$S\dot{S} < 0 \quad \forall t. \qquad (14)$$

The control law has the following form.

Thus, the vector control to be applied to the system is obtained by adding two control terms such as

$$U = U_{eq} + U_n, \qquad (15)$$

where U_{eq} on the sliding mode; U_n allows to influence the approach mode.

In order that the condition (19) is verified at any time, is chosen as follows [32] (a complete study of sliding-mode with ERL can be found in [32]

$$\dot{S} = -\frac{k}{\delta_0 + (1-\delta_0)e^{-\alpha|S|^p}} \text{sat}\left(\frac{S}{\phi}\right), \qquad (16)$$

where k is the discontinuous gain,

$$t_{rd} = \delta_0 \frac{|S(0)|}{k} + \frac{(1-\delta_0)}{k\alpha^{1/p}},$$

is the desired reaching time, $\alpha \geq 0$, $0 < \delta_0 < 1$ and $p > 0$, $\text{sat}\left(\frac{S}{\phi}\right)$ is the saturation function

$$\text{sat}\left(\frac{S}{\phi}\right) = \begin{cases} 1, \text{ if } \frac{S}{\phi} > 1; \\ \frac{S}{\phi}, \text{ if } -1 \leq \frac{S}{\phi} \leq 1; \\ -1, \text{ if } \frac{S}{\phi} < -1. \end{cases} \qquad (17)$$

The use of saturation function instead of *sign* function is justified to avoid chattering phenomenon.

The sliding mode applied to DFIG. We will use this technique to control the rotor currents of DFIG with a strongly coupled model [33, 34] (Fig. 5).

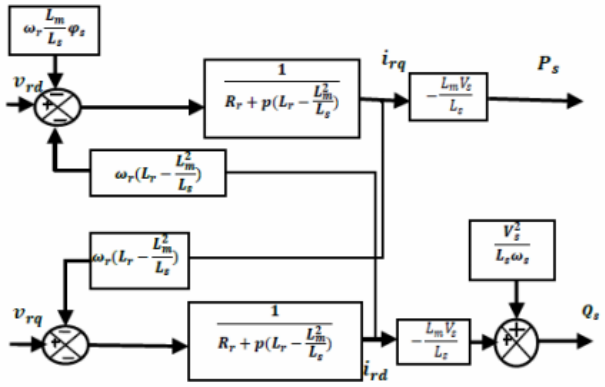

Fig. 5. Global scheme mode of the DFIG control

Recall the model of DFIG in Park's Den which is given by the following equations:

$$\begin{cases} V_{dqs} = R_s I_{dqs} + \frac{d\Phi_{dqs}}{dt} \mp \omega_s \cdot \Phi_{dqs}; \\ V_{dqr} = R_s I_{dqr} + \frac{d\Phi_{dqr}}{dt} \mp \omega_r \cdot \Phi_{dqr}; \end{cases} \qquad (18)$$

$$\begin{cases} \Phi_{dqs} = L_s I_{dqs} + M \cdot I_{dqr}; \\ \Phi_{dqr} = L_s I_{dqr} + M \cdot I_{dqs}. \end{cases} \qquad (19)$$

The vector of the state variables chosen for the control of the machine is given by:

$$x = \begin{pmatrix} \Phi_{ds} \\ \Phi_{qs} \\ I_{dr} \\ I_{qr} \end{pmatrix}.$$

The model of the machine with the consideration of the state variables is given by the following equations:

$$\begin{pmatrix} V_{ds} \\ V_{qs} \\ V_{dr} \\ V_{qr} \end{pmatrix} =$$

$$= \begin{bmatrix} R_s \cdot a\Phi_{ds} - R_s \cdot c\left(L_r \sigma I_{dr} + \frac{M}{L_s \omega_s} V_{qs}\right) - \omega_s \Phi_{qs} + \frac{d\Phi_{ds}}{dt}; \\ R_s \cdot a\Phi_{qs} - R_s \cdot c\left(L_r \sigma I_{qr} + \frac{M}{L_s \omega_s} V_{ds}\right) + \omega_s \Phi_{ds} + \frac{d\Phi_{qs}}{dt}; \\ R_r \cdot b\left(L_r \sigma I_{dr} + \frac{M}{L_s \omega_s} V_{qs}\right) - R_r \cdot c\Phi_{ds} - \omega_r\left(L_r \sigma I_{qr} + \frac{M}{L_s \omega_s} V_{ds}\right) + L_r \sigma \frac{dI_{dr}}{dt}; \\ R_r \cdot b\left(L_r \sigma I_{qr} + \frac{M}{L_s \omega_s} V_{ds}\right) - R_r \cdot c\Phi_{qs} + \omega_r\left(L_r \sigma I_{dr} + \frac{M}{L_s \omega_s} V_{qs}\right) + L_r \sigma \frac{dI_{qr}}{dt}. \end{bmatrix}$$

$$a = \frac{1}{\sigma L_s}, \; b = \frac{1}{\sigma L_r}, \; c = \frac{M}{\sigma L_s L_r}.$$

The state model of the machine is put in the following form:

$$\dot{X} = f(x,t) + g(x,t)U_{dq}; \qquad (20)$$

$$\dot{X} = \begin{bmatrix} \frac{d\Phi_{ds}}{dt} \\ \frac{d\Phi_{qs}}{dt} \\ \frac{dI_{dr}}{dt} \\ \frac{dI_{qr}}{dt} \end{bmatrix} \cdot g(x,t) = \begin{bmatrix} 1 & 0 & 0 & 0 \\ 0 & 1 & 0 & 0 \\ 0 & 0 & \frac{1}{\sigma L_r} & 0 \\ 0 & 0 & 0 & \frac{1}{\sigma L_r} \end{bmatrix};$$

$$U_{dq} = \left|V_{ds} V_{qs} V_{dr} V_{qr}\right|;$$

$$\begin{bmatrix} -R_s \cdot a\Phi_{ds} + R_s \cdot c\left(L_r \sigma I_{dr} + \frac{M}{L_s \omega_s} V_{qs}\right) + \omega_s \Phi_{qs} \\ -R_s \cdot a\Phi_{qs} + R_s \cdot c\left(L_r \sigma I_{qr} + \frac{M}{L_s \omega_s} V_{ds}\right) - \omega_s \Phi_{ds} \\ \frac{1}{\sigma L_r}\left(-R_r \cdot b\left(L_r \sigma I_{dr} + \frac{M}{L_s \omega_s} V_{qs}\right) + R_r \cdot c\Phi_{ds} + \omega_r\left(L_r \sigma I_{qr} + \frac{M}{L_s \omega_s} V_{ds}\right)\right) \\ \frac{1}{\sigma L_r}\left(-R_r \cdot b\left(L_r \sigma I_{qr} + \frac{M}{L_s \omega_s} V_{ds}\right) + R_r \cdot c\Phi_{ds} - \omega_r\left(L_r \sigma I_{dr} + \frac{M}{L_s \omega_s} V_{qs}\right)\right) \end{bmatrix} =$$

$= f(x,t)$.

Sliding surfaces in the Park marker are defined to control the rotor currents. They are given by the following equations:

$$\begin{cases} S_d = \lambda\left(I_{drref} - I_{dr}\right), \\ S_q = \lambda\left(I_{qrref} - I_{qr}\right), \end{cases}$$

where V_{dr} and V_{qr} are the two control vectors, to force the system path to converge to surfaces $S_{dq} = 0$.

The control vector U_{dqeq} is obtained by imposing $S_{dq} = 0$

$$f(x,t) + g(x,t)U_{dq} = 0\,; \qquad (21)$$

$$U_{eqdq} = \begin{bmatrix} -\left(-R_r \cdot b\left(L_r\sigma I_{dr} + \frac{M}{L_s\omega_s}V_{qs}\right) + R_r \cdot c\Phi_{ds} + \omega_r\left(L_r\sigma I_{qr} + \frac{M}{L_s\omega_s}V_{ds}\right)\right) \\ -\left(R_r \cdot b\left(L_r\sigma I_{qr} + \frac{M}{L_s\omega_s}V_{ds}\right) + R_r \cdot c\Phi_{qs} - \omega_r\left(L_r\sigma I_{dr} + \frac{M}{L_s\omega_s}V_{qs}\right)\right) \end{bmatrix}.$$

To have good performance, good dynamics and good switching around surfaces the control vector is imposed as follows:

$$U_{dq} = U_{dqeq} + Ksign(S_{dq})\,. \qquad (22)$$

Simulation results. The figures below (Fig. 6) represent the different curves by the simulation of the DFIG with sliding mode controllers.

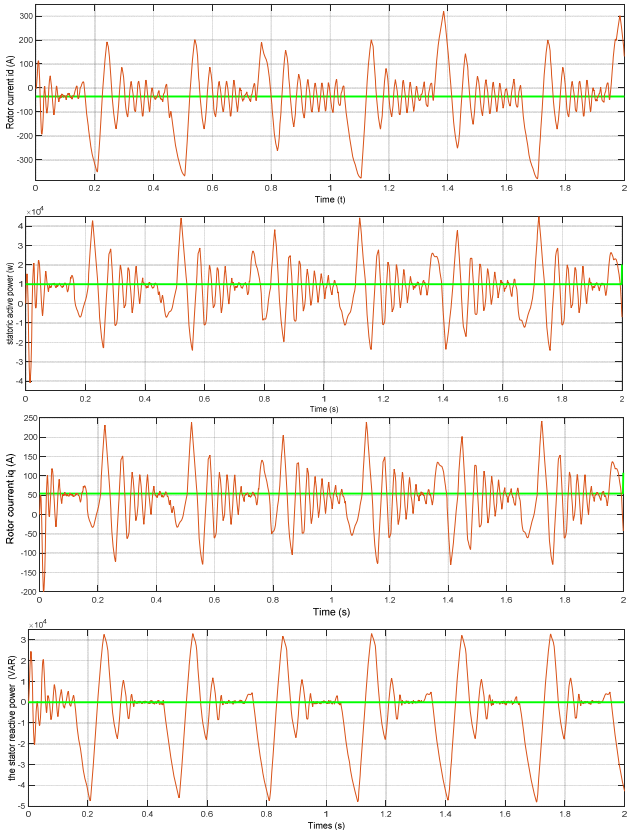

Fig. 6. Simulation results of the system GADA and voltage inverter

Its characteristics have allowed us to cite the performance of regulators in sliding mode, such as:

- good continues stator currents compared to references;
- perfect decoupling between the two components of the stator current.

Therefore, the control of the active power of the stator is by the direct component of the current, while the reactive power of the stator of the quadratic component of the stator current.

In order to test the robustness of this control structure by sliding mode, we studied the influence of parametric variations on the performance of the adjustment. We consider variations on all parameters that can undergo changes (stator and rotor resistors, stator, rotor and mutual inductors, and moment of inertia).

The results of the test of robustness to variations of the reference power simulation obtained show that decoupling is ensured at all times of the active and reactive powers, despite the presence of slight oscillations which are due to the Chattering phenomenon (Fig. 7).

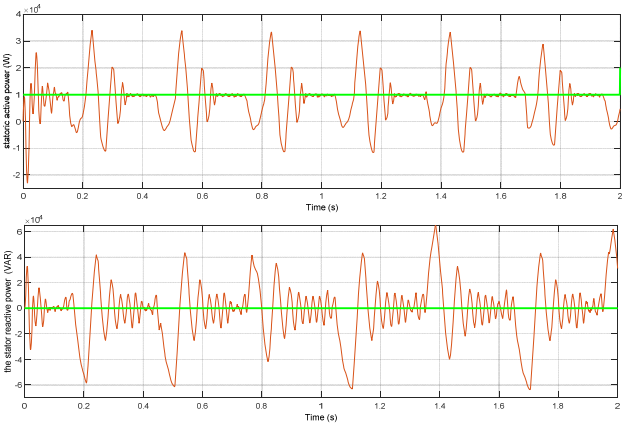

Fig. 7 Results of the system with the function sign

The results obtained in Fig. 8, 9 show that decoupling is ensured at all times of the active and reactive powers, despite the presence of slight oscillations that are due to the Chattering phenomenon.

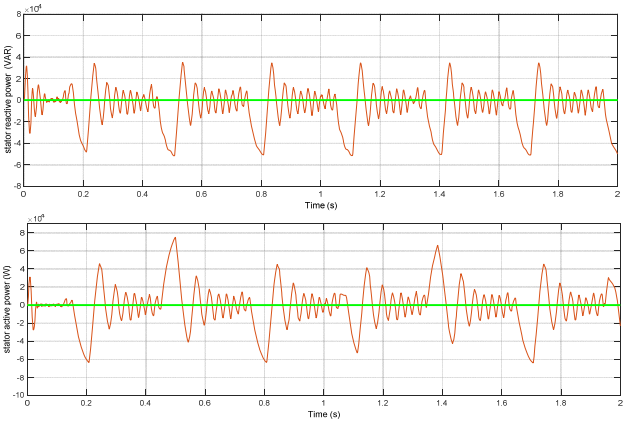

Fig. 8. Robustness test for a variation of R_s

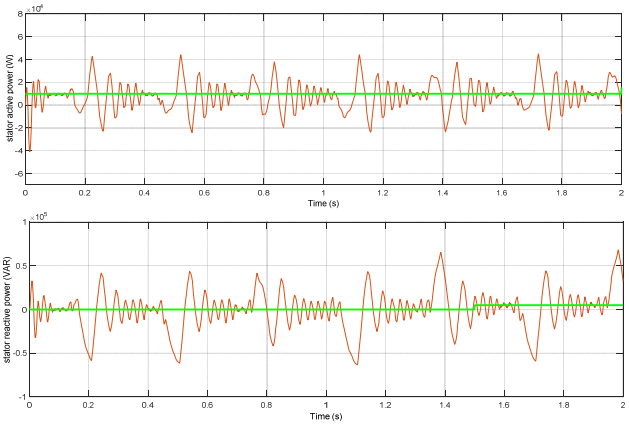

Fig. 9. Robustness test for a variation of R_r

Conclusion. In this paper, a complete system for electrical energy production has been done via wind

turbine by use of the doubly fed induction generator (DFIG). The studied system has been formed of a DFIG with stator and rotor, which in that stator has connected to the grid directly, machine converter and grid converter. With the consideration of turbine variable velocity state and design controller for DFIG in form of using of the sliding mode.

Firstly, we have introduced the simplicity of the control variable structure by sliding mode non-linear switching surface. Then, we are interested more closely in the application of this type of control on the asynchronous machine with double feeding. The setting of the active and reactive powers by the sliding mode brings a remarkable improvement and good system performance with DFIG.

The results of the simulations obtained are evaluated and carried out using the Matlab / Simulink software and show the performance and the effectiveness of the proposed control.

REFERENCES

1. Johnstone C.M., Nielsen K., Lewis T., Sarmento A., Lemonis G. EC FPVI co-ordinated action on ocean energy: A European platform ford sharing technical information and research outcomes in wave and tidal energy systems. *Renewable Energy*, 2006, vol.31, no.2, pp. 191-196. **doi: 10.1016/j.renene.2005.08.015.**

2. Ben Elghali S.E. et al. Les systèmes de génération d'énergie électriques à partir des courants de mare. *Revue 3EI*, 2008, no.52, pp. 73-85.

3. Benbouzid M.E.H. et al. Marine tidal current electric power generation technology: State of the art and current status. *Proceedings of IEEE IEMDC'07*, May 2007, Antalya (Turkey), vol.2, pp. 1407-1412.

4. Myers L., Bahaj A.S. Simulated electrical power potential harnessed by marine current turbine arrays in the Alderney Race. *Renewable Energy*, 2005, vol.30, no.11, pp. 1713-1731. **doi: 10.1016/j.renene.2005.02.008**.

5. Couch S.J., Bryden I. Tidal current energy extraction: Hydrodynamic resource characteristics. *Proceedings of the Institution of Mechanical Engineers, Part M: Journal of Engineering for the Maritime Environment*, 2006, vol.220, no.4, pp. 185-194. **doi: 10.1243/14750902jeme50**.

6. Taraft S., Rekioua D., Aouzellag D., Bacha S. A proposed strategy for power optimization of a wind energy conversion system connected to the grid. *Energy Conversion and Management*, 2015, vol.101, pp. 489-502. **doi: 10.1016/j.enconman.2015.05.047.**

7. Mobayen S., Tchier F. Robust global second-order sliding mode control with adaptive parameter-tuning law for perturbed dynamical systems. *Transactions of the Institute of Measurement and Control*, June 2017, p. 014233121770883. **doi: 10.1177/0142331217708832.**

8. Ansarifar G.R., Rafiei, M. Second-order sliding-mode control for a pressurized water nuclear reactor considering the xenon concentration feedback. *Nuclear Engineering and Technology*, 2015, vol.47, no.1, pp. 94-101. **doi: 10.1016/j.net.2014.11.003.**

9. Bartolini G., Levant A., Pisano A., Usai E. Adaptive second-order sliding mode control with uncertainty compensation. *International Journal of Control*, 2016, vol.89, no.9, pp. 1747-1758. **doi: 10.1080/00207179.2016.1142616.**

10. Benbouzid M., Beltran B., Mangel H., Mamoune A. A high-order sliding mode observer for sensorless control of DFIG-based wind turbines. *IECON 2012 – 38th Annual Conference on IEEE Industrial Electronics Society*, Oct. 2012, Montreal, Canada. pp. 4288-4292. **doi: 10.1109/iecon.2012.6389200**.

11. Evangelista C.A., Valenciaga F., Puleston P. Multivariable 2-sliding mode control for a wind energy system based on a double fed induction generator. *International Journal of Hydrogen Energy*, 2012, vol.37, no.13, pp. 10070-10075. **doi: 10.1016/j.ijhydene.2011.12.080.**

12. Sun H., Han Y., Zhang L. Maximum Wind Power Tracking of Doubly Fed Wind Turbine System Based on Adaptive Gain Second-Order Sliding Mode. *Journal of Control Science and Engineering*, vol. 2018, pp. 1-11. **doi: 10.1155/2018/5342971**.

13. Kassem A.M., Hasaneen K.M., Yousef A.M. Dynamic modeling and robust power control of DFIG driven by wind turbine at infinite grid. *International Journal of Electrical Power & Energy Systems*, 2013, vol.44, no.1, pp. 375-382. **doi: 10.1016/j.ijepes.2011.06.038.**

14. Belmokhtar K., Doumbia M.L., Agbossou K. Novel fuzzy logic based sensorless maximum power point tracking strategy for wind turbine systems driven DFIG (doubly-fed induction generator). *Energy*, 2014, vol.76, pp. 679-693. **doi: 10.1016/j.energy.2014.08.066.**

15. Weng Y.-T., Hsu Y.-Y. Sliding mode regulator for maximum power tracking and copper loss minimisation of a doubly fed induction generator. *IET Renewable Power Generation*, 2015, vol.9, no.4, pp. 297-305. **doi: 10.1049/iet-rpg.2014.0125.**

16. Abdeddaim S., Betka A. Optimal tracking and robust power control of the DFIG wind turbine. *International Journal of Electrical Power & Energy Systems*, 2013, vol.49, no.1, pp. 234-242. **doi: 10.1016/j.ijepes.2012.12.014.**

17. Myers L., Bahaj A.S. Power output performance characteristics of a horizontal axis marine current turbine. *Renewable Energy*, 2006, vol.31, no.2, pp. 197-208. **doi: 10.1016/j.renene.2005.08.022.**

18. Bossanyi E. *Wind Energy Handbook*. New York: Wiley, 2000.

19. Bin Wang. *On Discretization of Sliding Mode Control Systems*. Theses doctorate, School of Electrical and Computer Engineering RMIT University Melbourne, Australia, 2008.

20. Harmouche M. Contribution to the theory of higher order sliding mode control and the control of underactuated mechanical systems. Theses Doctorate, Universite de technologie de Belfort-Montbeliard, France, 2017.

21. Laghrouche S., Chitour Y., Harmouche M., Ahmed F.S. Path Following for a Target Point Attached to a Unicycle Type Vehicle. Acta Applicandae Mathematicae, 2012, vol.121, no.1, pp. 29-43. **doi: 10.1007/s10440-012-9672-8**.

22. Harmouche M., Laghrouche S., Ahmed F.S., Bagdouri M.E. Second-order sliding mode controllers: an experimental comparative study on a mechatronic actuator. *Proceedings of the Institution of Mechanical Engineers, Part I: Journal of Systems and Control Engineering*, 2012, vol.226, no.9, pp. 1231-1248. **doi: 10.1177/0959651812454061.**

23. Batten W.M.J., Bahaj A.S., Molland A.F., Chaplin J.R. Hydrodynamics of marine current turbines. *Renewable Energy*, 2006, vol.31, no.2, pp. 249-256. **doi: 10.1016/j.renene.2005.08.020.**

24. Harrouz A., ben Atialah A., Harrouz O. Modeling of small wind energy based of PMSG in south of Algeria. *2012 2nd International Symposium On Environment Friendly Energies And Applications*, Jun. 2012, pp. 191-195. **doi: 10.1109/efea.2012.6294042.**

25. Bahaj A.S., Molland A.F., Chaplin J.R., Batten W.M.J. Power and thrust measurements of marine current turbines under various hydrodynamic flow conditions in a cavitation tunnel and a towing tank. *Renewable Energy*, 2007, vol.32, no.3, pp. 407-426. **doi: 10.1016/j.renene.2006.01.012.**

26. Muller S., Deicke M., De Doncker R.W. Doubly fed induction generator systems. *IEEE Industry Applications Magazine*, 2002, vol.8, no.3, pp. 26-33. **doi: 10.1109/2943.999610.**

27. Park J.W., Lee K.W., Lee H.J. Wide speed operation of a doubly-fed induction generator for tidal current energy. *30th Annual Conference of IEEE Industrial Electronics Society, 2004. IECON 2004.* Busan (South Korea). **doi: 10.1109/iecon.2004.1431771.**

28. Multon B., Robin G., Gergaud O., Ben Ahmed H. Le génie électrique dans le vent : Etat de l'art dans le domaine de la génération éolienne. *congres Jeunes Chercheurs en Genie Electrique 2003,* June 2003, Saint Nazaire, France. 10 p.

29. Carrasco J.M., Franquelo L.G., Bialasiewicz J.T., Galvan E., PortilloGuisado R.C., Prats M.A.M., Leon J.I., Moreno-Alfonso N. Power-electronic systems for the grid integration of renewable energy sources: A survey. *IEEE Transactions on Industrial Electronics*, 2006, vol.53, no.4, pp. 1002-1016. **doi: 10.1109/tie.2006.878356.**

30. Tapia G., Tapia A., Ostolaza J.X. Proportional–integral regulator-based approach to wind farm reactive power management for secondary voltage control. *IEEE Transactions on Energy Conversion*, 2007, vol.22, no.2, pp. 488-498. **doi: 10.1109/tec.2005.858058.**

31. Tapia A., Tapia G., Ostolaza J.X., Saenz J.R. Modeling and control of a wind turbine driven doubly fed induction generator. *IEEE Transactions on Energy Conversion*, 2003, vol.18, no.2, pp. 194-204. **doi: 10.1109/tec.2003.811727.**

32. Koutroulis E., Kalaitzakis K. Design of a maximum power tracking system for wind-energy-conversion applications. *IEEE Transactions on Industrial Electronics*, 2006, vol.53, no.2, pp. 486-494. **doi: 10.1109/tie.2006.870658.**

33. Xu L., Cartwright P. Direct active and reactive power control of DFIG for wind energy generation. *IEEE Transactions on Energy Conversion*, 2006, vol.21, no.3, pp. 750-758. **doi: 10.1109/tec.2006.875472.**

34. Glaoui H., Abdelkader H., Messaoudi I., Saab H. Modelling of Wind Energy on Isolated Area. *International Journal of Power Electronics and Drive System* (IJPEDS), 2014, vol.4. no.2, pp. 274-280. **doi: 10.11591/ijpeds.v4i2.4859.**

Received 06.03.2018

Hachemi Glaoui[1]*, Ph.D.,*
Abdelkader Harrouz[2]*, Ph.D.,*
[1] Department of Electrical Engineering,
Tahri Mohamed Bechar University,
Bechar, Algeria,
e-mail: glaouih@yahoo.fr
[2] Department of Hydrocarbon and Renewable Energy,
Ahmed Draia University,
Adrar, Algeria,
e-mail: harrouz@univ-adrar.dz

How to cite this article:
Glaoui H., Harrouz A. Sliding mode control of the DFIG used in wind energy system. *Electrical engineering & electromechanics*, 2018, no.3, pp. 61-67. **doi: 10.20998/2074-272X.2018.3.08.**

UDC 621.316.99 **doi: 10.20998/2074-272X.2018.3.09**

I.V. Nizhevskyi, V.I. Nizhevskyi

A TECHNIQUE OF FULL-SCALE MEASUREMENTS OF THE RESISTANCE OF THE GROUNDING DEVICE

Purpose. *The measurements of the resistance of grounding devices for various purposes using a three-electrode installation under real conditions are considered.* ***Methodology.*** *On the basis of the use of a three-electrode installation, a technique for full-scale measurements of the resistance of a grounding device of any design in an arbitrary soil structure is presented.* ***Results.*** *Based on the measurement results, a system of sixth-order equations is solved which allows to determine the own and mutual resistances in a three-electrode installation with a sufficiently high accuracy.* ***Originality.*** *It is not necessary to find a point of zero potential.* ***Practical value.*** *The proposed technique allows to perform measurements in conditions of dense urban and industrial development.* References 9, tables 6, figures 2.

Key words: **grounding device, grounding resistance, full-scale measurements, technique, three-electrode installation, zero potential point, system of equations.**

Рассмотрены измерения сопротивления заземляющих устройств различного назначения с помощью трехэлектродной установки в реальных условиях. На основе использования трехэлектродной установки представлено обоснование методики измерения сопротивления заземляющего устройства любой конструкции в произвольной структуре грунта. По результатам измерений решается система уравнений шестого порядка, что позволяет определить собственные и взаимные сопротивления в трехэлектродной установке с достаточно высокой точностью и без отыскания точки нулевого потенциала. Библ. 9, табл. 6, рис. 2.

Ключевые слова: **заземляющее устройство, сопротивление заземления, натурные измерения, методика, трехэлектродная установка, точка нулевого потенциала, система уравнений.**

Introduction and problem definition. At present, a three-electrode measuring installation has been widely used to measure the resistance of grounding devices (GDs) [1]. One of the main tasks that must be solved in order to obtain sufficiently accurate results with this installation is, as indicated in [2], the correct choice of the locations of the measuring electrodes, i.e. such their arrangement at which the measured value of resistance differs from its true value by no more than 10 % in one direction or another. However, in a number of cases, the measurement of the resistance of the GD of urban and industrial substations presents a serious problem to this day.

Analysis of recent investigations and publications. Many domestic and foreign scientists solve the problem of increasing the accuracy of measuring the electrical parameters of the earth and GD.

The calculation method for determining the optimal arrangement of measuring electrodes at measuring the resistance of large-sized grounding devices with the help of the considered models has only limited application due to their external fields [3].

On the basis of a critical analysis of existing methods for determining the grounding resistance, a refined version of its definition was considered in [4]. By introducing the concept of special and quasi-equipotential regions of the grounding device, a new technique for measuring its resistance was proposed and experimentally tested. However, the proposed method in a number of cases does not allow measuring the resistance of grounding devices with acceptable accuracy.

In [5] a method of increased accuracy was proposed for measuring the grounding resistance of a substation at connecting a transmission line by measuring the grounding current using a specially developed wireless current sensor using GPS. Despite the fact that testing the method at an operating substation of 500 kV confirmed its validity, in some cases its use raises many questions and requires a serious and detailed analysis.

The principal possibility of an accurate measurement of the resistance of the grounding device was noted in [6]. However, unfortunately, in this case it will also be necessary to determine the location of the potential electrode by repeatedly finding the zero potential point at the measurement site.

Mathematical modeling of the process of measuring the resistance of the grounding device to the current of the power frequency in a multilayer soil showed [7] that it is impossible to choose by the experimental method for measurements on the terrain such an arrangement of electrodes in which the measured resistance of the grounding device is equal to the true.

In [8] the theoretical, and based on the use of the method of physical modeling in [9] the experimental justifications of a new method of measuring the resistance of the grounding device with the help of a three-electrode measuring installation for any character of ground heterogeneity, any size and configuration of GD and arbitrary placement of measuring electrodes without finding the zero potential point are presented.

The goal of the work is the development of a technique for full-scale measurements of the resistance of the grounding device by means of a three-electrode measuring installation without finding a zero potential point.

Recommended method of full-scale measurements in a group of grounding devices and processing of measurement results to obtain the values of own and mutual resistances in a three-element system. Preparation and carrying out of measurements of electrical parameters of the GDs of operating substations of voltage class above 1 kV must exclude dangerous situations that may arise in this case. For example, in

conditions of industrial or urban development, the removal of electrodes over long distances is associated with the possibility for potential outflow which poses a serious danger.

Wires and cables connecting the source of electricity, instruments, grounding devices, usually have a significant length, especially at large dimensions of the tested grounding device. In this case, it is necessary to observe two rules [2]:

a) the connecting lines must not be laid parallel or at a slight acute angle to the overhead line (OL) route. The position of the electrodes (grounding conductors), in addition to the tested one, should be chosen so that the connecting lines are located with respect to the OL route either at an angle close to the right angle or in the direction opposite to the OL route connected for the substation (the latter only applies to the dead-end substations);

b) first the current ground electrode and the potential electrode are mounted and the connecting wires are connected to them. Then they begin to unfold and connect to the subject.

At the end of the work, the measuring circuit is disassembled in the reverse order. Initially, the connecting wires are disconnected from the GD device and from the devices, then the wires are rewound and only at the end are disconnected from the current and potential electrodes.

In connection with the above, the technique of full-scale measurements in a group of grounding devices is as follows.

Fig. 1 shows in the plan the circuit for the implementation of the method of measuring the resistance of individual interacting grounding devices in a sequence of operations.

In the initial state, a system of three independent (to check the absence of galvanic connection) grounding electrodes 1, 2, 3 is used each having its own value R_{xi}, where i = 1, 2, 3. One of the grounding electrodes can be set to measure its resistance, others or already exist, or are created additionally. In general, the grounding electrodes 1, 2 and 3 are located in the ground.

Below we consider a system of three interacting grounding electrodes in the shape of circular plates with a diameter of 4 m, 2 m and 3.6 m. The plates are made of from foamed polystyrene foam and placed on the surface of a water basin (30×20 m) with a specific resistance of water ρ = 12 Ω·m at distances between them of 0.4 m. First, the resistance of the grounding electrodes was measured by a single-beam circuit [1], i.e. by the existing method (see Table 6 for the values). Measurements were made in early spring.

According to the new technique, a series of measurements are made in experiments A (Fig. 1,*a*), B (Fig. 1,*b*) and C (Fig. 1,*c*).

The circuit of the measurement circuit is assembled: the voltmeter 8 is connected to a pair of grounding electrodes (1-2) by means of wires 7, the voltmeter 10 is connected to a pair of grounding electrodes (2-3) by means of wires 9, the voltmeter 12 is connected to a pair of grounding electrodes (1-3) by means of wires 11. The source 6 of the current monitored by the ammeter 5 is connected to a pair of grounding electrodes (1-2) by means of wires 4 and ensures current flow through the circuit (Fig. 1,*a*). We record the readings of the ammeter 5 ($I_{1\text{-}2}$), voltmeter 8 ($U_{1\text{-}2}$), voltmeter 10 ($U_{2\text{-}3}$), voltmeter 12 ($U_{1\text{-}3}$). From the grounding electrode 2 we disconnect wire 4, move it to grounding electrode 3 and connect to it. We provide the current flow through the circuit (Fig. 1,*b*). We record the readings of the ammeter 5 ($I_{1\text{-}3}$), voltmeter 8 ($U_{1\text{-}2}$), voltmeter 10 ($U_{2\text{-}3}$), voltmeter 12 ($U_{1\text{-}3}$). From the grounding electrode 1, we disconnect the wire 4, move it to the grounding electrode 2 and connect to it. We ensure the current flow through the circuit (Fig. 1,*c*). We record the readings of the ammeter 5 ($I_{2\text{-}3}$), voltmeter 8 ($U_{1\text{-}2}$), voltmeter 10 ($U_{2\text{-}3}$), voltmeter 12 ($U_{1\text{-}3}$).

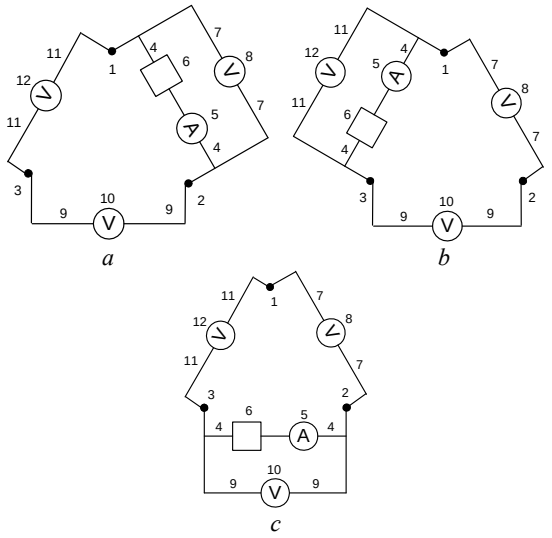

Fig. 1. . Schematic location of grounding electrodes and connection of measuring instruments

As a result of measurements, we obtain the values of parameters which we enter in Table 1.

Table 1

Results of full-scale measurements of parameters

Experiment	A	B	C
Measured parameter	Source introducing in points 1, 2	Source introducing in points 1, 3	Source introducing in points 2, 3
I_{12}, A	112.64	–	–
I_{13}, A	–	165.76	–
I_{23}, A	–	–	112.16
U_{12}, V	379.9	169.41	243.275
U_{13}, V	128.296	351.4	124.273
U_{23}, V	251.638	182	367.5

The treatment of given in Table 1 data allows to obtain input resistances for each pair of grounding electrodes in a system of three interfering grounding electrodes. The input resistance at input of a source between grounding electrodes, for example 1 and 2, is determined by expression

$$R_{12\text{inp}} = U_{12} / I_{12}.$$

Similarly, we obtain the values of the input resistances $R_{13\text{inp}}$ и $R_{23\text{inp}}$. The results are summarized in Table 2.

Table 2

Input resistances for corresponding pairs of grounding electrodes

Determined parameter	Input resistances between grounding electrodes, Ω		
	R_{12inp}	R_{13inp}	R_{23inp}
Parameter value	3.37	2.11	3.27

According to the results of Table 2 and taking into account Fig. 2 we compose a system of three equations with six unknown values of a three-element grounding system:

$$\begin{aligned} R_1 + R_2 - 2R_{12} &= R_{12inp}; \\ R_1 + R_3 - 2R_{13} &= R_{13inp}; \\ R_2 + R_3 - 2R_{23} &= R_{23inp}. \end{aligned} \quad (1)$$

Neglecting (as an assumption) the mutual resistances (R_{12}, R_{13} and R_{23}) and the influence of the third grounding electrode within each pair, by solving the system of three equations with three unknowns obtained in this way, we calculate the approximate values of the own resistances of grounding electrodes (R_{10}, R_{20} and R_{30}) and summarize them in Table 3.

Table 3

Approximate values of the own resistances of grounding electrodes

Determined parameter	Own resistances, Ω		
	R_{10}	R_{20}	R_{30}
Parameter value	1.11	2.26	1

The obtained approximate values of the own resistances of grounding electrodes make it possible to estimate the approximate values of the mutual resistances between the grounding electrodes within each pair. Such an estimate is based on the fact that the mutual resistance between two grounding electrodes is always less than the smallest of them. The results of calculations are summarized in Table 4.

Table 4

Estimation of mutual resistances between the corresponding pairs of grounding electrodes

Determined parameter	Mutual resistances between grounding electrodes, Ω		
	R_{12mut}	R_{13mut}	R_{23mut}
Parameter value	1	0.8	1

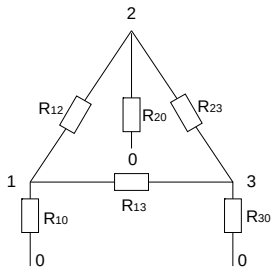

Fig. 2. Substitution circuit of the system of three interfering grounding electrodes

According to the measurement data (Table 1) of the currents (I_{12}, I_{13}, I_{23}) and voltages (U_{12}, U_{13}, U_{23}) obtained in each current measurement, we form a system of six equations with six unknowns representing the substitution (Fig. 2) of a system of three interfering grounding electrodes. The system has the following form:

$$\begin{cases} R_{(1-3)A} = \left[(R_1 - R_{12}) - \dfrac{(R_{13} - R_{32})R_{13}}{R_3} \right] - (R_{13} - R_{32}); \\ R_{(3-2)A} = \left[(R_2 - R_{12}) + \dfrac{(R_{13} - R_{32})R_{32}}{R_3} \right] + (R_{32} - R_{13}); \\ R_{(1-2)B} = \left[(R_1 - R_{13}) - \dfrac{(R_{23} - R_{12})R_{12}}{R_2} \right] - (R_{23} - R_{12}); \\ R_{(3-2)B} = \left[(R_3 - R_{13}) + \dfrac{(R_{23} - R_{12})R_{23}}{R_2} \right] - (R_{23} - R_{12}); \\ R_{(1-2)C} = \left[(R_2 - R_{32}) + \dfrac{(R_{13} - R_{12})R_{12}}{R_1} \right] + (R_{12} - R_{13}); \\ R_{(1-3)C} = \left[(R_3 - R_{32}) - \dfrac{(R_{13} - R_{12})R_{13}}{R_1} \right] + (R_{12} - R_{13}). \end{cases} \quad (2)$$

The obtained approximate values of the parameters of the circuit (see Table 3, 4), in accordance with the procedure described in [8], are used as initial values for the solution of the system of six equations with six unknowns (2) for which the left-hand sides are presented on the basis of the measurements given in Table 1 as follows.

For example, in experiment A, the results of measuring the voltages U_{13} and U_{23} and the current I_{12} when a source is input between grounding electrodes 1 and 2 make it possible to obtain input resistances, i.e. the left-hand sides of the system of equations (2):

$$\begin{aligned} R_{13A} &= U_{13} / I_{12}; \\ R_{32A} &= U_{23} / I_{12}. \end{aligned}$$

The results of similar calculations for the input of a source between grounding electrodes 1 and 3 (experiment B), as well as grounding electrodes 2 and 3 (experiment C), are summarized in Table 5.

Table 5

The results of estimating the left-hand sides of the equations in the input of the source between the respective grounding electrodes

The source connection	Points 1, 2		Points 1, 3		Points 2, 3	
Determined parameter	R_{13A}	R_{32A}	R_{12B}	R_{32B}	R_{12C}	R_{13C}
Parameter value, Ω	1.139	2.234	1.022	1.098	2.169	1.108

Using the as initial approximate values of own (Table 3) and mutual (Table 4) resistances of the grounding electrodes and substituting the resulting left-hand parts (Table 5) into equations (2), we solve the system of equations using the program developed in the Mathcad package and summarize the results in Table 6.

Table 6

Results of measurements of own and mutual resistances of grounding electrodes by new and existing techniques and estimation of discrepancies

Parameter, Ω	R_1	R_2	R_3	R_{12}	R_{13}	R_{23}
Initial value	1.11	2.26	1	1	0,8	1
Using new technique	1.534	2.694	1.594	0.525	0.464	0.565
Using existing technique	1.5	2.7	1.6	0.53	0.47	0.57
Discrepancy, %	2.26	0.22	0.37	0.94	1.27	0.87

Analyzing the data of Table 6, we come to the conclusion that the results of the calculations agree satisfactorily with the results of measurements obtained in the experiments. In this case, the discrepancy does not exceed 2.3 %, which is a very good error result.

Thus, we obtain the required values of the own and mutual resistances of the grounding electrodes making up the three-element system.

Conclusions.

For the first time, the technique of full-scale measurements of the resistance of grounding devices for various purposes using a three-electrode installation without finding a zero potential point is presented.

The proposed technique provides the minimal possible separation of measuring electrodes outside the GD which removes restrictions on building up the area outside the investigated GD, by several times reduces the length of the connecting wires of the measurement circuit which increases the signal-to-interference ratio.

Experimental full-scale measurements showed that the developed technique allows to obtain a fairly accurate result in all cases of GD resistance measurements of electrical installations.

REFERENCES

1. *Natsional'nyy standart Ukrayiny. SOU 31.2-21677681-19:2009. Viprobuvannya ta kontrol' prystroyiv zazemlennya elektroustanovok. Tipova instruktsiya* [National Standard of Ukraine SOU 31.2-21677681-19:2009. Test and control devices, electrical grounding. Standard instruction]. Kyiv, Minenergovugillya Ukrayiny Publ., 2010. 54 p. (Ukr).

2. Burgsdorf V.V., Yakobs A.I. *Zazemlyayushchie ustroystva elektroustanovok* [Grounding device of electrical installations]. Moscow, Energoatomizdat Publ., 1987. 400 p. (Rus).

3. Oslon A.B., Kostruba S.I. Measuring the resistance of large grounding devices. *Electrichestvo*, 2006, no.8. pp. 49-56. (Rus).

4. Chernov K.P. Resistance of grounding conductor and method of its determination with the help of two additional earth leads with unknown resistances. *Proceedings of higher educational establishments. Energy problems.* 2012, no.5-6, pp. 55-61. (Rus).

5. Yue Yong-gang, Huang Zhi, Dang Da-wei, Meng Qing-da, Wang Ya-ping, Huo Feng, Ye Tao. Grounding impedance measurement for 500 kV substation with lightning line. *Journal of Electric Power Science and Technology*, 2013, iss.4, pp. 83-87. (Chinese).

6. Oslon A.B., Tselebrovskii Iu.V. The intersection of the potential curves and the resistance of the grounding device *III Rossiiskaia konferentsiia po zazemliaiushchim ustroistvam: Sbornik dokladov* [3rd Russian Conf. on Grounding Devices: Collected Papers]. Novosibirsk, Russia, 27-31 October 2008, pp. 121-130. (Rus).

7. Oslon A.B., Kostruba S.I. Mathematical modeling of the process of grounding resistance measurement current of industrial frequency in multilayer soil. *Electrichestvo*, 2008, no.5, pp. 12-17. (Rus).

8. Nizhevskyi I.V., Nizhevskyi V.I. A technique of measuring of resistance of a grounding device. *Electrical engineering & electromechanics*, 2016, no.3, pp. 50-57. (Rus). **doi: 10.20998/2074-272X.2016.3.08.**

9. Nizhevskyi I.V., Nizhevskyi V.I., Bondarenko V.E. The experimental validation of the grounding device resistance measurement method. *Electrical engineering & electromechanics*, 2016, no.6, pp. 60-64 (Rus). **doi: 10.20998/2074-272X.2016.6.10.**

Received 01.02.2018

I.V. Nizhevskyi[1], *Candidate of Technical Sciences,*
V.I. Nizhevskyi[1], *Candidate of Technical Sciences, Associate Professor,*
[1] National Technical University «Kharkiv Polytechnic Institute», 2, Kyrpychova Str., Kharkiv, 61002, Ukraine,
phone +380 57 7076977,
e-mail: victornizhevski@gmail.com

How to cite this article:
Nizhevskyi I.V., Nizhevskyi V.I. A technique of full-scale measurements of the resistance of the grounding device. *Electrical engineering & electromechanics*, 2018, no.3, pp. 68-71. **doi: 10.20998/2074-272X.2018.3.09.**

Матеріали приймаються за адресою:
Кафедра "Електричні апарати", НТУ "ХПИ", вул. Кирпичова, 21, м. Харків, 61002, Україна
Електронні варіанти матеріалів по e-mail: a.m.grechko@gmail.com

Довідки за телефонами: +38 050 653 49 82 Клименко Борис Володимирович
+38 067 359 46 96 Гречко Олександр Михайлович